

University of Arkansas, Fayetteville

ScholarWorks@UARK

Graduate Theses and Dissertations

12-2019

Probing of Carbohydrate-Protein Interactions Using Galactonoamidine Inhibitors

Jessica B. Pickens

University of Arkansas, Fayetteville

Follow this and additional works at: <https://scholarworks.uark.edu/etd>



Part of the [Amino Acids, Peptides, and Proteins Commons](#), [Biochemistry Commons](#), and the [Organic Chemistry Commons](#)

Citation

Pickens, J. B. (2019). Probing of Carbohydrate-Protein Interactions Using Galactonoamidine Inhibitors. *Graduate Theses and Dissertations* Retrieved from <https://scholarworks.uark.edu/etd/3462>

This Dissertation is brought to you for free and open access by ScholarWorks@UARK. It has been accepted for inclusion in Graduate Theses and Dissertations by an authorized administrator of ScholarWorks@UARK. For more information, please contact scholar@uark.edu.

Probing of Carbohydrate-Protein Interactions Using Galactonoamidine Inhibitors.

A dissertation submitted in partial fulfillment
of the requirements for the degree of
Doctor of Philosophy in Chemistry

by

Jessica B. Pickens
University of Arkansas at Fort Smith
Bachelor of Science in Chemistry, 2013

December 2019
University of Arkansas

This dissertation is approved for recommendation to the Graduate Council.

Susanne Striegler, Ph.D.
Dissertation Director

Roger Koeppe, Ph.D.
Committee Member

Joshua Sakon, Ph.D.
Committee Member

Suresh Kumar Thallapuranam. Ph.D.
Committee Member

Abstract

Glycoside hydrolases are ubiquitous and one of the most catalytically proficient enzymes known, and thus understanding their mechanisms are crucial. Most research has focused on the interaction of the glycon of substrates and their inhibitors within the active site of glycoside hydrolases. The inhibitors employed to probe these interactions generally had small aglycons (i.e. a hydrogen atom, amidines, small aliphatic groups, or benzyl groups). Here, the interactions of the aglycon with glycoside hydrolases are examined by probing the active sites with a library of 25 galactonoamidines. The studies described in this dissertation aim to increase the understanding of stabilization of the transition state by glycoside hydrolases, which allows for the acceleration of substrate hydrolysis by the enzymes up to 10^{17} over non-enzymatic hydrolysis. To understand this stabilization, the active sites of β -galactosidases from *Aspergillus oryzae*, bovine liver, and *Escherichia coli* were evaluated using spectroscopic, molecular docking, and modeling analyses to determine transition state analogs (TSAs) and how the TSAs interact within the active site of glycoside hydrolases.

The probing with the galactonoamidine library revealed hydrophobic interactions, π - π interactions, and CH- π interactions within the active sites to varying extent. Further, three TSAs were found for the hydrolysis of substrates by β -galactosidase (*A. oryzae*), and two TSAs for the β -galactosidases from bovine liver and *E. coli*. Upon TSA binding to the three β -galactosidases, conformational changes occurred to stabilize the galactonoamidines within the active sites, which did not occur when fortuitous binders interacted with the enzyme. The conformational changes within the active sites of β -galactosidases from bovine liver and *E. coli* closes off the active site via a loop movement resulting in a substantially higher binding affinity than those observed with β -galactosidase (*A. oryzae*). A subsequent evaluation of galactonoamidine

specificity in the presence of other proteins revealed an increase of inhibitory activity two orders of magnitude more than a purified β -galactosidase (*E. coli*).

©2019 by Jessica B. Pickens
All Rights Reserved

Acknowledgements

I thank my advisor, Dr. Susanne Striegler, for her support and guidance throughout my studies at the University of Arkansas. I greatly appreciate the time and advice given to me throughout this project, without which this dissertation would not have been possible. She has mentored me to be a better chemist and has been very understanding of the personal and familial trials that I faced in graduate school. I thank my committee members for their guidance in both my research and professional matters. I thank Dr. Feng Wang for his time, expertise, and advice on all molecular dynamics simulations. I acknowledge and thank Logan G. Mills for his hard work and help during spectroscopic evaluations for **Chapter 2**. I also acknowledge and thank Dr. Rami Kanso, Dr. Qui-Hua Fan and Ifedi Orizu for their contributions by synthesis of the glycosides used in this study. I thank my lab mates Dr. Babloo Sharma and Ifedi Orizu for their support and friendship.

Support for this research to Dr. Susanne Striegler by National Science Foundation (CHE-1305543) and the Arkansas Biosciences Institute are gratefully acknowledged. I am thankful to the Scharlau family, whom gave a gift to the laboratory that allowed the purchase of the protein purification equipment. I am also grateful for the Don Bobbitt Fellowship, which was awarded to Jessica B Pickens during the 2019 Spring semester. All molecular dynamics simulations were performed with the Arkansas High-Performance Computing Center, which is supported by the National Science Foundation (ACI0722625, ACI0959124, ACI0963249, and ACI0919070) and the Division of Science and Technology at the Arkansas Economic Development Commission.

Last, but not least, I would like to thank my family for their unwavering support during this journey.

Table of Contents

1 Introduction	1
1.1 Glycoside Hydrolase in Nature	1
1.2 Inhibitors of Glycoside Hydrolases	4
1.3 Transition states and transition state analogs	9
1.4 Initial evaluations of galactonoamidines	14
2 Examination of galactonoamidines with hydrophobic aglycons as putative TSAs for β-galactosidase (<i>A. oryzae</i>)	21
2.1 Introduction:	21
2.2 Results and Discussion:	22
2.2.1 Docking analysis of galactonoamidines.	22
2.2.2 Linear Free Energy Relationship Analysis	23
2.2.3 Molecular dynamic evaluation of galactonoamidine-protein complexes	26
2.3 Conclusion	29
2.4 Materials and Methods	29
2.4.1 Instrumentation	29
2.4.2 Materials	30
2.4.3 Spectroscopic Evaluation of galactonoamidines	30
2.4.4 Docking Analysis	32
2.4.5 Molecular dynamics analysis:	33
3 Exploration of the active site of β-galactosidase (bovine liver) reveals loop closure over active site	35
3.1 Introduction	35
3.2 Results and Discussion	37
3.2.1 Spectroscopic evaluations	37
3.2.2 Development of model for β -galactosidase (bovine liver)	43
3.2.3 Molecular dynamics evaluations of galactonoamidine-enzyme complexes	45
3.3 Conclusion:	47
3.4 Materials and Methods	48
3.4.1 Instrumentation	48
3.4.2 Materials	48
3.4.3 Spectroscopic evaluations	49
3.4.4 Development of β -galactosidase (bovine liver) model	50
3.4.5 Molecular Dynamics Simulations	51
4 Investigation of galactonoamidine inhibition of β-galactosidase (<i>E. coli</i>) under isolated and cell-like conditions.	53

4.1 Introduction	53
4.2 Results and Discussion	55
4.2.1 Active site independence and SAR study	55
4.2.2 Molecular docking and modeling of galactonoamidines	60
4.2.3 Spectroscopic evaluation of galactonoamidines as TSA.	67
4.2.4 Inhibition of β -galactosidase in cell assays	69
4.2.5 Purification of β -galactosidase (<i>E. coli</i>)	72
4.2.6 Inhibition of purified (<i>E. coli</i>)	73
4.3 Conclusions	74
4.4 Materials and Methods	75
4.4.1 Instrumentation:	75
4.4.2 Materials:	76
4.4.3 Spectroscopic evaluations of commercial enzyme.	77
4.4.4 Inhibitor cooperativity analysis:	78
4.4.5 Molecular docking and modeling of protein inhibitor complexes.....	79
4.4.6 Propagation of <i>E. coli</i> cells for cell assays	80
4.4.7 Purification of β -galactosidase (<i>E. coli</i>)	81
4.4.8 Spectroscopic analysis with lysed cells, crude protein extract, and purified protein. ..	85
4.4.9 Assay to determine β -galactosidase activity.....	86
4.4.10 Assay to determine inhibition constants with purified β -galactosidase	87
5 Conclusions and Outlooks	88
6 References	90
7 Appendix 1: Supplemental Information from Chapter 2.....	103
7.1 Molecular docking analysis with β -galactosidase (<i>A. oryzae</i>)	103
8 Appendix 2: Supplemental Information from Chapter 3	104
8.1 Determination of molar absorptivity of nitrophenylates.	104
8.1.1 Stock solution of phenols:	104
8.1.2 Molar absorptivity Assay:	104
8.1.3 Data analysis:.....	104
8.2 Molecular Dynamics snapshots of FQ248 in complex with β -galactosidase (bovine liver)	105
9 Appendix 3: Supplemental information for Chapter 4	106
9.1 Molecular Dynamics Simulations	106
9.1.1 RMSD Plots of β -galactosidase (<i>E. coli</i>) in complex with galactonoamidines:	106
9.1.2 Hydrogen bond Formation	107
9.1.3 Images	107

9.2 SDS-PAGE	109
---------------------------	------------

Table of Figures

Figure 1.1 Koshland's mechanism for inverting and retaining glycoside hydrolases. ¹³	2
Figure 1.2 Structure of some covalent inhibitors used to probe glycoside hydrolase active sites..	5
Figure 1.3 Structures of activated 2-deoxy-2-fluoro glycosides.....	6
Figure 1.4 Transition state theory of a non-enzymatic reaction (top) and enzymatic reaction (bottom).....	10
Figure 1.5 Vasella's gluconojiritetrazole (3l) and mannonojiritetrazole (3m).	12
Figure 1.6 Xylobiose based inhibitors of Cex xylanase.	13
Figure 1.7 Free-energy relationship studies of xylobiose based inhibitors 3n (A) and 3r (B) with Cex xylanase. ⁶⁹	14
Figure 1.8 (A) Initial seven galactonoamidines synthesized to inhibit hydrolysis of substrate by β -galactosidases. ⁸² (B) Lineweaver-Burk plot with 5h as a model substrate showing competitive inhibition of β -galactosidase (<i>A. oryzae</i>) in the absence of inhibitor (cyan), 0.2 μ M 4b (navy), and 0.5 μ M 4b (blue). ⁸²	15
Figure 1.9 Aryl- β -D-galactopyranosides 5a-j developed as model substrates for β -galactosidase (<i>A. oryzae</i>) in evaluation of N-benzylgalactonoamidines as TSAs. ⁸³	16
Figure 1.10 Correlation of the binding energy of inhibitor ($\log K_i$), 4a (navy) and 4b (orange) to binding energy at the transition state ($-\log k_{cat}/K_M$) of the hydrolysis of ten galactopyranoside substrates by β -galactosidase (<i>A. oryzae</i>). ⁸³	17
Figure 2.1 Galactonoamidines selected for TSA analysis. ⁷⁹	22
Figure 2.2 Galactonoamidines (4l-o, 4r-t) docked within the active site of β -galactosidase (<i>A. oryzae</i>) with the catalytically active residues shown in green. The galactonoamidines are overlaid with the know TSA (4b): (A) 4o (red), (B) 4s (purple), 4t (grey), 4r (pink), 4n (olive), and 4l (blue). ⁷⁹	23
Figure 2.3 Double-logarithmic correlation of catalytic efficiency (k_{cat}/K_M) and the inhibition constant (K_i) with linear fit $y = ax + b$ for the 9 nitrophenyl- β -D-galactopyranosides in the presence of (A); (4o) (red triangle) $a = 1.02 \pm 0.10$, $R^2 = 0.93$; (4s) (purple pentagon) $a = 1.08 \pm 0.10$, $R^2 = 0.95$; and (B) (4n) (green diamond) $a = 1.16 \pm 0.21$, $R^2 = 0.83$; (4r) (pink hexagon) $a = 0.44 \pm 0.19$, $R^2 = 0.46$; (4t) (grey pentagon) $a = 1.17 \pm 0.32$, $R^2 = 0.69$. ⁷⁹	26
Figure 2.4 (A) Frequency of hydrogen bonding interactions in correlation to the number of hydrogen bonding of galactonoamidines with β -galactosidase (<i>A. oryzae</i>). (B) Occupancy of the catalytic residues throughout the 30ns simulations with galactonoamidines. ⁷⁹	27

Figure 2.5 Overlay of the molecular dynamics simulations of β -galactosidase from <i>A. oryzae</i> (dark grey) with 4b (orange) and β -galactosidase from <i>A. oryzae</i> (blue) with 4t (cyan). Catalytic residues are shown as ball and stick (red). ⁷⁹	28
Figure 3.1 Sequence similarities of β -galactosidases from <i>A. oryzae</i> and bovine liver surrounding the two catalytically active residues. ¹¹³	35
Figure 3.2 Predicted active site of β -galactosidase from bovine liver. ¹²⁴	36
Figure 3.3 Lineweaver-Burk plot of the hydrolysis of model substrate by β -galactosidase (bovine liver) in the presence of 0nM (grey triangle), 0.05nM (green triangle) 4b, and 0.1nM (olive triangle) 4b. ⁹⁰	37
Figure 3.4 Double-logarithmic correlation of catalytic efficiency (k_{cat}/K_M) and the inhibition constant (K_i) with linear fit $y = ax + b$ for the 8 nitrophenyl- β -D-galactopyranosides in the presence of (A) (4a) (navy circle) $a = 1.08 \pm 0.15$, $R^2 = 0.92$; (4b) (orange square) $a = 1.06 \pm 0.11$, $R^2 = 0.95$; and (B) (4o) (red triangle) $a = 0.66 \pm 0.24$, $R^2 = 0.60$; (4s) (purple pentagon) $a = 1.07 \pm 0.23$, $R^2 = 0.87$.	41
Figure 3.5 Models from M4T server (red), and model 1 (cyan), model 2 (green), model 3 (yellow), model 4 (pink), and model 5 (orange) from Robetta server.	44
Figure 3.6 (A) Frequency of hydrogen bonding interactions in correlation to the number of hydrogen bonding of galactonoamidines and derivatives with β -galactosidase (bovine liver). (B) Occupancy of the catalytic residues throughout the 30ns simulations with galactonoamidines and derivatives. ⁹⁰	46
Figure 3.7 Snapshots of from the 30ns simulation of the 4b (orange) and β -galactosidase (bovine liver) complex showing the active site (A) before, (B) during, and (C) after the loop closure event. The catalytic residues are shown in green and TRP272 and TYR484 are shown in magenta.	47
Figure 4.1 Current compounds synthesized to mimic the transition state that have been crystalized within the active site of β -galactosidase (<i>E. coli</i>). ¹⁴⁶ Galactonoamidines designed to mimic the transition state of substrate hydrolysis.	54
Figure 4.2 (A) Lineweaver-Burk plots of the hydrolysis of 5h by β -galactosidases (<i>E. coli</i>) in the presence of 4b show competitive inhibition. (B) Cooperativity analysis of interaction of galactonoamidines in the active sites of β -galactosidases (<i>E. coli</i>) shows the independence of active sites of the homotetramers.	56
Figure 4.3 Substrate, 2-fluoro-2-deoxy- β -D-galactopyranoside (2a), crystallized within the active site of β -galactosidase (<i>E. coli</i>), PDB ID 4V45. ¹⁴⁶	61
Figure 4.4 Hydrogen bonding interactions of 2a and 3k with β -galactosidase (<i>E. coli</i>)	62

Figure 4.5 A) Crystallized (purple) β -galactosidase (*E. coli*) in complex with 2FG (yellow) and the final coordinates of β -galactosidase (*E. coli*) after 48ns of simulation (grey) within 15Å of the active site. B) Active site residues from the crystal structure (purple) and simulated β -galactosidase (grey) after 48ns with 2FG in yellow. C) Crystallized (red) β -galactosidase (*E. coli*) in complex with GTZ (blue) and the final coordinates of β -galactosidase (*E. coli*) after 48ns of simulation (grey) within 15..... 63

Figure 4.6 Hydrogen bonding interactions of galactonoamidines **4a** (A), **4b** (B), **4c** (C), **4f**(D), **4g**(E) and **4i**(F) with β -galactosidase (*E. coli*)..... 65

Figure 4.7 Snap shot of the loop closure with complex of β -galactosidase (*E. coli*) and **4a**. Only protein within 10Å of **4a** is shown for clarity. 66

Figure 4.8 Transition state of model substrates' (**5a-k**) hydrolysis by β -galactosidases (grey).⁷⁰ 68

Figure 4.9 Double-logarithmic correlation of inverse catalytic efficiency (K_M/k_{cat}) and the inhibition constant (K_i) with linear fit $y = ax + b$ for the 9 nitrophenyl- β -D-galactopyranosides in the presence of (A); **4a** (navy circle) $a = 0.99 \pm 0.10$, $R^2 = 0.92$ and **4b** (orange square) $a = 0.91 \pm 0.11$, $R^2 = 0.91$; (B) (**4s**) (purple pentagon) $a = 1.15 \pm 0.35$, $R^2 = 0.61$ 69

Figure 4.10 Hydrolysis of model substrate, 4-methylumbelliferyl β -D-galactopyranoside (**5m**).70

Figure 4.11 Activity of β -galactosidase (*E. coli*) from crude protein extract (half squares) and purified protein (half circles) in the presence of (A) **4a**, (B) **4b**, and (C) **4s**. 71

Figure 4.12 A) Comparison of commercial (red) and purified (blue) β -galactosidases by GPC analysis. B) Comparison of estimated $\Delta\epsilon$ by PDB2CD (black) to the experimental CD obtained with purified (blue) and commercial (red) β -galactosidase (*E. coli*).¹⁶⁰ 73

Figure 5.1: Structure of the galactonoamidine (**4b**) that determined to be a TSA of the three examined β -galactosidases..... 89

Figure 7.1 Snap shots of from the 30 ns simulation of the **4o** (red) and β -galactosidase (bovine liver) complex showing the active site (A) before, (B) during, and (C) after the loop closure event. The catalytic residues are shown in green and TRP272 and TYR484 are shown in magenta. 105

Figure 8.2 Frequency of hydrogen bonding interactions in correlation to the number of hydrogen bonding of galactonoamidines with β -galactosidase (*E. coli*). 107

Figure 8.3 Snap shots of **2a** and **3k** within the active site of β -galactosidase (*E. coli*). Catalytic residues are shown as green sticks, Trp999 and Trp568 are shown as cyan sticks, and the metal ions are shown as spheres (cyan = Mg^{2+} and yellow = Na^+) 107

Figure 8.4 Snap shots of the galactonoamidines within the active site of β -galactosidase (*E. coli*). Green sticks are catalytic residues, cyan sticks are Trp999 and Trp568, and the metal ions are shown as spheres (cyan = Mg^{2+} and yellow = Na^+). (A) 4a, (B) 4b, (C) 4c, (D) 4f, (E) 4g, (F) 4j, (G) 4i, (H) 4p, and (I) 4s. 108

Figure 8.5 SDS PAGE analysis of fractions from the ion exchange column, DEAE Sephacel. The fractions containing β -galactosidase (*E. coli*) were from the 300mM and 400mM NaCl buffer solutions. 109

Figure 8.6 SDS PAGE analysis of fractions from the affinity column, p-aminobenzyl-1-thio- β -D-galactopyranoside agarose. Pure β -galactosidase (*E. coli*) eluted in fractions 19-25. Since fraction 21 contained some contamination it was not pooled with the other fractions for the final stock solution. 109

Figure 8.7 SDS PAGE comparison of purified β -galactosidase (*E. coli*) and the commercial β -galactosidase (*E. coli*). 110

Figure 8.8 Activity of β -galactosidase (*E. coli*) from (A) lysed cells, (B) crude protein extract, and (A) purified protein in the presence of 4a (navy circle), 4b (orange square), 4i (grey diamond) 4n (green triangle), and 4s (purple pentagon)..... 110

Table of Tables

Table 1.1 Inhibition constants (K_i ; μM) of β -galactosidases by azasugars designed to mimic the transition state of hydrolysis of substrates.	8
Table 1.2 Inhibition of hydrolysis of 2-chloro-4-nitrophenyl- β -D-galactopyranoside ($k_{\text{cat}} = 2381 \pm 135 \text{ min}^{-1}$ and $K_M = 0.70 \pm 0.1 \text{ mM}$) by β -galactosidase (<i>A. oryzae</i>) in the presence of galactonoamidines. 50mM Acetate buffer solution at pH 5.00 ± 0.05 and $30.0 \pm 0.1^\circ\text{C}$. ⁶⁷	19
Table 2.1 Model Substrates for TSA analysis with β -galactosidases. ⁷⁹	24
Table 2.2 Galactonoamidine inhibition of hydrolysis of 9 nitrophenyl- β -D-galactopyranosides by β -galactosidase (<i>A. oryzae</i>); 50 mM acetate buffer solution at pH 5.00 ± 0.05 and $30.0 \pm 0.1^\circ\text{C}$. ⁷⁹	25
Table 3.1 Inhibition of hydrolysis of 4-nitrophenyl- β -D-galactopyranoside ($k_{\text{cat}} = 4.24 \pm 0.26 \text{ min}^{-1}$ and $K_M = 0.51 \pm 0.01 \text{ mM}$) by β -galactosidase (bovine liver) in the presence of galactonoamidines. 5mM HEPES buffer solution at pH 7.50 ± 0.05 and $30.0 \pm 0.1^\circ\text{C}$. ⁹⁰	39
Table 3.2 Galactonoamidine inhibition of hydrolysis of 8 nitrophenyl- β -D-galactopyranosides by β -galactosidase (Bovine Liver); 5mM HEPES buffer solution at pH 7.50 ± 0.05 and $30.0 \pm 0.1^\circ\text{C}$	40
Table 3.3 Inhibition of hydrolysis of 4-nitrophenyl- β -D-galactopyranoside by β -galactosidase (bovine liver) in the presence of galactonoamidines. 5mM HEPES buffer solution at pH 7.50 ± 0.05 and $30.0 \pm 0.1^\circ\text{C}$. R = $-\text{CH}_2-\text{C}_6\text{H}_4-\text{CH}_3$. ⁹⁰	42
Table 4.1 Inhibition of hydrolysis of 4-nitrophenyl- β -D-galactopyranoside ($k_{\text{cat}} = 5478 \pm 107 \text{ min}^{-1}$ and $K_M = 0.040 \pm 0.004 \text{ mM}$) by β -galactosidase (<i>E. coli</i>) in the presence of galactonoamidines. 5mM HEPES buffer solution at pH 7.50 ± 0.05 and $30.0 \pm 0.1^\circ\text{C}$. ⁵⁶	58
Table 4.2 Galactonoamidine inhibition of hydrolysis of 9 nitrophenyl- β -D-galactopyranosides by β -galactosidase (<i>E. coli</i>); 5mM HEPES buffer solution at pH 7.50 ± 0.05 and $30.0 \pm 0.1^\circ\text{C}$. ..	68
Table 4.3 Inhibition of hydrolysis of 4-methylumbelliferyl- β -D-galactopyranoside (5l) by β -galactosidase (<i>E. coli</i>) in the presence of galactonoamidines. 5mM HEPES buffer solution at pH 7.50 ± 0.05 and $37.0 \pm 0.1^\circ\text{C}$	71
Table 4.4 Inhibition of hydrolysis of 4-nitrophenyl- β -D-galactopyranoside (5h) by β -galactosidase (<i>E. coli</i>) in the presence of galactonoamidines. 5mM HEPES buffer solution at pH 7.50 ± 0.05 and $30.0 \pm 0.1^\circ\text{C}$	74
Table 6.1 Hydrogen bonding interactions of the galactonoamidines (4b, 4l, 4n-o, and 4r-t) and amino acid residues in the active site of β -galactosidase (<i>A. oryzae</i>). From Section 2.2.1	103

1 Introduction

Carbohydrates account for approximately two-thirds of the carbon atoms on Earth.¹ Therefore, reactions with these glycosides must be considered as one of the most important to occur. Similarly, the enzymes that interact with these carbohydrates must be considered equally important.² The carbohydrate processing enzymes have been divided into three classes: glycoside hydrolases, glycosyl transferases, and polysaccharide phosphorylases.² Due to the fact that glycoside hydrolases can accelerate the non-enzymatic hydrolysis of glycosidic bonds by an astounding 17 orders of magnitude, understanding the mechanisms and stabilization of the transition states of hydrolysis by the glycoside hydrolases are paramount.³

The first mechanism for their hydrolysis of substrates was proposed by Koshland in 1953 and has not changed much since.⁴ However, the mechanism does not account for the role of the aglycon during the reaction. Summarized here is the general mechanism and classification of glycoside hydrolases, design of azasugars inhibitors, transition state theory and its application to glycoside hydrolases, and finally the contribution of the Striegler laboratory to the field.

1.1 Glycoside Hydrolase in Nature

Glycoside hydrolases (GHs) cleave di-, tri-, oligo-, and polysaccharides, making them essential in biological processes such as:⁵ hydrolysis of storage and structural polysaccharides,⁶ defense against viruses and pathogens,^{7, 8} and cell surface interactions.^{9, 10} The fundamental necessity for the GHs is evident based on all organisms containing genes to code for these enzymes, with the exception of some Archaeans and some unicellular eukaryotes.³ The GHs cleave these saccharides with either a retention or inversion of the stereochemistry at the anomeric carbon atom.² Koshland proposed that the inverting enzymes cleave the glycosidic bond in a single step, while the retaining GHs do so through a double-displacement mechanism

involving an glycosyl-enzyme intermediate, **Figure 1.1.**⁴ Both of these mechanisms have an oxocarbenium transition state during cleavage of the glycosidic bond, **Figure 1.1.**¹¹

In the inversion mechanism, a residue acts as a catalytic acid to donate a proton to the anomeric carbon atom while a different residue acts as catalytic base to remove a proton from a water molecule, which facilitates a nucleophilic attack on the anomeric center.¹² In the double-displacement mechanism of the retaining GHs a residue acts as both a general acid and general base in a two-step process: glycosylation and deglycosylation.² In the glycosylation step, the general acid/base facilitates the aglycon to leave by donating a proton to the glycosyl oxygen atom, while a residue acts as a nucleophile to form a glycosyl-enzyme intermediate.¹² In the deglycosylation step, the general acid/base activates a water molecule, which attacks the covalent intermediate and facilitates the release of the glycon.¹²

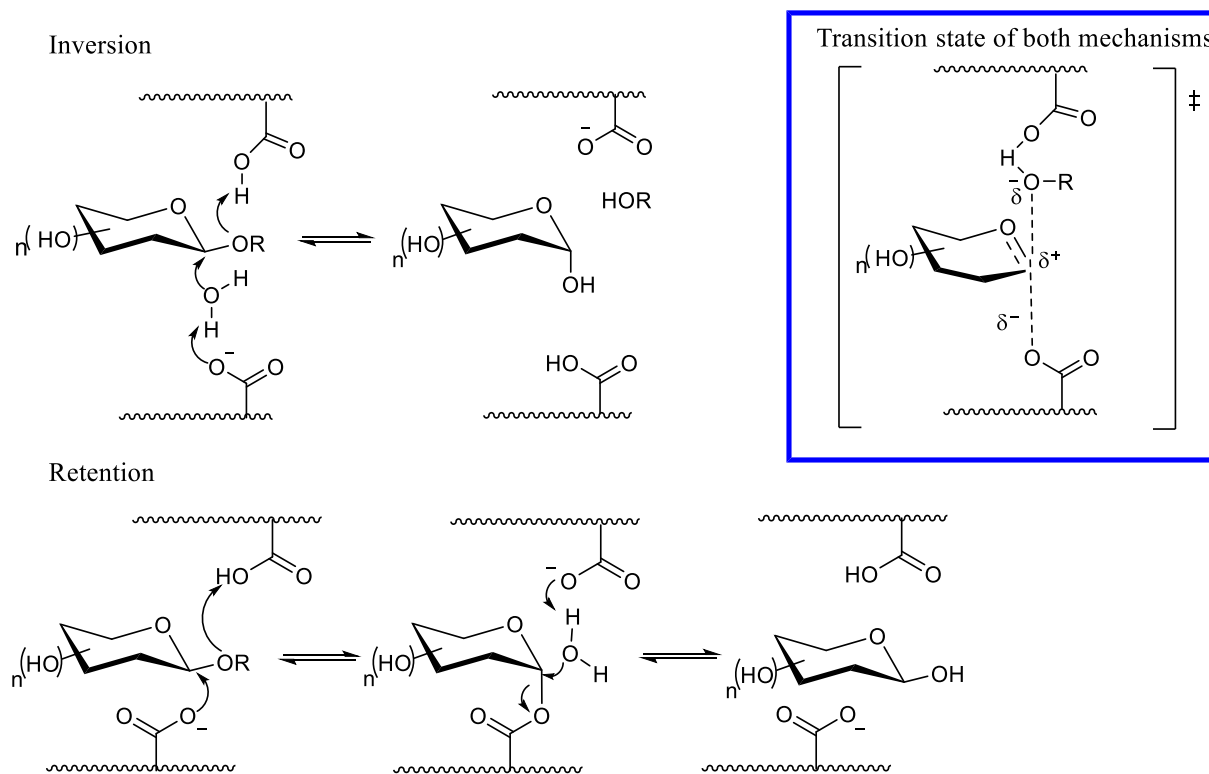


Figure 1.1 Koshland's mechanism for inverting and retaining glycoside hydrolases.¹³

A few alternative mechanisms have been proposed over the years.^{14, 15} In the mechanism proposed by Phillips protonation of the glycosidic oxygen atom by a general acid/base residue leads to cleavage of the bond and formation of an oxocarbenium ion.¹⁴ The oxocarbenium ion is stabilized by the negative charge of an Asp residue within the active site until a hydroxyl group binds to the positively charged anomeric carbon atom and the general acid/base is re-protonated.¹⁴ In the mechanism proposed by Post and Karplus, the oxygen atom at position five of the glycon is protonated, which results in the cleavage of the bond between the anomeric carbon and this oxygen atom.¹⁵ Then, attack by a water molecule, cleavage of the glycosidic bond and a subsequent ring closure result in the final products.¹⁵ Three main differences between the mechanisms are: (1) the ring opening that occurs with the Post and Karplus mechanism,¹⁵ (2) the Koshland and Phillips mechanisms require catalysis by enthalpic stabilization (distortion of the glycon),^{4, 14} whereas the Post-Karplus mechanism catalyzes by entropic contributions (orientation of the glycon),¹⁵ and (3) only the Koshland mechanism has a glycosyl-protein intermediate.¹⁵ The glycosyl protein intermediate and the oxocarbenium transition state of Koshland's mechanism have been proven through kinetic isotope studies,¹⁶ inhibition with irreversible fluoro-glycosyl inhibitors,¹⁷ and NMR studies.¹⁸

In order to differentiate the tremendous number of GHs in nature as retaining or inverting enzymes as well as specificity, they have been grouped into clans and subdivided into families.¹⁹ At first the GHs were classified based off of mechanism (retention or inversion) and then subdivided based on sequence similarity.²⁰ However, the subdivision based off of sequence alone was inefficient.⁵ Therefore, they were examined by hydrophobic cluster analysis, which has a high reliability with low sequence identity, and has the ability to detect secondary structure based on an enzyme's sequence.⁵ Using the second method, they were classified based on mechanistic

similarities, and sequence conversion was focused on the areas surrounding the catalytic residues.^{21, 22} This new classification system has classified all GHs into 18 clans (A-R) and 156 families.²³ The families have similar substrate specificity, evolutionary relationships, structure, and of course mechanisms.²³ Much that is known about the mechanistic details has been acquired by using inhibitors to probe the active sites of the enzymes. The probing has helped understand the importance of conserved residues, whether it is retaining or inverting, and the specificity.

1.2 Inhibitors of Glycoside Hydrolases

Glycoside hydrolases have been studied using covalent and noncovalent inhibitors.^{24 25 24,}
²⁶ The covalent inhibitors of glycoside hydrolases usually form a covalent bond when the catalytic residue that acts as a nucleophile attacks an electrophilic portion of the inhibitor.²⁷ These inhibitors can be categorized as affinity labels or mechanism based inhibitors.²⁵ Two classes of affinity labels have been employed to investigate the active site of the glycoside hydrolases: molecules that require stimuli to bind and those that do not.²⁸ Both classes of affinity labels have been used to label active sites of glycosides.²⁷ Some photoactivated labels employed are 3,7-Anhydro-2-azi-1,2-dideoxy-D-galactopyranoside (**1a**) and 4-[azidosalicyl-amido] butylamido-N-pentyl-1-deoxynojirimycin (**1b**), with β -galactosidase from *E. coli* and α -glucosidase from humans respectively, **Figure 1.2**.^{29, 30} The inhibitors that do not require activation have a tendency to spontaneously hydrolyze; however, a few (**1c-e**) have been used to examine the active site of retaining β -galactosidases, **Figure 1.2**.^{31, 32} The main drawback with these probes is that the aglycons are unspecific in binding.³³ Therefore, not all residues labeled are important in the binding of substrates within the active site.³³

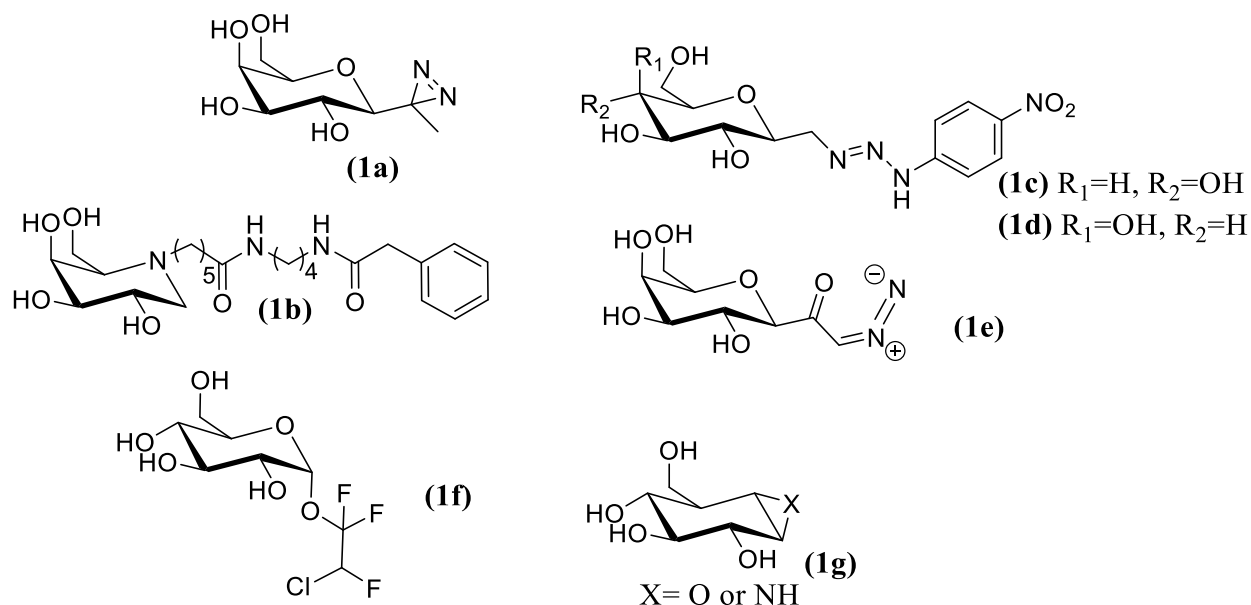


Figure 1.2 Structure of some covalent inhibitors used to probe glycoside hydrolase active sites.

Mechanism-based inhibitors (MBIs) are substrate analogs that are stable until acted upon by the enzyme.²⁵ Three main types of MBIs exist for glycoside hydrolases: glycosides with reactive aglycons, epoxide- and aziridine-based inhibitors, and activated fluorinated glycosides.²⁷ All MBIs with reactive aglycons are derived from difluoroalkyl glucoside (**1f**), which was the first developed.³⁴ After cleavage of the glycosidic bond, the *aglycon* decomposes into a reactive alkyl fluoride which in turn binds to the protein.³⁴ The enzymatic attack on epoxide and aziridine-based MBIs (**1g**) results in labeling of the nucleophile by the *glycon* of the MBI. Some of the resulting inhibitor-protein complexes have been characterized by X-ray diffraction, allowing for determination of nucleophiles of these enzymes.³⁵⁻³⁷

The final class of MBIs, activated fluorinated glycosides, can also be labeled as slow enzymatic substrates.^{38, 39} The glycosyl-enzyme intermediate created during inhibition can be hydrolyzed, allowing for the rescue of the enzyme activity³⁸. The first fluorinated glycosides, 2-deoxy-2-fluoro glycosides (**2a-b**), were developed by Withers in 1987, **Figure 1.3**.¹⁷ The

substitution of the hydroxyl group at C-2 in the glycon slows the formation of the glycosyl enzyme intermediate and its hydrolysis by destabilization of both transition states.²⁷ The two-fold destabilization is attributed to the inductive effects of the addition of the fluorine as well as the removal of key hydrogen bonding interactions over the hydroxyl group at C-2 in the glycon.⁴⁰

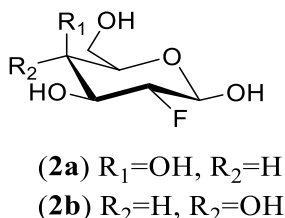


Figure 1.3 Structures of activated 2-deoxy-2-fluoro glycosides.

The fluorinated glycosides have been influential in three major mechanistic studies with glycoside hydrolases. Firstly, the fluorinated glycosides, along with the other MBIs, have helped identify the catalytic nucleophile in glycoside hydrolases by covalent attachment.⁴¹ Secondly, the fluorinated glycosides were instrumental in solidifying the double-displacement mechanism proposed by Koshland,⁴ rather than the ion-pair intermediate mechanism proposed by Phillips,¹⁴ as the glycoside hydrolase mechanism.⁴² Finally, an elegant study conducted by titration of glycoside hydrolases with ¹³C labeled catalytic residues in the presence and absence of the inhibitors exposed the role of the proton donor throughout the reaction.⁴³ Unlike the affinity labels, the MBIs are specific however, only the interactions of the *glycon* within the active site are revealed.

The general trend for design of the noncovalent inhibitors is to synthesize inhibitors that mimic the transition state of substrate hydrolysis by the GHs.⁴⁴ The discussion of these noncovalent inhibitors will be focused on azasugars designed to mimic the transition state (**3a-k**)

due to the similarities to the galactonoamidines used in the Striegler laboratory. In efforts to mimic the oxocarbenium ion-like transition state (TS), the inhibitors are endowed with one or more of the following characteristics: a flattened half-chair conformation of the glycon due to sp^2 -like character at the anomeric carbon atom, a positive charge that is delocalized over the anomeric carbon atom, and aglycons that mimic the bond lengthening of the glycosidic bond during the TS.⁴⁴⁻⁴⁷

Though deoxynojirimycin (**3a**), isofagomine (**3b**), and azaisofagomine (**3c**) lack the flattened chair characteristic most desired, the endocyclic nitrogen atom mimics the charge desired at the anomeric carbon atom during cleavage.⁴⁸ In order to incorporate some sp^2 nature into these compounds a similar compound, isofagomine lactam (**3d**), was synthesized. In addition to addition of sp^2 -character, this compound is able to tautomerize to form a hydroxyl group in at C-2 position of the glycon unlike **3b** and **3c**, **Table 1.1**.^{49, 50} As previously stated, the hydroxyl group at C-2 of the glycon has been shown to be important in the binding of substrates and inhibitors to the active sites of glycoside hydrolases.^{51, 52}

The first inhibitors that mimicked the delocalized positive charge and the flattening of the glycon due to sp^2 -hybridization of the anomeric carbon atom were developed by Ganem in the 1990s, **3e-h**.^{45, 53} These inhibitors were established to be broad spectrum inhibitors based on their ability to inhibit β -glucosidase (Almonds; **3g** K_i = 8.4 μ M), α -mannosidase (jack beans; **3h** K_i = 0.17 μ M), α -galactosidase (green coffee bean, **3f** K_i =8.3 μ M), and β -galactosidase (bovine liver, **3f** K_i = 6.5 μ M).⁵³ There was initial speculation if these inhibitors were able to be transition state analogs because of the lack of specificity and the various accounts of the placement of the double bond.^{54, 55} However, the glyconoamidines tautomerize and thus the double bond is not fixed as endo or exocyclic. Further, the pKa of the glyconoamidines is typically between 8-10, and thus

the amidines are protonated under all conditions discussed here in. Therefore, the inhibitors have a delocalization of positive charge that would result from either an exo- or endocyclic double bond.^{53, 56} Vasella's imidazole- (**3i**), triazoles- (**3j**), and tetrazole-based (**3k**) azasugars mimic both the flattened chair and the positive charge of the transition state.⁵⁷ The Vasella inhibitors were more effective inhibitors for the β -galactosidase (*E. coli*) than **3a-c**, with the inhibitor's effectiveness decreasing with increasing number of nitrogen atoms within the cycles, **Table 1.1**, (K_i **3i**<**3j**<**3k**).^{58, 59} Though these and other inhibitors are designed to mimic the transition state of the enzymes, relatively few have been experimentally proven to be a transition state analog. These experiments and the reason for desiring a TSA will be discussed in the following section.

Table 1.1 Inhibition constants (K_i ; μ M) of β -galactosidases by azasugars designed to mimic the transition state of hydrolysis of substrates.

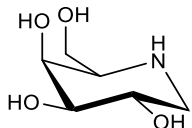
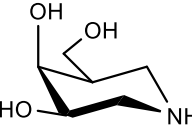
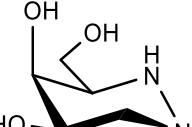
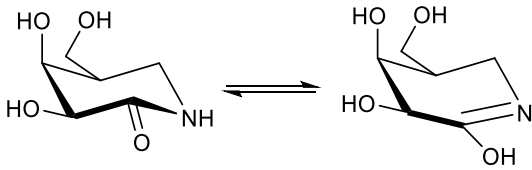
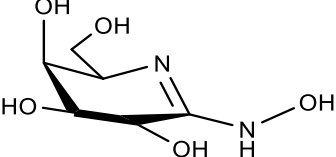
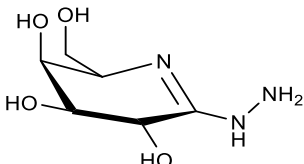
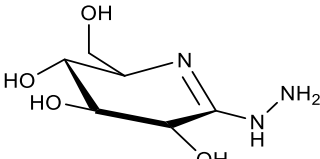
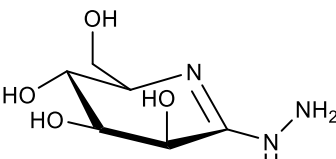
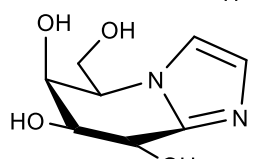
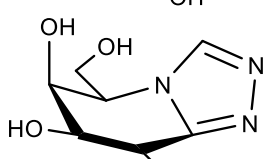
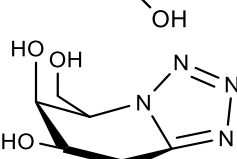
Compound	Inhibitor	<i>A. oryzae</i>	<i>E. coli</i>	bovine liver
3a		n.d.	13 ²⁴	12.5 ⁵³
3b		n.d.	0.2 ⁶⁰	n.d.
3c		n.d.	0.30 ⁶⁰	n.d.
3d		0.018 ⁶¹	n.d.	n.d.
3e		n.d.	0.1 ⁶²	10 \pm 0.5 ⁵³

Table 1.1 cont'd Inhibition constants (K_i ; μM) of β -galactosidases by azasugars designed to mimic the transition state of hydrolysis of substrates.

Compound	Inhibitor	<i>A. oryzae</i>	<i>E. coli</i>	bovine liver
3f		n.d.	n.d.	6.5 ± 0.1^{53}
3g		n.d.	n.d.	19 ± 1^{53}
3h		n.d.	n.d.	57 ± 2.5^{53}
3i		n.d.	0.004^{59}	n.d.
3j		n.d.	0.2^{59}	n.d.
3k		n.d.	1.0^{63}	n.d.

1.3 Transition states and transition state analogs

During enzymatic reactions, the active sites stabilize the transition state (TS) by optimization of noncovalent interactions of the substrate to a greater extent than the substrates' ground state.⁶⁴ This ability to stabilize the TS reduces the activation energy of the reaction and thus allows the enzymes to accelerate chemical reactions.⁶⁵ Using Eyring's theory of transition

states, Lienhard and Wolfenden established the thermodynamic relationship between ground-state binding and TS binding for enzymes and their substrates (**Figure 1.4**).⁶⁶⁻⁶⁸

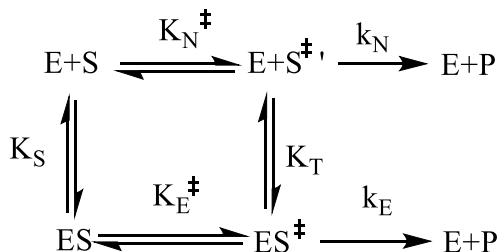


Figure 1.4 Transition state theory of a non-enzymatic reaction (top) and enzymatic reaction (bottom).

According to transition state theory, enzymatic catalysis (k_E) is faster than non-enzymatic catalysis (k_N) due to the tighter binding of the TS within the active site than the substrate.⁶⁸ Since most measured substrate binding affinities (K_S) to date are approximately 10^3 - 10^5 M^{-1} , the binding affinity of the transition state (K_T) could potentially reach up to 10^{15} M^{-1} .⁶⁸ The known binding ratios for transition states and substrates to enzymes (K_T/K_S) are 10^8 - 10^{14} , ideally a TSA would have a similar binding ratio (K_{TSA}/K_S).⁶⁸ However, current TSA's K_{TSA}/K_S are quite lower than this expected ratio, only 10^2 - 10^5 .⁶⁸ The inability of current TSAs to meet the theoretical enhancement of binding is attributed to the fact that no stable molecule can accurately mimic the electronic and geometric characteristics of the unstable TS structure.⁶⁵ This is especially true for areas at which bond cleavage and/or formation occurs.⁶⁵

With these general TS and TSA properties in mind, the TSs and TSAs of glycoside hydrolases can be examined.^{54, 69, 70} As discussed previously, the current methods of designing TSA for glycoside hydrolases involve the incorporation of the electronic mimicry by addition of nitrogen atoms within the heterocycles, and interchanging a glycoside's normal tetrahedral sp^3 anomeric carbon atom for the planar sp^2 aromatic carbon atom to mimic the chair flattening

during the TS.⁷¹ Usually these glycoside hydrolase inhibitors are called TSAs on a conceptual basis, for having the characteristics of the TS.⁶⁵ Yet, some well-designed studies have been developed that distinguish true TSAs from fortuitous binders with the characteristics of a TS.^{54, 69, 72, 73} Methods by which enzyme TS or its TSA have been examined include kinetic isotope effects of the substrate,¹⁶ QM/MM of substrate itinerary,⁷⁴ crystallography of enzymes with TSAs in the active sites,^{75, 76} mutations of residues within the active sites,⁷⁷ and spectroscopic analysis.⁷⁸ For brevity, only the mutation of active site residues and spectroscopic analysis methods will be discussed here due to their similarities to methods in later sections.^{70, 79}

Both of these methods take advantage of the thermodynamics of substrate and TSA binding to enzymes by the free energy relationship that correlates the free energy of activation for substrate turnover (k_{cat}/K_M) with the free energy of inhibitor binding to the enzyme (K_i).⁷⁸ In order for an inhibitor to be classified as a TSA, the slope of this free energy relationship plot, as well as the correlation factor (R^2), should be near 1.⁷⁸ These methods have been employed to test whether seven inhibitors similar to inhibitors in Error! Reference source not found. were TSAs of glycoside hydrolases in two studies.^{54, 69}

The first study was conducted by Ermert *et al* with Vasella's gluco- (**3l**) and manno-nojiritetrazole (**3m**), **Figure 1.5**.⁵⁴ Here, the ability of **3l** and **3m** to inhibit the hydrolysis of model substrates by five enzymes was examined: α -mannosidase (jack bean), α -mannosidase (almonds), β -mannosidase (snail), α -glucosidase (yeast), and β -glucosidase (Agrobacter).⁵⁴ The inhibition of hydrolysis of both manno- and glucopyranosides with the corresponding inhibitor was examined spectroscopically with each enzyme.⁵⁴ A double logarithmic plot of the catalytic efficacy and inhibition constants of each enzyme with each substrate showed a high linearity ($R^2=0.90$), but the slope of the line was not 1, rather it was 0.82 ± 0.10 .⁵⁴ Ermert classifies these

nojiritetrazoles as broad spectrum TSAs of the hydrolysis of glycosides by gluco- and mannosidases.⁵⁴ However, we will be more rigorous in our classifications in later chapters, and not classify any inhibitor as TSA unless the slope of the linear free-energy relationship is 1.00 ± 0.10 .

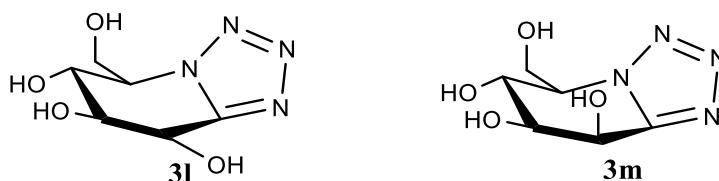


Figure 1.5 Vasella's gluconojiritetrazole (**3l**) and mannonojiritetrazole (**3m**).

The other examinations for TSAs used the mutation method for evaluation of five inhibitors as TSAs of Cex xylanase, **Figure 1.6**. All of the inhibitors were able to inhibit Cex xylanase, an exoglucanase, with inhibition constants between 0.13 and 5.8 μM .⁵⁰ Ten mutations were made to Cex xylanase and the catalytic turnover and binding affinity were determined in the presence and absence of the five inhibitors.⁶⁹ All ten of the mutations were made within the active site of the enzyme: Glu43Ala, Asn44Ala, Lys47Ala, His80Asn, His80Ala, His80Gln, Gln87Met, Gln87Thr, Asn126Ala, and Asn169Ala.⁶⁹ In efforts to determine if the sp^2 -hybridization is needed at the anomeric carbon atom, three xylobiose based inhibitors with sp^2 -hybridization, lactam oxime (**3n**), imidazole (**3o**), and isofagomine lactam (**3p**), were compared to two inhibitors with sp^3 -hybridization at the anomeric center: deoxynojirimyxine (**3q**) and isofasomine (**3r**). All of the inhibitors analyzed were charged under the assay conditions.⁶⁹

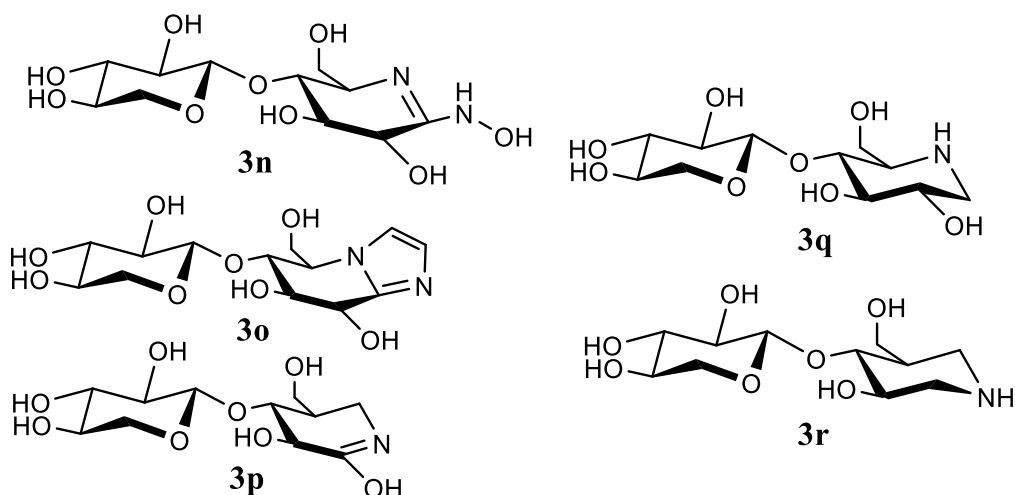
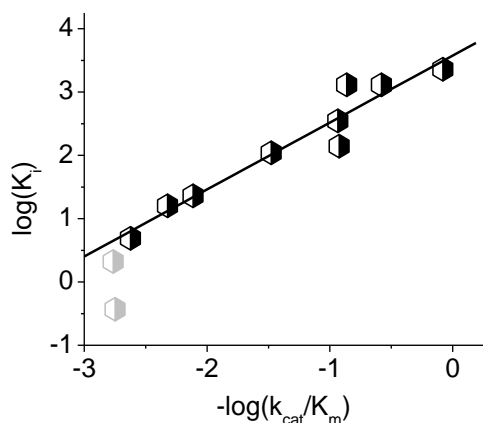


Figure 1.6 Xylobiose based inhibitors of Cex xylanase.

All the inhibitors with sp^2 hybridization of the anomeric carbon had slopes similar to one with the excellent correlations (**3n** **Figure 1.7**, **3o**, and **3p**).^{69, 80} Based on the criteria set out by Bartlett and Lienhard, these three inhibitors are TSAs of the Cex xylanase hydrolysis of substrates.^{69, 78} The two inhibitors with sp^3 -hybridization of the anomeric carbon had a slope very different than one (**3q**- 0.82 ± 0.10) or poor correlation of the free energy plot (**3r**- $R^2=0.74$), **Figure 1.7**.⁶⁹ The isofagomine-based inhibitor's low correlation was attributed to the sp^3 -hybridization at the anomeric carbon atom and the missing hydroxyl group at the C-2 of the gluco-moiety, which is known to be important in binding (See section **1.2 above**).^{17, 69} Up to this point only gluco- and manno- azasugars had been examined as TSAs, with little to no evaluation of how the aglycon interacts during substrate hydrolysis. The research presented here is aimed at filling these gaps.

A



B

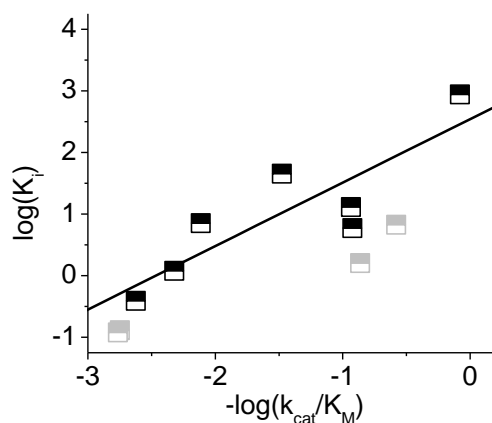
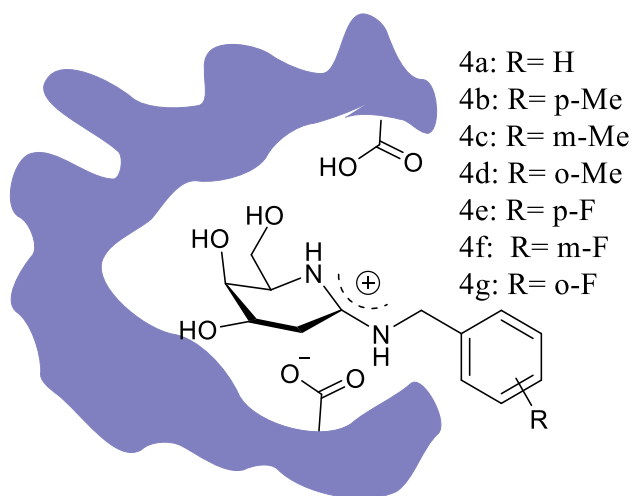


Figure 1.7 Free-energy relationship studies of xylobiose based inhibitors **3n** (A) and **3r** (B) with Cex xylanase.⁶⁹

1.4 Initial evaluations of galactonoamidines

Most of the azasugars developed have only been able to inhibit glycoside hydrolases in the micromolar range with few delving into the high nanomolar range.⁷¹ Previous endeavors to increase the binding affinity of these azasugars have been aimed at addition of electrostatic interactions into the aglycons with and without additional hydrogen bonding groups and addition of hydrophobic groups to the aglycon.⁸¹ The Striegler laboratory endeavored to create galactonoamidines with the ability to inhibit in the nanomolar concentration range.⁸² To accomplish this increase in binding affinity, the above mentioned aliphatic aglycons were incorporated, as well as lengthening of the distance between the glycon and aglycon by addition of a methylene spacer, **Figure 1.8A**.⁸² The seven synthesized N-benzyl galactonoamidines (**4a-g**) were first evaluated in their inhibition ability of β -galactosidase (*A. oryzae*).⁸²

A



B

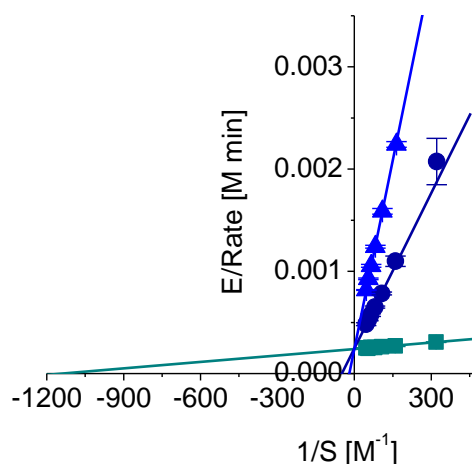


Figure 1.8 (A) Initial seven galactonoamidines synthesized to inhibit hydrolysis of substrate by β -galactosidases.⁸² (B) Lineweaver-Burk plot with **5h** as a model substrate showing competitive inhibition of β -galactosidase (*A. oryzae*) in the absence of inhibitor (cyan), 0.2 μ M **4b** (navy), and 0.5 μ M **4b** (blue).⁸²

The N-benzyl galactonoamidines were able to competitively inhibit the hydrolysis of galactopyranosides by β -galactosidase (*A. oryzae*) in the low nanomolar concentration range (12-48 nM), **Figure 1.8B**.⁸² The low nanomolar inhibition pointed towards the inhibitors being TSA. No other galacto- azasugar had previously been examined as a TSA.⁸³ Rather than performing mutations and having to express and purify multiple proteins, a different method for TSA analysis was employed.⁸³ The analysis consisted of an examination of the hydrolysis of ten structurally related substrates (**Figure 1.9**) through a method developed by Bartlett *et al.*⁷⁸ The binding energy of the TS is compared to the binding energy of the inhibitor similarly to the previously discussed evaluations.⁷⁸ However, prior to this work, only two galactopyranoside substrates were commercially available, **5a** and **5h**. Therefore, substrates **5b-g** and **5i-j** were synthesized by modification of procedures for related compounds developed by Thiem *et al.*^{70 84}

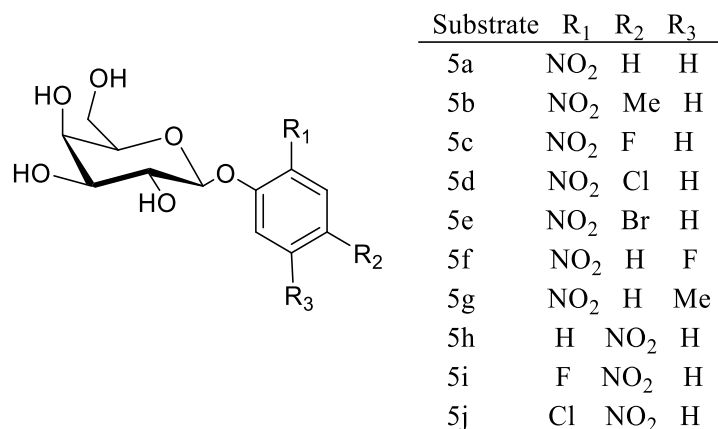


Figure 1.9 Aryl- β -D-galactopyranosides **5a-j** developed as model substrates for β -galactosidase (*A. oryzae*) in evaluation of N-benzylgalactonoamidines as TSAs.⁸³

The initial study of the seven aryl-D-galactonoamidines as a TSA identified a single putative TSA, **4b**,⁸⁵ **Figure 1.10**.⁷⁰ The binding of the *N*-substituted galactonoamidines is strongly affected by stereoelectronic effects at the *para* position of the aromatic ring, observed in the comparison of **4b** and **4e**.⁷⁰ The stereoelectronic effect influences the strength of the inhibitor, as well as its ability to successfully function as a TSA.⁸³ The ability of one (**4b**) of the seven to effectively mimic the TS of the hydrolysis led to the conclusion that the aglycon plays a significant role in the binding of the inhibitor within the active site.⁸³

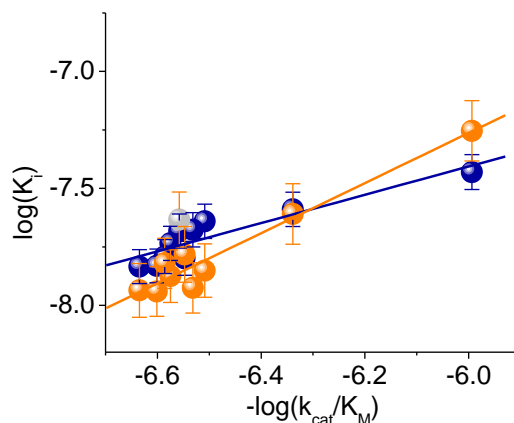


Figure 1.10 Correlation of the binding energy of inhibitor ($\log K_i$), **4a** (navy) and **4b** (orange) to binding energy at the transition state ($-\log k_{\text{cat}}/K_M$) of the hydrolysis of ten galactopyranoside substrates by β -galactosidase (*A. oryzae*).⁸³

The observed importance of the galactonoamidines' aglycon prompted a more in-depth investigation of interactions occurring between the aglycon and the active site of β -galactosidase. Probing of the active site was accomplished with a library of 20 galactonoamidines.⁸⁶ The library was designed to initiate various interactions including: π - π stacking, steric, electronic, hydrophobic, van der Waals interactions, and spacing effects, **Table 1.2**.⁸⁶ The binding affinities of the galactonoamidine library to the β -galactosidase were some of the highest observed prior to this study (6.3-602nM).⁸⁶ The structure activity relationship study showed that the β -galactosidase (*A. oryzae*) was significantly more inhibited with the addition of the methylene spacer to the aglycon as expected due to the bond lengthening during hydrolysis of substrates (K_i **4r** and **4t** << **4p** and **4s**).⁸⁶ The study also showed that hydrophobic interactions with the aglycon were more favorable than π - π interactions (K_i **4s** < **4a**).⁸⁶ These new inhibitors' high binding affinities and diversity make them excellent probes not only for the interactions occurring within the active site of the β -galactosidase (*A. oryzae*), but a host of other glycoside hydrolases. Probing of active sites with these galactonoamidines will lead to increased understanding of the

transition states of the enzymes and interactions that occur to promote the stability of the transition state within the enzyme, allowing for accelerated reactions.

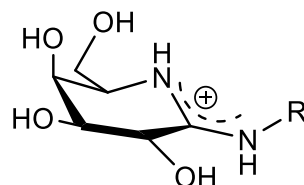
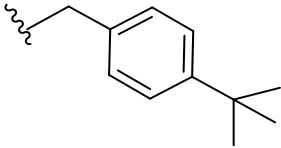
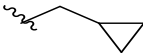
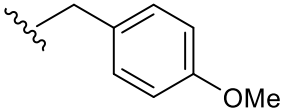
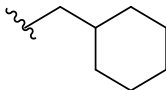
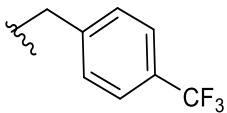
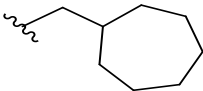


Table 1.2 Inhibition of hydrolysis of 2-chloro-4-nitrophenyl- β -D-galactopyranoside ($k_{\text{cat}} = 2381 \pm 135 \text{ min}^{-1}$ and $K_M = 0.70 \pm 0.1 \text{ mM}$) by β -galactosidase (*A. oryzae*) in the presence of galactonoamidines. 50mM Acetate buffer solution at pH 5.00 ± 0.05 and $30.0 \pm 0.1^\circ\text{C}$.⁶⁷

Compound	Aglycon	K_i [nM] ⁶⁶	Compound	Aglycon	K_i [nM] ⁶⁶
4a		21.1 ± 1.2	4k		149 ± 2
4b		8.0 ± 0.5	4l		10.8 ± 0.7
4c		29.4 ± 5.2	4m		48.4 ± 3.3
4d		23.6 ± 2.4	4n		7.8 ± 1.4
4e		10.1 ± 2.5	4o		8.6 ± 1.2
4f		20.3 ± 2.3	4p		31.9 ± 1.8
4g		16.1 ± 0.3	4q		602 ± 52

Table 1.2 cont'd: Inhibition of hydrolysis of 2-chloro-4-nitrophenyl- β -D-galactopyranoside ($k_{\text{cat}}=2381\pm135\text{min}^{-1}$ and $K_{\text{M}}=0.70\pm0.1\text{mM}$) by β -galactosidase (*A. oryzae*) in the presence of galactonoamidines. 50mM Acetate buffer solution at pH 5.00 ± 0.05 and $30.0\pm0.1^{\circ}\text{C}$.⁶⁷

Compound	Aglycon	K_{i} [nM] ⁶⁶	Compound	Aglycon	K_{i} [nM] ⁶⁶
4h		20.6 ± 2.5	4r		9.5 ± 1.1
4i		17.1 ± 3.4	4s		11.3 ± 0.9
4j		15.7 ± 0.1	4t		6.3 ± 0.6

2 Examination of galactonoamidines with hydrophobic aglycons as putative TSAs for β -galactosidase (*A. oryzae*)

2.1 Introduction:

Evaluations of the transition state are difficult due to its fleeting nature. Thus, transition state analogs (TSAs) are designed to probe the active sites of enzymes in an effort to learn about the transition state.⁸⁷ During the transition state of glycoside hydrolysis, the substrate's aglycon interacts differently than its ground state.^{68, 69} The aglycon orientation and interactions during the transition state requires that bond lengthening be incorporated into a good inhibitor.^{88, 89} Other interactions that occur with the aglycon of the substrates during transition state have not been examined as in depth as the interaction of the glycons. Prior to the previously discussed evaluation of the seven N-benzyl galactonoamidines no TSAs for a β -galactosidase were known.⁷⁰ The subsequent structure activity relationship (SAR) study using the library of galactonoamidines (**4a-t**) revealed that hydrophobic interactions with the aglycon of inhibitors were the most stabilizing interaction in the active site of β -galactosidase (*A. oryzae*).⁹⁰

In the SAR study, six galactonoamidines were determined to have IC₅₀ and inhibition constants (K_i) similar to **4b** (K_i=6-11nM and IC₅₀=12-36nM).⁸⁶ These six galactonoamidines had aglycons with a linear aliphatic heptyl chain (**4l**), a branched aliphatic 2-ethylhexyl group (**4n**), aromatic substituents with extended spacers (**4o**), cyclopropyl (**4r**), cyclohexyl (**4s**) and cycloheptyl groups (**4t**).⁷⁹ Here, we examine these six inhibitors,

Figure 2.1, through linear free energy relationship analysis to determine TSA,^{70, 79} docking analysis,⁷⁹ and molecular modeling.⁷⁹

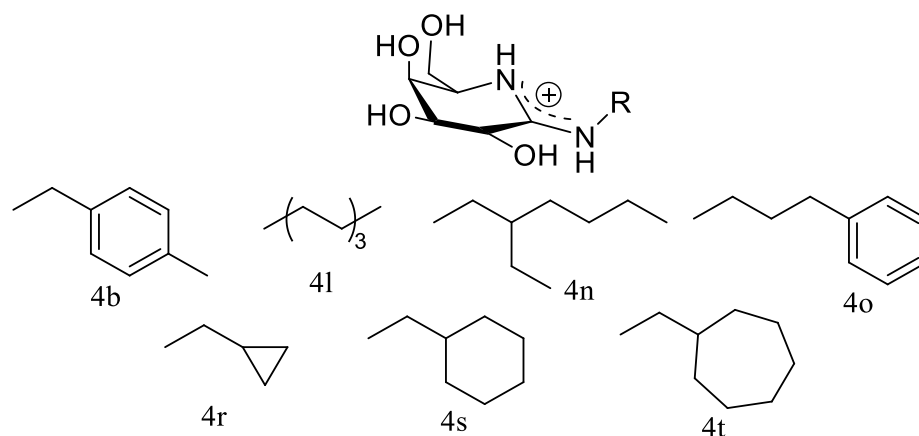


Figure 2.1 Galactonoamidines selected for TSA analysis.⁷⁹

2.2 Results and Discussion:

2.2.1 Docking analysis of galactonoamidines.

Although all of the galactonoamidines are competitive binders of β -galactosidase (*A. oryzae*),⁸² the interactions occurring within the active site had not been established.⁹⁰ Docking analysis with AutoDock Vina was employed to determine the binding of the seven galactonoamidines using the crystal structure available through the protein data bank (4IUG).⁹¹ It was speculated that galactonoamidines bound in a similar manner to **4b** will also be a TSA.⁷⁹ Therefore, the binding of galactonoamidines (**4l-o**, and **4r-s**) were compared to the binding of **4b**.⁷⁹

All of the inhibitors' glycons bound within the active site in a similar manner (deviation of $> 0.5\text{\AA}$ for all non-hydrogen atoms in the glycon), **Table 7.1**; however, deviations were seen in the aglycon position within the active site.⁷⁹ Two inhibitors, **4o** and **4s**, had very little deviation from **4b**'s position within the active site (less than 30° rotation of the aglycon), **Figure 2.2A** and **B**.⁷⁹ Inhibitors **4n**, **4r**, and **4t** showed greater deviation of the aglycon position from that of **4b** (82° , 76° , and 115° respectively), **Figure 2.2C-E**.⁷⁹ The final inhibitor **4l** showed the most deviation from **4b** (120°) and thus was excluded from further study **Figure 2.2F**.⁷⁹

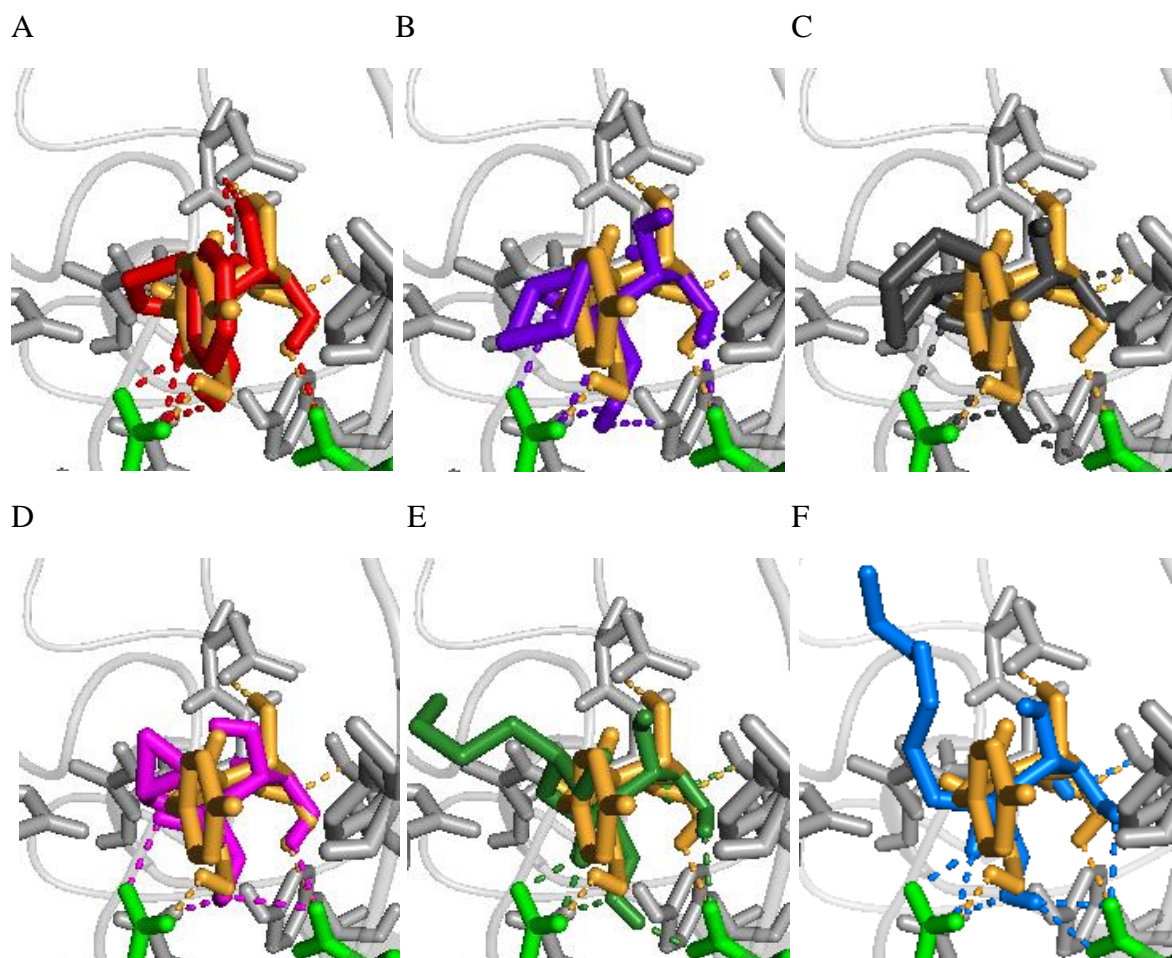


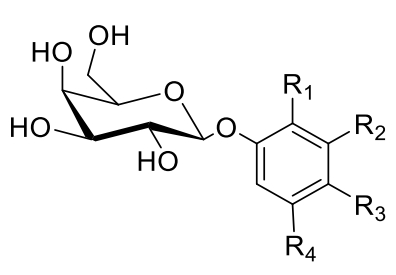
Figure 2.2 Galactonoamidines (**4l-o**, **4r-t**) docked within the active site of β -galactosidase (*A. oryzae*) with the catalytically active residues shown in green. The galactonoamidines are overlaid with the know TSA (**4b**): (A) **4o** (red), (B) **4s** (purple), **4t** (grey), **4r** (pink), **4n** (olive), and **4l** (blue).⁷⁹

2.2.2 Linear Free Energy Relationship Analysis

The five remaining galactonoamidines (**4n-o**, **4r-t**) were then examined as TSAs by employing the linear free energy relationship method developed by Bartlett.⁷⁸ In short, the hydrolysis of a library of substrates (**5a-j**, **Table 2.1**) in the presence and absence of inhibitors is observed spectroscopically.⁷⁰ The inhibition constants of each inhibitor with the nine substrates were determined by the average of independent experiments with at least three concentrations of inhibitor ranging from 0.25-1 μ M, **Table 2.1**.⁷⁹ Then, the relationship of inhibition constant (K_i)

to the catalytic efficacy (k_{cat}/K_M) is determined.⁷⁹ For the inhibitor to be a TSA, the slope of the linear free energy relationship and the correlation factor of the line must be near to 1.⁷⁸ Any deviation from this criteria shows that the inhibitor is not a TSA, rather just an opportunistic binder within the active site of the β -galactosidase (*A. oryzae*).⁷⁹

Table 2.1 Model Substrates for TSA analysis with β -galactosidases.⁷⁹



Entry	S	R ₁	R ₂	R ₃	R ₄
1	5a	NO ₂	H	H	H
2	5b	NO ₂	H	Me	H
3	5c	NO ₂	H	F	H
4	5d	NO ₂	H	Cl	H
5	5f	NO ₂	H	H	F
6	5g	NO ₂	H	H	Me
7	5h	H	H	NO ₂	H
8	5i	F	H	NO ₂	H
9	5j	Cl	H	NO ₂	H

The galactonoamidines were all able to inhibit the hydrolysis of the model substrates with nanomolar inhibition constants (6-170nM), **Table 2.2**.⁷⁹ However, only two of the five galactonoamidines (**4o** and **4s**) have a correlation of the inhibition constants to the catalytic efficiency near 1, along with a R^2 near 1(**Figure 2.3A**).⁷⁹ The slope of the free energy relationship of the galactonoamidines with the branched linear aglycon (**4n**) and cycloheptyl aglycons (**4t**) were within error of 1; however, the correlation factor for the fit these data is very poor (0.83 and 0.69 respectively), **Figure 2.3**.⁷⁹ The correlation of the data obtained for **4r** resulted in scattered data ($R^2=0.46$) and a slope very different than 1.⁷⁹

Table 2.2 Galactonoamidine inhibition of hydrolysis of 9 nitrophenyl- β -D-galactopyranosides by β -galactosidase (*A. oryzae*); 50 mM acetate buffer solution at pH 5.00 \pm 0.05 and 30.0 \pm 0.1 $^{\circ}$ C.⁷⁹

S	$k_{cat}/K_M \times 10^6$ [min ⁻¹][M ⁻¹] ⁹²	K _i [nM] 4n	K _i [nM] 4o	K _i [nM] 4r	K _i [nM] 4s	K _i [nM] 4t
5a	3.61	28.6 \pm 0.5	17.4 \pm 0.6	35.8 \pm 2.7	24.2 \pm 1.2	30.4 \pm 2.3
5b	3.23	20.8 \pm 5.3	11.1 \pm 0.1	37.9 \pm 2.0	20.3 \pm 1.3	42.8 \pm 0.9
5c	3.76	31.9 \pm 0.8	13.5 \pm 0.1	29.7 \pm 1.4	20.5 \pm 0.1	13.3 \pm 3.3
5d	4.31	26.5 \pm 0.6	11.8 \pm 0.1	14.6 \pm 0.1	20.1 \pm 4.5	39.2 \pm 3.2
5f	2.18	81.5 \pm 2.8	21.2 \pm 1.8	30.6 \pm 0.4	35.5 \pm 1.1	135 \pm 12
5g	9.86	145 \pm 0.7	60.7 \pm 2.0	64.9 \pm 1.6	87.5 \pm 3.2	168 \pm 1.9
5h	3.85	40.2 \pm 1.4	15.7 \pm 1.4	35.2 \pm 0.6	16.2 \pm 0.1	61.8 \pm 2.6
5i	3.99	36.7 \pm 0.2	14.2 \pm 2.3	51.5 \pm 4.0	18.7 \pm 1.5	40.6 \pm 1.0
5j	3.59 ⁸⁶	7.8 \pm 1.4 ⁸⁶	8.6 \pm 1.2 ⁸⁶	9.5 \pm 1.1 ⁸⁶	11.3 \pm 0.9 ⁸⁶	6.3 \pm 0.6 ⁸⁶

These spectroscopic evaluations revealed only two galactonoamidines (**4o** and **4s**) met the criteria to be TSA.⁷⁹ The two new TSAs (**4o** and **4s**) had the least deviation from the binding orientation of previously determined TSA (**4b**) in the molecular docking studies (section **2.2.1**).⁷⁹ These three inhibitors (**4b**, **4o**, and **4s**) are in better orientation to interact with residues that form a tunnel-like hydrophobic region at the rim of the active site than the other inhibitors (**4n**, **4r**, and **4t**).⁷⁹ In order to understand why only two of the five inhibitors were TSA, the protein-inhibitor complexes were examined by molecular dynamics.⁷⁹

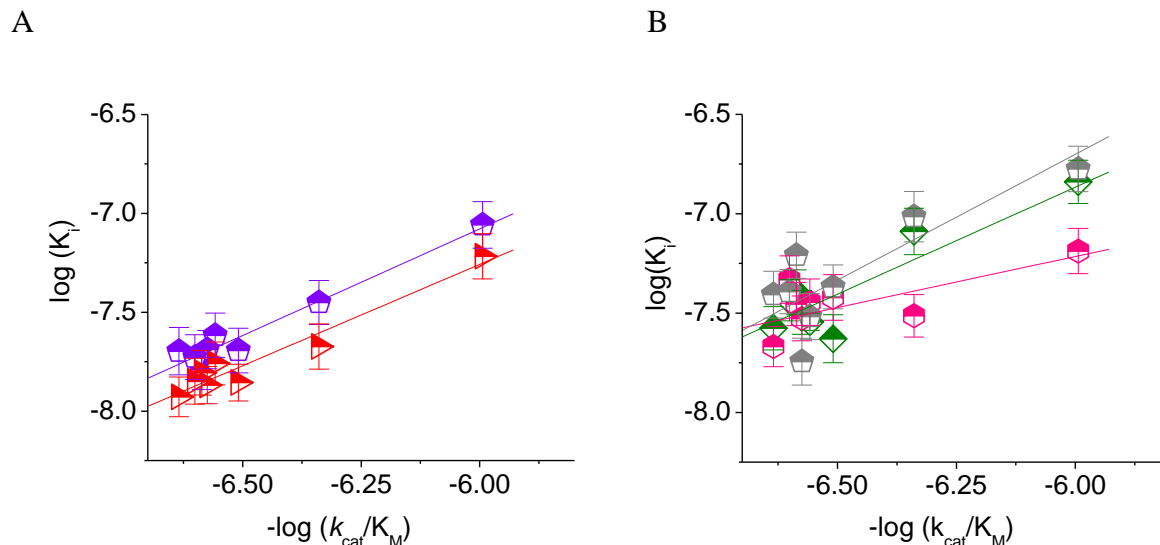


Figure 2.3 Double-logarithmic correlation of catalytic efficiency (k_{cat}/K_M) and the inhibition constant (K_i) with linear fit $y = ax + b$ for the 9 nitrophenyl- β -D-galactopyranosides in the presence of (A); (**4o**) (red triangle) $a = 1.02 \pm 0.10$, $R^2 = 0.93$; (**4s**) (purple pentagon) $a = 1.08 \pm 0.10$, $R^2 = 0.95$; and (B) (**4n**) (green diamond) $a = 1.16 \pm 0.21$, $R^2 = 0.83$; (**4r**) (pink hexagon) $a = 0.44 \pm 0.19$, $R^2 = 0.46$; (**4t**) (grey pentagon) $a = 1.17 \pm 0.32$, $R^2 = 0.69$.⁷⁹

2.2.3 Molecular dynamic evaluation of galactonoamidine-protein complexes

Complexes of galactonoamidines and β -galactosidase from *A. oryzae* (PDB ID 4IUG) were built from the lowest energy conformation determined by AutoDock Vina using the GROMOS 96-43A1 model in GROMACS.^{79, 91} The hydrogen bonding interactions of the glycon and interactions of the aglycon and the surrounding residues were evaluated over 30 ns of molecular dynamics.⁷⁹ First, the hydrogen bonding interactions of the inhibitors with all residues within the active site were examined, **Figure 2.4A**.⁷⁹ This showed that **4r** and **4t** had the least number of hydrogen bonds to residues within the active site.⁷⁹ The field was then narrowed to the two catalytic residues, Glu200 (proton donor) and Glu298 (nucleophile).⁷⁹ All galactonoamidines showed high occurrence of hydrogen bonding interactions with the nucleophile.⁷⁹ However, **4n** and **4r** showed very little interaction with the proton donor, **Figure 2.4B**.⁷⁹ This observation is

similar to previous indications that suggested the need of an inhibitor to interact with both catalytic residues to be considered a TSA.⁹³ The orientation of the **4b**, **4o**, and **4s** remained near identical throughout the simulation ($\text{RMSD} \leq 0.65\text{\AA}$), while the galactonoamidines that were not TSA (**4n**, **4r**, and **4t**) were much different ($\text{RMSD} \leq 2.26\text{\AA}$).⁷⁹ The similar orientations and high probability of hydrogen bonding interactions with catalytic residues reveal that the TSAs are stabilized differently in the active site than the non-TSAs.⁷⁹

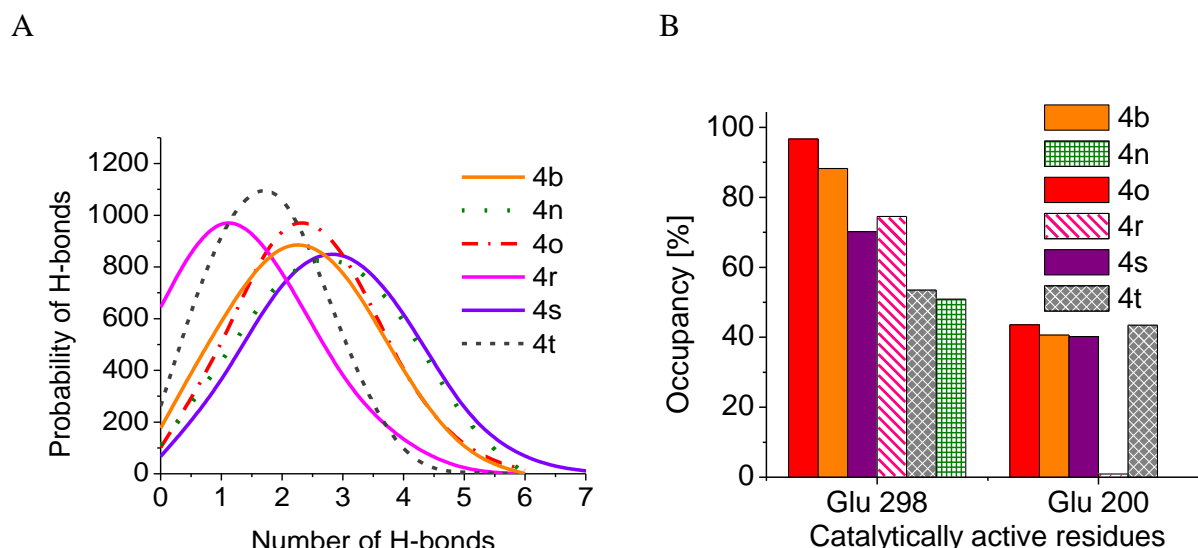


Figure 2.4 (A) Frequency of hydrogen bonding interactions in correlation to the number of hydrogen bonding of galactonoamidines with β -galactosidase (*A. oryzae*). (B) Occupancy of the catalytic residues throughout the 30ns simulations with galactonoamidines.⁷⁹

After the glycon interactions were examined, focus shifted to establishing what interactions were occurring with the aglycon throughout the simulations.⁷⁹ Along these lines, special attention was paid to the interactions with the hydrophobic residues surrounding the active site (Ala237, Pro261, Lue262, Phe264, Phe278, Phe281, Ala301, Ala303, Phe304, Ala317, Val391, Met343, and Trp806).⁷⁹ These hydrophobic residues make up a hydrophobic tunnel leading towards the active site.⁷⁹ The *p*-methyl substituent of the aglycon of **4b** is oriented towards

Ala237, Pro261, Lue262, Phe264, Pro278 and Phe281 within acceptable distance for hydrophobic interactions.⁷⁹ The propylene spacer of **4o**'s aglycon allows for interactions with the same residues as well as Ala301, Ala303, Phe304, Ala317, Val319, Met343, and Trp806.⁷⁹ The ability of the three TSAs to interact with these hydrophobic residues is due to small conformational changes in the loops surrounding the active site that orient the residues in a way that promotes interaction with the aglycons. These orientation shifts of the hydrophobic tunnel are also seen in **4s**.⁷⁹ The rearrangement of the hydrophobic residues surrounding the aglycons of the TSAs result in an overall conformational change of the active site of β -galactosidase (*A. oryzae*) which stabilizes the TSAs within the active site.⁷⁹ This change in active site conformation is not observed in molecular dynamics with an unbound β -galactosidase (*A. oryzae*), nor when bound to the opportunistic binders (**4n**, **4r**, and **4t**), **Figure 2.5**.⁷⁹

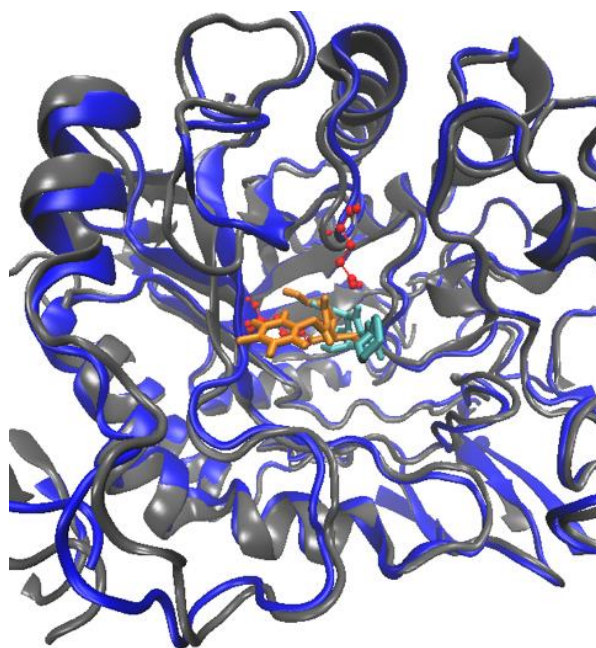


Figure 2.5 Overlay of the molecular dynamics simulations of β -galactosidase from *A. oryzae* (dark grey) with **4b** (orange) and β -galactosidase from *A. oryzae* (blue) with **4t** (cyan). Catalytic residues are shown as ball and stick (red).⁷⁹

2.3 Conclusion

Galactonoamidines **4b**, **4o**, and **4s** have been spectroscopically determined to be TSAs and show similar interactions through docking and molecular dynamics simulations that account for their ability to accurately mimic the transition state.⁷⁹ The TSAs' glycons and aglycons interact within the active site with similar orientation, whereas galactonoamidines **4n**, **4r**, and **4t** are not in the same orientation within the active site, **Figure 2.5**.⁷⁹ The strong interactions with the catalytic residues, as well as a conformational change when binding to a TSAs **4b**, **4o**, and **4s**, allow for sustained interactions with the hydrophobic tunnel surrounding the active site.⁷⁹ In contrast, galactonoamidines **4n**, **4r**, and **4t** lack interaction with the catalytic residues and the conformation change upon binding.⁷⁹ This difference in binding interactions and orientation differences account for these three inhibitors being classified as opportunistic binders within the active site of β -galactosidase (*A. oryzae*) and not true TSA.⁷⁹

2.4 Materials and Methods

2.4.1 Instrumentation

UV/Vis data were collected on a FilterMax F5 Multi-Mode Microplate Reader from Molecular Devices using a 96-well medium-binding microton ELISA-plate from Greiner Bio-one.⁷⁹ A Φ 250 pH meter (Beckman) with a refillable ROSS combination pH electrode (Orion) with an epoxy body and an 8mm semi-micro tip. Prior to each use, the pH meter was calibrated using standard buffers (4.00, 7.00, and 10.01) purchased from VWR.⁷⁹ All water used was Nanopure water at a resistance of 18.2 M Ω cm was obtained from a ThermoScientific Barnstead E-pureTM purification system.⁷⁹ All compounds were weighed on either an AB135-S Classic Balance (Mettler Toledo) or a M-120 Balance (Denver Scientific). All molecular dynamics simulations were performed in the Arkansas High-Performance Computation Center.⁷⁹

2.4.2 Materials

Acetic acid (99.7% purity) was purchased from VWR. Sodium hydroxide (99.999% purity) and β -galactosidase (*A. oryzae*) were obtained from Sigma-Aldrich.⁸² The β -galactosidase was received as a lyophilized powder, which was stabilized with dextran, and stored at -18°C until use.⁸² The protein content was previously determined to be 10%.⁸² The molecular weight was determined to be 86,800 g/mol⁻¹ by microchip electrophoresis.⁸² The synthesis of the galactonoamidines and nitrophenyl β -D-galactopyranoside substrates were described previously.^{94, 95} Gibson P-200, P-1000, and SL10 pipettes or a multichannel FinnPipette F2 (Thermo Scientific) were used to for dilutions and addition of compounds into 96-Well plates. All solutions were prepared using 5mL, 10mL, 20mL, or 500mL volumetric flasks (Duran).

2.4.3 Spectroscopic Evaluation of galactonoamidines

2.4.3.1 Acetate Buffer solution

A 500mL aliquot of 50mM Acetate buffer solution was prepared at ambient temperature for use at 30°C by standard methods. The buffer solution was stored at ambient temperature and discarded if not used within 10 days.⁷⁹

2.4.3.2 Stock solutions of β -galactosidase (*A. oryzae*)

A typical stock solution was prepared by dissolving 4.5 mg of lyophilized β -galactosidase from *A. oryzae* in 5mL of the buffer solution.⁷⁹ A 518nM enzyme stock solution was obtained by dilution of a 500 μ L aliquot to 10mL of buffer solution in a volumetric flask.⁷⁹

2.4.3.3 *Stock solutions of galactonoamidine inhibitors*

Typically, a 1.0mM stock solution of galactonoamidine inhibitor was serially diluted to 0.25, 0.50, 0.75, and 1.0mM with nanopure water in 5mL volumetric flasks.⁷⁹ The four stock solutions were kept at ambient temperature until use.⁷⁹

2.4.3.4 *Stock solutions of nitrophenyl β -D- galactopyranosides:*

A typical stock solution was prepared by dissolving 7-11mg of a nitrophenyl β -D- galactopyranoside (**5a-d** and **5f-j**) in 5mL of acetate buffer solution.⁷⁹ These solutions were used within four hours of preparation and kept at ambient temperature.⁷⁹

2.4.3.5 *Kinetic assay*

A 0-70 μ L aliquot of the substrate stock solution was added in increasing 10 μ L increments in a 96-well plate.⁷⁹ Stock solutions of inhibitor were added in constant 10 μ L aliquots and the appropriate amount of buffer solution was then added to maintain 80 μ L in each well.⁷⁹ The plate solutions were equilibrated to 30°C then a 20 μ L aliquot of the stock solution of enzyme was added to the wells.⁷⁹ The product formation was observed at a wavelength of 405nm by change in absorbance over 15min in 27s intervals, for a total of 34 cycles.⁷⁹

2.4.3.6 *Data Analysis*

The formation of product, nitrophenylate, was determined by absorbance at a wavelength of 405nm using previously determined apparent extinction coefficients.⁸³ A linear regression of the change in product concentration overtime gave the initial rate of hydrolysis.⁷⁹ These data were then corrected for enzyme concentration by dividing by the concentration of enzyme in the well, then the data were averaged for the triplicated samples.⁷⁹ This average product formation per minute was then plotted as a function of substrate concentration.⁷⁹ A non-linear regression fitting

was performed to determine the catalytic activity and apparent catalytic activity (k_{cat} and k_{cat}') and the Michaelis constant and apparent Michaelis constant (K_m and K_m'). The inhibition constant (K_i) was determined by the following equation:⁷⁹

$$K_i = \frac{[I]K_m}{K_m' - K_m} \quad \text{Eq 1}$$

All kinetic parameters were determined in triplicate. The inhibition constants were determined by averaging the data obtained by 3-4 different inhibitor concentrations.⁷⁹

2.4.4 Docking Analysis

The PDB coordinates of β -galactosidase (*A. oryzae*) were obtained from the Protein Data Bank (PDB ID 4IUG).⁹⁶ All water and solvent molecules and substrates were removed from the structure. The pdb coordinate file was converted to pdbqt files using PMV-1.5.6 software.⁹⁷ Using AutoDock Vina Tools, Kollman partial charges were added to all atoms and all polar hydrogens added to all residues.⁹⁸ Structures of galactonoamidines were energy minimized using MM2 force field and converted to a pdb coordinate file using PYMOL.⁷⁹ The coordinate files were converted to pdbqt coordinate files with all non-ring bonds rotatable.⁷⁹ A 30x30x30 Å³ grid box was centered in the active site of the β -galactosidase.⁷⁹ All parameters for docking analysis were set to default of AutoDock Vina 1.1.2 Software with the exception of exhaustiveness, which was set to 100.⁷⁹ The software yielded nine inhibitor conformations that were ranked based on the binding score in kcal/mol.⁷⁹ The inhibitor conformation with the lowest binding score was used as an enzyme-inhibitor complex and analyzed for hydrogen bonding interactions.⁷⁹

2.4.5 Molecular dynamics analysis:

All molecular dynamic simulations of galactonoamidines and β -galactosidase (*A. oryzae*) assemblies were carried out with GROMACS 4.6.7 software employing the GROMOS96 43A1 force field.⁹⁹ The pdb coordinate file of β -galactosidase (*A. oryzae*) prepared in docking section was converted to a GROMACS coordinate and topology file using pdb2gmX program.¹⁰⁰ The pdb coordinate file of the lowest energy conformation of each galactonoamidine from docking, were imported into PRODRG, a free software.¹⁰¹ Topology and coordinate files were generated by maintaining chirality and defining partial charges on all atoms of the galactonoamidine as GROMOS96 43a1 force field.^{101, 102} The energy minimization function was not employed to keep the lowest energy conformation determined by docking analysis.⁷⁹ The galactonoamidine topology file was corrected for partial charge on all atoms within the galactonoamidines and all charge groups were reduced atoms to 3-4 atoms per group.⁷⁹ The corrections were accomplished with guidance from a study conducted Lemkul *et al.*¹⁰³

A protein-inhibitor complex was created by appending the edited topology and the coordinates files of the galactonoamidine to the coordinate and topology files of the β -galactosidase.⁷⁹ This protein-inhibitor complex was then centered in a 2389.39nm³ cubic box and solvated with 75,211-75,214 water molecules using the simple point charge model (SPC).¹⁰⁴ Next, the system was neutralized by replacing random water molecules with 28 sodium cations.⁷⁹ Systems were then equilibrated to less than 1000kJ/mol using the steepest-decent method. An NVT simulation using a stochastic scaling thermostat was conducted over 100ps at experimental conditions of 303K. This was followed by a NPT simulation at 1 bar over 500ps.¹⁰⁵ A 1ns stability NPT simulation was performed on the system followed by a 30ns NPT. The last 30ns of NPT were treated as the production.⁷⁹

The following constraints were placed on the system during production which allowed for an integration time step of 2fs.⁷⁹ Coulomb interactions were calculated to 12Å of each atom,¹⁰⁶ outside of this distance a particle-mesh Ewald summation was employed with a spacing of 13Å and a fourth-order-B-spline interpolation,¹⁰⁷ a Verlet scheme was used to cut off London-Jones interactions,¹⁰⁸ and LINCS was used to constrain bond lengths.¹⁰⁹ The temperature was maintained using Nosé-Hoover coupling with a time constant of 2ps and the pressure was maintained with a Parrinello-Rahman coupling with a time constant of 5ps.^{110 111} The H-bond plugin in the Visual Molecular Dynamics (VMD) was implemented to determine the number of hydrogen bonds with a donor-acceptor cut-off distance of 3.0Å and a donor-H atom-acceptor 20°.^{79, 112}

3 Exploration of the active site of β -galactosidase (bovine liver) reveals loop closure over active site

3.1 Introduction

Glycoside hydrolases (GH) have been categorized into multiple families based on their mechanism, evolutionary relationship, structure, and sequence.¹⁹ These similarities in the enzymes' active sites led to speculation that multiple glycoside hydrolases will stabilize their transition states with similar interactions.⁹⁰ Since examining the transition state itself is not within reason, the interactions with a transition state analog (TSA) and residues within the active site are examined instead.⁹⁰ Along these lines, examination of another β -galactosidase from the same family as β -galactosidase (*A. oryzae*) was desired.⁹⁰ Two potential enzymes from GH family 35 were β -galactosidase from humans and β -galactosidase from bovine liver.^{19, 23} The β -galactosidase from bovine liver was determined to be the best candidate to examine the interactions because of its commercial availability, previous studies with similar inhibitors by others,^{44, 71} and similarities within the active site to the β -galactosidase (*A. oryzae*), **Figure 3.1**.⁹⁰

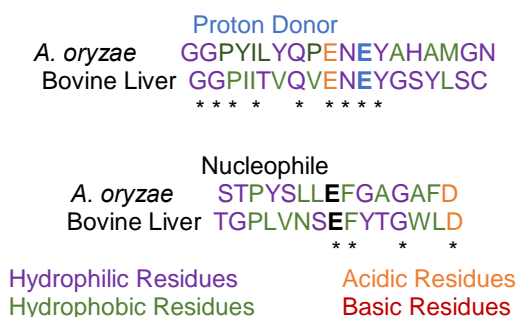


Figure 3.1 Sequence similarities of β -galactosidases from *A. oryzae* and bovine liver surrounding the two catalytically active residues.¹¹³

Though the crystal structure for the β -galactosidase (bovine liver) is currently unknown,⁹⁰ previous inhibition studies led to speculation that the binding domain has a separate binding area

for the glycon and aglycon, **Figure 3.2.**⁵³ Based on this speculation, the active site will be examined with the previously discussed galactonoamidines, three derivatives of a TSA, and two similar inhibitors lacking an aglycon. Spectroscopic evaluations and homology templating have been previously used to explore active sites of enzymes that lack a crystal structure.¹¹⁴⁻¹¹⁷ Though predicting a model for an enzyme by homology templating is a difficult task, multiple state-of-the-art programs for calculating models and ensuring the model is accurate and of high quality are available.¹¹⁸⁻¹²³ With the software and a library of 25 galactonoamidines and their derivatives on hand, we set out to explore the active site of β -galactosidase (bovine liver) using Michaelis-Menten kinetics,⁸⁶ transition state analog (TSA) studies,⁷⁰ and molecular dynamics.⁹⁰ The spectroscopic evaluations showed drastic differences in binding affinities compared to those observed with β -galactosidase (*A. oryzae*), which are attributed to a loop closure over the active site of β -galactosidase (bovine liver).⁹⁰

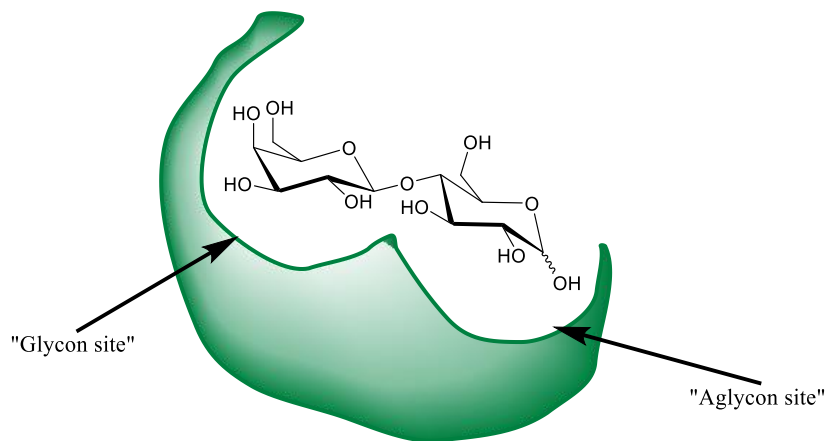


Figure 3.2 Predicted active site of β -galactosidase from bovine liver.¹²⁴

3.2 Results and Discussion

3.2.1 Spectroscopic evaluations

Initially, a structure activity relationship (SAR) study was performed with the various galactonoamidines previously synthesized along with galactonoamidines with derivatives at the glycon.^{56, 86} Kinetic evaluations for the SAR study were performed using the Michaelis-Menten model for enzyme kinetics in the presence and absence of galactonoamidines (**4a-y**).^{86, 90} All inhibitors were determined to be competitive inhibitors of β -galactosidase (bovine liver), **Figure 3.3**.⁹⁰ We expected to see similar inhibition constants to those observed in the SAR evaluation of β -galactosidase (*A. oryzae*) because of the sequence similarities leading to the enzymes being classified in the same GH family.¹⁹ However, the affinities of inhibitors show an astounding increase of about two orders of magnitude towards the β -galactosidase (bovine liver) (0.05-2.34nM) than those observed with β -galactosidase from *A. oryzae* (K_i = 6.3-604nM), **Table 3.1**.^{86, 90} The drastic affinity difference revealed that the β -galactosidase (bovine liver) active site was able to stabilize the galactonoamidines better than the β -galactosidase (*A. oryzae*).⁹⁰

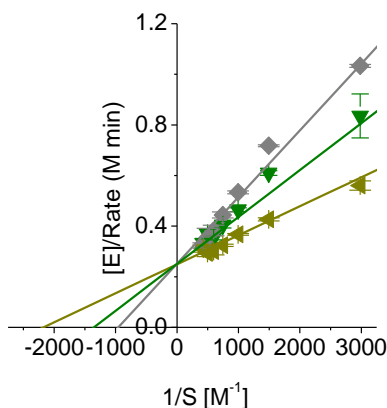


Figure 3.3 Lineweaver-Burk plot of the hydrolysis of model substrate by β -galactosidase (bovine liver) in the presence of 0nM (grey triangle), 0.05nM (green triangle) **4b**, and 0.1nM (olive triangle) **4b**.⁹⁰

Moreover, a clear preference for galactonoamidines with an aglycon promoting π - π interactions were observed within the active site of β -galactosidase from bovine liver (Ki **4a** 0.05nM < **4n** 0.18nM).⁹⁰ Unlike the β -galactosidase (*A. oryzae*),⁸⁶ the β -galactosidase (bovine liver) bound the 1-,2-, and 3-fluoro-N-benzylgalactonoamidines (**4e-g**) with far less affinity than that of the unsubstituted N-benzylgalactonoamdine (**4a**), with inhibition constants of 0.13-0.23nM compared to 0.05nM.⁹⁰ The addition of the electron-withdrawing groups to the benzyl aglycon in **4e-g** reduces the ability of these inhibitors to form π - π interactions within the active site and thus results in a lower binding affinity than **4a**.⁹⁰ Though **4s** cannot have π - π interactions, it still binds with a similar affinity to the N-benzylgalactonoamidines (**4a-b**); it is possible that this inhibitor forms a CH- π bond with an amino acid within the active site similar to the suspected π - π bonds of **4a-b** and **4o**.⁹⁰ The size of the inhibitor also seems to be more critical for binding within the active site of β -galactosidase (bovine liver) than β -galactosidase (*A. oryzae*).^{86, 90} The inhibitors with small aglycons, **4k** and **4p-r**, have much weaker binding affinities than **4a** (0.32-2.34nM >0.05nM). This reduction in binding is likely due to a combination of bad fitting in the “aglycon binding site” and the lack of any π - π interactions.⁹⁰

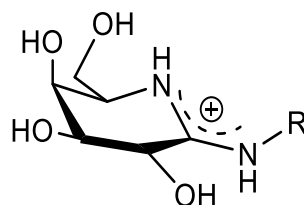


Table 3.1 Inhibition of hydrolysis of 4-nitrophenyl- β -D-galactopyranoside ($k_{\text{cat}} = 4.24 \pm 0.26 \text{ min}^{-1}$ and $K_M = 0.51 \pm 0.01 \text{ mM}$) by β -galactosidase (bovine liver) in the presence of galactonoamidines. 5mM HEPES buffer solution at pH 7.50 ± 0.05 and $30.0 \pm 0.1^\circ\text{C}$.⁹⁰

Compound	Aglycon	K_i [nM]	IC_{50} [nM]	Compound	Aglycon	K_i [nM]	IC_{50} [nM]
4a		0.05 ± 0.01	18.9	4k		0.32 ± 0.02	1030
4b		0.07 ± 0.01	57.6	4l		0.11 ± 0.01	24.1
4c		0.11 ± 0.01	16.2	4m		0.24 ± 0.03	42.7
4d		0.20 ± 0.02	118	4n		0.18 ± 0.02	21.6
4e		0.19 ± 0.02	9.1	4o		0.06 ± 0.01	41.3
4f		0.13 ± 0.02	9.4	4p		0.32 ± 0.02	>1000
4g		0.23 ± 0.01	43.1	4q		2.34 ± 0.30	>1000

Table 3.1 Cont'd: Inhibition of hydrolysis of 4-nitrophenyl- β -D-galactopyranoside ($k_{\text{cat}} = 4.24 \pm 0.26 \text{ min}^{-1}$ and $K_M = 0.51 \pm 0.01 \text{ mM}$) by β -galactosidase (bovine liver) in the presence of galactonoamidines. 5mM HEPES buffer solution at pH 7.50 ± 0.05 and $30.0 \pm 0.1^\circ\text{C}$.

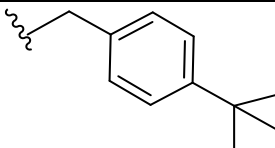
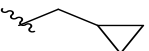
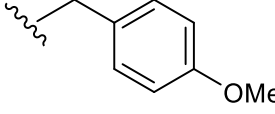
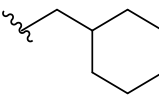
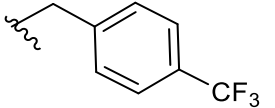
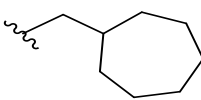
Compound	Aglycon	K_i [nM]	IC_{50} [nM]	Compound	Aglycon	K_i [nM]	IC_{50} [nM]
4h		0.11 ± 0.01	412	4r		0.39 ± 0.07	>1000
4i		0.12 ± 0.01	26.2	4s		0.08 ± 0.01	11.6
4j		0.16 ± 0.01	15.2	4t		0.16 ± 0.03	45.4

Table 3.2 Galactonoamidine inhibition of hydrolysis of 8 nitrophenyl- β -D-galactopyranosides by β -galactosidase (Bovine Liver); 5mM HEPES buffer solution at pH 7.50 ± 0.05 and $30.0 \pm 0.1^\circ\text{C}$.

Entry	S	k_{cat} [min ⁻¹]	K_M [mM]	K_i [pM] 4a	K_i [pM] 4b	K_i [pM] 4o	K_i [pM] 4s
1	5a	4.53 ± 0.46	0.55 ± 0.18	70 ± 2	148 ± 2	250 ± 8	378 ± 48
2	5b	5.29 ± 0.20	0.29 ± 0.07	77 ± 8	110 ± 2	198 ± 9	138 ± 11
3	5c	8.43 ± 0.89	0.72 ± 0.24	62 ± 9	143 ± 22	174 ± 4	524 ± 48
4	5d	20.4 ± 1.7	0.39 ± 0.11	8.6 ± 0.3	26 ± 3	49 ± 5	44 ± 3
5	5f	7.07 ± 0.85	1.58 ± 0.41	132 ± 3	424 ± 13	279 ± 13	516 ± 32
6	5h	4.24 ± 0.26	0.51 ± 0.10	46 ± 2	71 ± 6	60 ± 11	81 ± 5
7	5i	6.82 ± 0.38	0.47 ± 0.09	60 ± 7	121 ± 5	357 ± 6	299 ± 32
8	5j	7.27 ± 0.40	0.48 ± 0.10	58 ± 6	78 ± 9	266 ± 42	349 ± 42

Remarkably, the four inhibitors (**4a**, **4b**, **4o**, and **4s**) with the lowest K_i and IC_{50} values (K_i 50-80pM and IC_{50} 18-59nM) were some of those observed to have the lowest binding affinities with β -galactosidase (*A. oryzae*).^{86, 90} Of these, three (**4b**, **4o**, and **4s**) had previously been determined to be TSAs of the hydrolysis of galactosides by β -galactosidase (*A. oryzae*).⁷⁹ Thus, the four inhibitors were examined as potential TSAs of the hydrolysis of galactosides by β -galactosidase (bovine liver) using the method developed by Bartlett,⁷⁸ **Table 3.2**. Galactonoamidines **4a** and **4b** were found to be TSAs, whereas **4o** and **4s** were determined to be opportunistic binders, **Figure 3.4**. These results show the need for π - π interactions in the active site with the aglycon of the inhibitors to be classified as a TSA. It is probable that there is a conserved tryptophan in the “aglycon binding site” similar to those observed in other glycoside hydrolases.^{6, 128, 129}

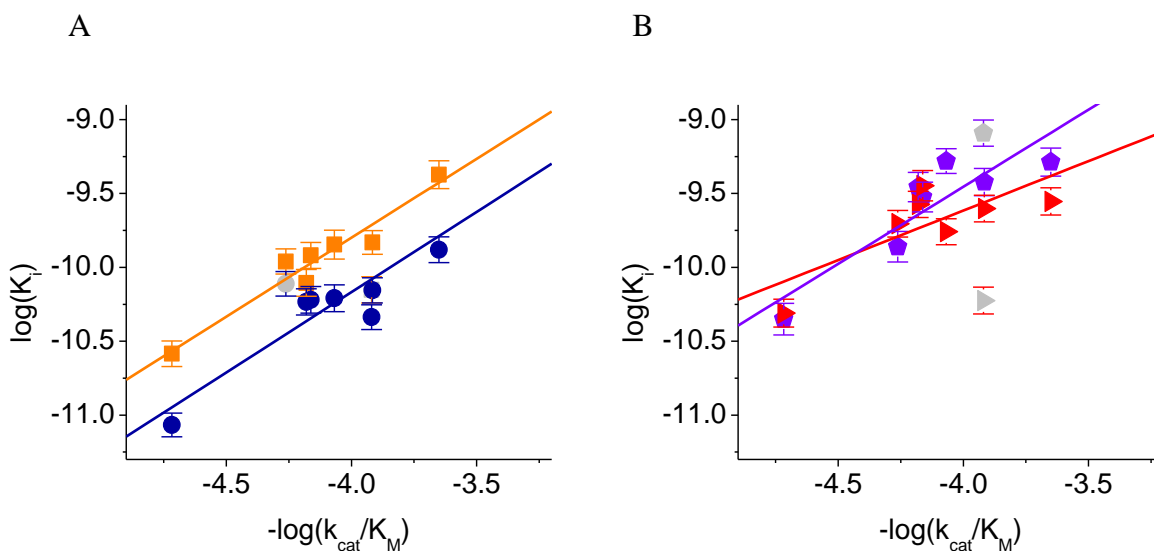
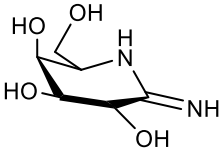
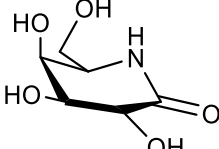
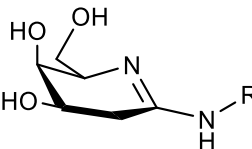
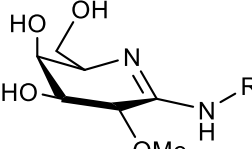
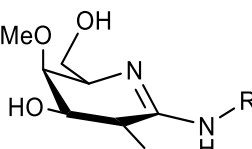


Figure 3.4 Double-logarithmic correlation of catalytic efficiency (k_{cat}/K_M) and the inhibition constant (K_i) with linear fit $y = ax + b$ for the 8 nitrophenyl- β -D-galactopyranosides in the presence of (A) (**4a**) (navy circle) $a = 1.08 \pm 0.15$, $R^2 = 0.92$; (**4b**) (orange square) $a = 1.06 \pm 0.11$, $R^2 = 0.95$; and (B) (**4o**) (red triangle) $a = 0.66 \pm 0.24$, $R^2 = 0.60$; (**4s**) (purple pentagon) $a = 1.07 \pm 0.23$, $R^2 = 0.87$.

After determining that **4b** was a TSA, this inhibitor was used as a parent molecule to design inhibitors with derivatizations at the glycon, **Table 3.3**.⁹⁰ Similar inhibitors that lacked aglycons were also employed to study the effect of the aglycon (**4u** and **4v**).^{86, 90} Similar studies of the active site interactions of β -galactosidase (*E. coli*) and glycons of inhibitors have been carried out with fluorinated substrates and galactonoamidines derivatives by us and others.^{52, 125-127, 56} As previously stated, azasugar inhibitors had been employed to examine the active site of β -galactosidase (bovine liver).⁵³ One of these inhibitors was **4u**, which was synthesized by Ganem *et al.* This inhibitor was used as a control for all other inhibition constants; the values determined here were within error of those found by Ganem.⁵³

Table 3.3 Inhibition of hydrolysis of 4-nitrophenyl- β -D-galactopyranoside by β -galactosidase (bovine liver) in the presence of galactonoamidines. 5mM HEPES buffer solution at pH 7.50 ± 0.05 and $30.0 \pm 0.1^\circ\text{C}$. R= $-\text{CH}_2-\text{C}_6\text{H}_4-\text{CH}_3$.⁹⁰

Compound	Glycon Structure	K _i [nM]	IC ₅₀ [nM]
4u		2000 \pm 200	>50,000
4v		2700 \pm 260	8700
4w		0.60 \pm 0.07	850
4x		1540 \pm 220	10,800
4y		838 \pm 60	9200

As in the previously discussed fluorinated glycoside experiments, the hydroxyl group at the C-2 position of the glycon was determined to be the most important in binding of the glycon to the active site of this glycoside hydrolase.⁹⁰ The hydroxyl group in this position is an important hydrogen bond donor and without it **4w** and **4x** are not as stable within the active site (K_i = 0.06nM and 1540nM respectively).⁹⁰ The large difference in inhibition observed between **4w** and **4y** is most likely due to steric effects induced by addition of the methoxy group at C-4 of the glycon.⁹⁰ Also notable is the fact that the inhibitors lacking an aglycon (**4u** and **4v**) are less potent inhibitors than the derivatives of **4b**.⁹⁰ This shows that the aglycon is very important in the stabilization of the glycon within the active site.⁹⁰ Molecular dynamics simulations were employed in order to understand this stabilization and why the galactonoamidines bind to the β -galactosidase from bovine liver 2 orders of magnitude better than to β -galactosidase from *A. oryzae*.⁹⁰

3.2.2 Development of model for β -galactosidase (bovine liver)

To examine the differences between bindings of the galactonoamidines in the two β -galactosidases, a homology model of β -galactosidase (bovine liver) was prepared.⁹⁰ Two different servers were employed to develop a model structure: the M4T server and the Robetta server.^{130,120,119, 131, 132} Both servers selected crystal structures from β -galactosidase (human) (3TDH from M4T and 3WF3 from Robetta).⁹⁰ The sequences of the β -galactosidase (human) and β -galactosidase (bovine liver) show a 82% sequence identity, which makes the match reliable for simulation screenings.^{133, 134} The data were obtained on June 23, 2016 from M4T server and May 30, 2017 from Robetta; therefore, any crystal structures added after this point have no bearing on the modeled enzyme.⁹⁰

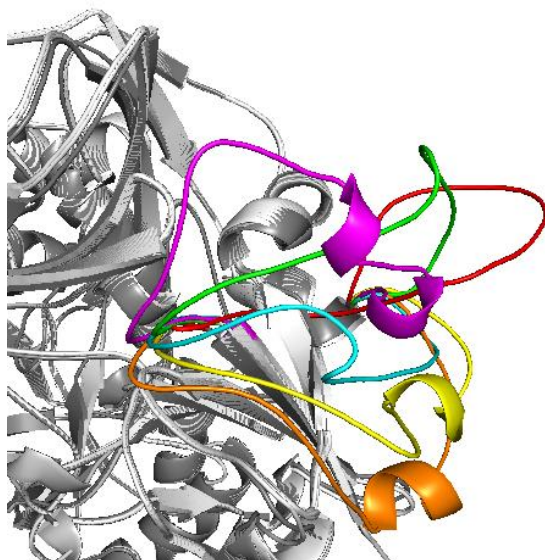


Figure 3.5 Models from M4T server (red), and model 1 (cyan), model 2 (green), model 3 (yellow), model 4 (pink), and model 5 (orange) from Robetta server.

The six models were all very similar, with the only differences being at the C-terminal tail (the last 6 residues, 621-626) and a loop that is distal to the active site made up of residues 500-521, **Figure 3.5**.⁹⁰ The active sites of the Robetta models were all nearly identical surrounding the active site, with a maximum root mean square error (RMDE) of 0.13 Å within 20 Å of the active site.⁹⁰ A comparison of the sequences of β -galactosidase (human) and β -galactosidase (bovine liver) using BLAST revealed 518 identical residues and 73 residues determined to be similar, resulting in a 90.5% sequence similarity.⁹⁰ To establish the model that was built with the most reliability and therefore should be used for further analysis the models were ranked based on statistical analysis using the Quality Model Energy ANalysis (QMEAN) server.⁹⁰ Each model was given a QMEAN6 score, which range from a high score of 1 and low score of -1, to ascribe certainty of the model.¹²¹ The M4T server had a much lower QMEAN6 score (-0.37) than all of the models obtained by Robetta (0.55-0.98).⁹⁰ Model 1 of Robetta had the highest QMEAN6 score (0.98), and therefore this model was selected for further docking and modeling analyses.⁹⁰

3.2.3 Molecular dynamics evaluations of galactonoamidine-enzyme complexes

Six inhibitors were selected for the molecular dynamics studies: the two putative TSAs discovered (**4a** and **4b**) and the two inhibitors that were determined to be opportunistic binders (**4o** and **4s**) through spectroscopic evaluation, an similar inhibitor that lacks an aglycon (**4u**), and an inhibitor with the aglycon of a TSA but a derivatized glycon (**4x**).⁹⁰ Analysis of hydrogen bonding interactions with the galactonoamidines revealed a similar number of overall hydrogen bonding interactions with the glycon of the inhibitors, **Figure 3.6A**.⁹⁰ As expected, the inhibitors which are TSAs (**4a** and **4b**) show the highest probability of interaction with both catalytic residues (Glu187 and Glu267), **Figure 3.6B**.⁹⁰ The inhibitor with the cyclohexyl aglycon, **4s**, shows less probability with both catalytic residues, showing the importance of π - π interactions with the aglycon in the aglycon binding center of the active site, **Figure 3.6B**.

Simulations with the glycon derivatives showed greater differences in the hydrogen bonding interactions of **4x** and **4b** (**Figure 3.6A**) leading to a drastic 30,000-fold potency difference, inhibition constants of 0.05nM and 1,500nM respectively.⁹⁰ The 2-methoxy derivative, **4x**, was found to rotate so that the methoxy group at C-2 of the glycon is no longer completely within the active site; and thus, is no longer allows for interactions with both catalytic residues, **Figure 3.6B**.⁹⁰ The inhibitor lacking an aglycon, **4u**, has a similar number of overall hydrogen bonding interactions to **4a** and **4b**, **Figure 3.6A**.⁹⁰ Yet, **4u** had about 2x less interactions with the proton donor than **4a**.⁹⁰ Without an aglycon bound within its pocket in the active site, **4u** cannot interact with the catalytic residues to the extent of **4a**.⁹⁰ This inability to interact results in the reduction of in binding affinity of **4u** compared to **4a** (**4u** K_i = 2,000nM).⁹⁰

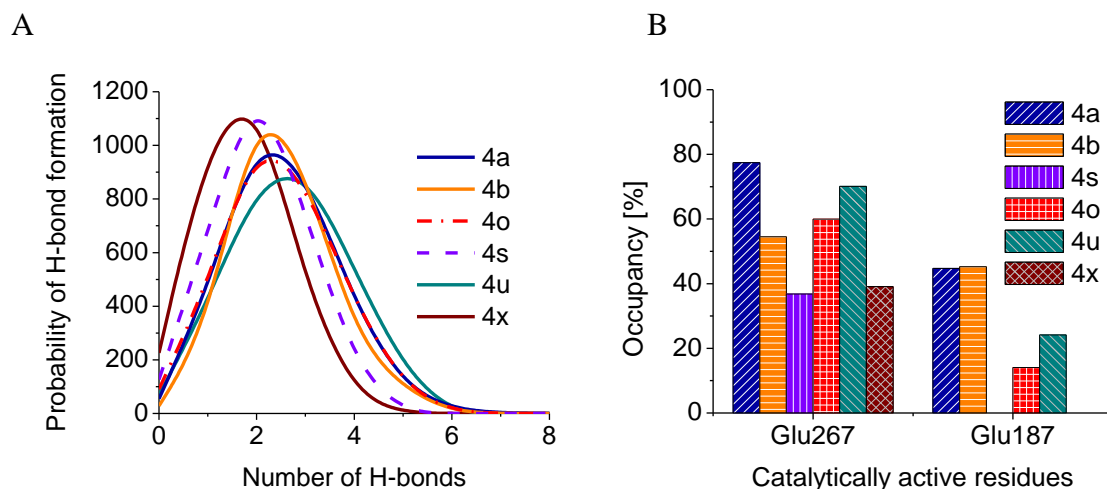


Figure 3.6 (A) Frequency of hydrogen bonding interactions in correlation to the number of hydrogen bonding of galactonoamidines and derivatives with β -galactosidase (bovine liver). (B) Occupancy of the catalytic residues throughout the 30ns simulations with galactonoamidines and derivatives.⁹⁰

As previously stated, molecular dynamics simulations of TSAs in complex with β -galactosidase (*A. oryzae*) showed an induced fit movement that was not observed when fortuitous binders were simulated within the active site.⁷⁹ Astonishingly, not only was an induced fit to stabilize the active site of β -galactosidase (bovine liver) observed, but this induced fit resulted in a conformational shift that shuts off the active site completely via loop closure upon binding to a TSA, **Figure 3.7**.⁹⁰ The molecular dynamics show the binding of **4a** and **4b** to the glycon pocket within the active site of β -galactosidase (bovine liver), followed by the binding of the aglycon in its pocket, resulting in the subsequent loop closure.⁹⁰ During the conformation change, interaction of the aglycons with residues at the outside of the active site cause a π -CH interaction between a Tyr484 and Trp272 that results in a loop movement and closure of the active site, **Figure 3.7**.⁹⁰ Simulations with opportunistic binders did not show this loop closure or any significant loop movement in the active site,⁹⁰ **Figure 8.1 appendix 8.2**. The binding of **4u** to the glycon pocket within the active site results in a partial closure of the active site loop.⁹⁰

However, binding of both glycon and aglycon to their respective pockets within the active site are mandatory for full loop closure over the active site.⁹⁰

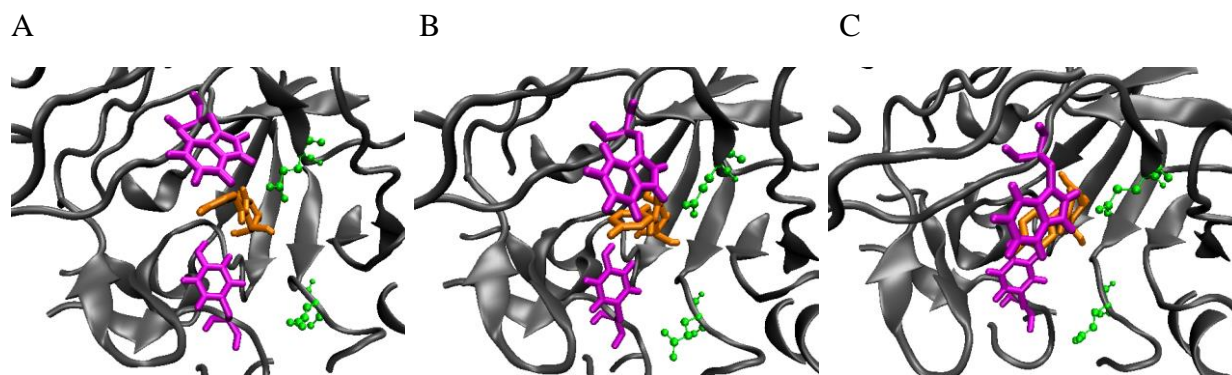


Figure 3.7 Snapshots of from the 30ns simulation of the **4b** (orange) and β -galactosidase (bovine liver) complex showing the active site (A) before, (B) during, and (C) after the loop closure event. The catalytic residues are shown in green and TRP272 and TYR484 are shown in magenta.

3.3 Conclusion:

The active site of a second β -galactosidase from the glycoside hydrolase family 35 was evaluated to compare to the efficacy of the β -galactosidase (*A. oryzae*).⁹⁰ The active sites of the two β -galactosidases should impart similar binding affinities and interactions over the aglycon given the enzymes are classified into the same family.⁹⁰ Though the galactonoamidines were competitive inhibitors of both β -galactosidases, the galactonoamidines had a two orders of magnitude increase in binding towards the β -galactosidase (bovine liver) than those observed with β -galactosidase (*A. oryzae*) resulting in inhibition constants in the picamolar scale.⁹⁰

Spectroscopic evaluations using a library of galactonoamidines revealed that the β -galactosidase (bovine liver) active site preferred aglycons with the ability to form π - π interactions with residues within the active site.⁹⁰ Four galactonoamidines (**4a**, **4b**, **4o**, and **4s**) exhibited the strongest binding affinities with the β -galactosidases from bovine liver.⁹⁰ Three of

these inhibitors were previously shown to be TSA of the β -galactosidase from *A. oryzae* (**4a**, **4b**, and **4s**).^{79, 90} Yet, only **4a** and **4b** are TSAs for the hydrolysis of galactosides by β -galactosidase (bovine liver). This difference in TSAs again shows the preference for π - π interactions over hydrophobic interactions within the aglycon binding pocket of the β -galactosidase (bovine liver).

Exploration of this binding difference by molecular dynamics revealed that when β -galactosidase (bovine liver) binds to a TSA (**4a** or **4b**), a loop closure is observed that closes off the active site to further interaction.⁹⁰ This closure is reminiscent of other loop closures that have been observed in similar TIM barrel type active sites.¹³⁵ This loop closure combined with hydrogen bonding over the glycon and hydrophobic interactions and π - π interactions with the aglycon are the source of the drastic variance in potency of the galactonoamidines on the two β -galactosidases.⁹⁰

3.4 Materials and Methods

3.4.1 Instrumentation

All instrumentation in this chapter was described previously in **section 2.4.1**.

3.4.2 Materials

All commercially obtained chemicals were reagent-grade or higher and were used as received unless noted otherwise. The β -galactosidase (bovine liver) was obtained through Sigma Aldrich as a lyophilized powder and stored at -18 °C until further use.⁹⁰ Sodium hydroxide at 99.999% metal-free purity and HEPES buffer were purchased from Sigma Aldrich and used as received.⁹⁰ The 5mM HEPES buffer solutions were prepared at ambient temperature with compensation for the temperature difference in the UV/vis experiments (pH 7.50 \pm 0.05 and 30.0 \pm 0.1 °C).⁹⁰ Substrates **5a** and **5h** were purchased from Sigma Aldrich and stored at -8 °C.⁹⁰ Substrates **5b-g** and **5i-k** were

synthesized by previously disclosed methods.¹³⁶ Synthesis of the galactonoamidines (**4a-g**,⁸² **4h-t**,⁸⁶ **4u** and **4v**¹³⁷) were synthesized previously by described methods.

3.4.3 Spectroscopic evaluations

3.4.3.1 Stock solution of β -galactosidase (bovine liver)

The stock solution of enzyme was prepared by dissolving the lyophilized β -galactosidase from bovine liver in 5mL of 5mM HEPES buffer solution and stored at -80°C in 50 μ L aliquots until use.⁹⁰ The concentration of the enzyme stock solution was determined to be 139 \pm 6.25 μ M by BCA assay.⁹⁰ Prior to IC₅₀ and K_i value determination, an aliquot was thawed.⁹⁰ The entire 50 μ L aliquot was diluted to 5mL with 5mM HEPES buffer solution and stored on ice until use for IC₅₀ value determination.⁹⁰ However, for determination of inhibition constants a 20 μ L aliquot was diluted to 5mL with 5mM HEPES buffer solution and stored on ice until use.⁹⁰

3.4.3.2 Stock solution of galactonoamidines inhibitors

Typically, 0.005, 0.05, 0.125, 0.25, 0.5, 2.5, 10, 20, 30, 50 and 100 μ M inhibitor solutions were prepared by diluting aliquots of 100 μ M aqueous solution of the galactonoamidines with nanopure water.⁹⁰ All resulting inhibitor stock solutions were used in 10 μ L aliquots in IC₅₀ and K_i assays and kept at ambient temperature until pipetted into plates.⁹⁰ Stock solutions of inhibitors in concentrations of 0.05nM and 0.075nM for **4f** and **4s**, 0.05nM, 0.075nM, and 0.1nM for **4a**, **4b**, and **4g**, 0.075nM and 0.10nM **4c**, and **4e**, **4h-j**, **4l-m**, **4o**, and **4t**, 0.10nM and 0.125nM for **4n**, 0.15nM and 0.17nM for **4d**, 0.15nM and 0.20nM for **4k** and **4r**, 0.2nM and 0.50nM for **4t**, 0.5nM and 0.6nM for **4w**, 0.5 μ M, 1.25 μ M and 2.5 μ M for **4v**, 1.0 μ M and 2.0 μ M for **4u**, 0.25 μ M and 0.5 μ M for **4y**, and 0.5 μ M and 0.1 μ M for **4x** were used in the determination of K_i values.⁹⁰

3.4.3.3 Stock solution of model substrates

Substrate solutions were prepared by dissolving 4.20-7.84mg (0.013-0.025mmol) of nitrophenyl- β -D-galactopyranoside (**5a-e** and **5h-j**) in 5mL of 5mM HEPES buffer solution in a volumetric flask (2.66-4.94mM).⁹⁰ The substrate solution was prepared immediately before use and kept at ambient temperature until pipetted into microplates.⁹⁰

3.4.3.4 Kinetic Assay

The kinetic assay was prepared the same as **section 2.4.3.5** with the following changes: The plate was read at a wavelength of 405nm at 30°C for 45 minutes with data obtained every 27s.⁹⁰

3.4.3.5 Data Analysis

The formation of nitrophenylate was determined by absorbance at a wavelength of 405nm using apparent extinction coefficients (see **Chapter 8; appendix 2**). All kinetic parameters were determined in at least duplicate and data analysis was carried out as described in **section 2.4.3.6**. An average of 2-3 inhibition concentrations were employed to determine the inhibition constants (K_i).⁹⁰

3.4.4 Development of β -galactosidase (bovine liver) model

3.4.4.1 M4T model

A β -galactosidase (bovine liver) model was obtained through the M4T [server](#) vers. 4,^{130,120,131} through the [Protein Model Portal](#).⁹⁰ The data was obtained from the portal on June 30, 2016; therefore, any crystal structures added after this point have no bearing on the modeled enzyme. A model was prepared using Multiple Model Mapping and Modeller.^{138, 139}

3.4.4.2 Robetta model

The FASTA sequence of β -galactosidase (bovine liver) was imported from UniProt (ID Q58D55) into the Robetta server with the signal peptide (residues 1-28) removed from the sequence.⁹⁰ A GRINZU method homology templated was used to determine β -galactosidase from human, 3wf3, was the best match for templating the sequence again, with a high confidence of 96%.⁹⁰ A structure calculation by homology and *de novo* calculations returned five punitive models.⁹⁰

3.4.4.3 Quality assessment of models

All six models were uploaded as a pdb's onto the Quality Model Energy ANalysis (QMEAN) server and analyzed.⁹⁰ The model with the highest quality score, which was a QMEAN6 score of 0.98, was selected for further analysis.⁹⁰

3.4.5 Molecular Dynamics Simulations

The coordinates of the selected model were imported into PMV, where all polar hydrogens were added to residues and Kollman charges were added to each atom with AutoDock Vina Tools.^{98, 140} A 15x15x15Å grid box was centered in the active site of β -galactosidase (bovine liver).⁹⁰ Galactonoamidine inhibitors were prepared for docking analysis as described in **section 2.4.4**.⁹⁰ All parameters in AutoDock Vina were set to default for all calculations.¹⁴¹ The nine conformations of each inhibitor were visualized with PYMOL and the conformation with the lowest free energy estimate was exported as a pdb file for further analysis.¹⁴²

Inhibitor topologies and coordinates, enzyme topologies and coordinates, and inhibitor-enzyme complexes were obtained as previously described in **section 2.4.5**.⁹⁰ The complexes were then solvated with 41,945-41,956 single point charge water molecules in a 1367nm³ cubic box.⁹⁰ Then, a random water molecule was replaced by a sodium ion to neutralize the systems.⁹⁰

Energy minimization, equilibration, and the production phase were carried out as described in **section 2.4.5**. All analysis of production simulations were carried out with Visual Molecular Dynamics as previously described in **section 2.4.5**.^{90 79}

4 Investigation of galactonoamidine inhibition of β -galactosidase (*E. coli*) under isolated and cell-like conditions.

4.1 Introduction

The active site of all glycoside hydrolases from Clan A are within a TIM barrel motif.²³ The entrance to the active sites is made up of eight loops connecting the beta strands to the alpha helices, which are called the beta/alpha loops.¹⁴³ The catalytic residues are located on the fourth and seventh beta strands of the TIM barrel.⁶ In enzymes with similar TIM barrels as the catalytic core, motion of the beta/alpha loops help to create microenvironments that accelerate catalysis by closing over the active site when a ligand binds.^{135, 144, 145} An excellent example of the loops acting as a gate occurs during the hydrolysis of substrates by β -galactosidase from *E. coli*.¹⁴⁶

A loop closure over the active site of β -galactosidase (*E. coli*) occurs during the transition state of substrate hydrolysis and when a transition state analog (TSA) is bound within the active site.¹⁴⁶ Thus far, only *assumed* TSAs, galactonolactone (**3l**) and galactotetrazole (**3k**), have been studied within the active site of β -galactosidase (*E. coli*).^{51, 146, 147} Both of these inhibitors lack experimental evidence of them being TSA and lack an aglycon. Previous studies have shown that the aglycon of glycoside hydrolase inhibitors, TSAs in particular, have key roles in stabilization of the molecule within the active sites.^{70, 79, 90} Galactonoamidines have been shown to be TSAs of two other β -galactosidases within clan A^{Error! Reference source not found.}^{70, 79} Considering the similarities in active sites of GHs,¹³ it is plausible that these galactonoamidines are TSAs of the β -galactosidase (*E. coli*) as well. Establishing the interactions of a TSA with aglycons provides a full picture of the interactions occurring with substrates during the hydrolysis by GHs.

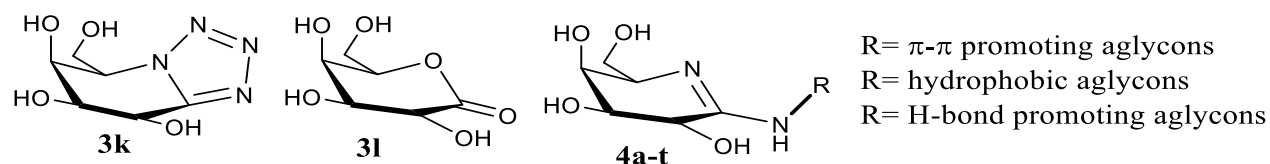


Figure 4.1 Current compounds synthesized to mimic the transition state that have been crystallized within the active site of β -galactosidase (*E. coli*).¹⁴⁶ Galactonoamidines designed to mimic the transition state of substrate hydrolysis

This enzyme has two binding modes: a “shallow” and a “deep” mode.¹⁴⁸ The interactions that occur in each mode have been established through crystallization and kinetic experiments with deoxy- and fluoro- analogs of 2, 4-dinitrophenyl galactopyranosides, **Error! Reference source not found.k** and **3l**.^{51, 146, 147} During hydrolysis, substrates first bind within the “shallow” mode of the active site.¹⁴⁶ In this position, the glycosidic oxygen atom of the substrate is positioned over the indole of W999 and the following hydrogen bonding interactions are observed: Glu461 (C2-OH), Glu537 (C3-OH), water mediated interaction to Asn460 (C3-OH), Asp201 (C4-OH), Asn604 (C6-OH), and His540 (C6-OH).^{148, 149} In this position, there is also a hydrophobic interaction with the C-6 of the glycon and Phe601.¹⁴⁸ This residue becomes important in the binding at the “deep” mode.¹⁴⁶ An additional hydrogen bond is observed with ONPG substrates with His418 through the nitro group.¹⁴⁸

A 90° rotation of the substrate and movement 3-4Å deeper into the active side occurs to transition the substrate into the “deep” mode of the active site.¹⁴⁶ When in the “deep” mode of the active site, galactose stacks with Trp568 and has hydrogen bonding interactions with Glu461 (C1-OH), Glu537 (C2-OH), Asn460 (C2-OH), His391 (C3-OH), Asp201 (C4-OH), Asn604 (C6-OH) and His540 (C6-OH).^{148, 150} The glucose binding site has only been characterized as having stacking interactions with Trp999.¹⁴⁶ After the substrate has moved to the “deep” mode, Phe601 moves to have a cation- π interaction with Arg599. As a result, Gly794, Ser796, and Glu797 are

no longer anchored by interactions with Arg599, and a beta/alpha loop (Gly794-Pro803) moves to close over the active site.¹⁵¹⁻¹⁵³ This loop closure event is instrumental in the enzyme's transglycosylation mechanism to produce allolactose for LacZ regulation.^{76, 154}

It is speculated that the galactonoamidines will inhibit β -galactosidase (*E. coli*) with similar binding affinities, in the low picomolar concentration range, as observed with other β -galactosidases with loop closures. Summarized here are the evaluations of binding interactions with galactonoamidines with spectroscopic evaluation, molecular docking, and molecular modeling, as well as the exploration of binding interactions in the presence of other proteins and/or cell components (i.e. lipids and organelles).

4.2 Results and Discussion

4.2.1 Active site independence and SAR study

The GH-2 β -galactosidases, unlike the previously examined GH-35 β -galactosidases,^{82, 90} are homotetramers at catalytic pH (7.50-8.00) and temperature (25-40°C).¹⁵⁵ Prior to extensive SAR studies, the binding of the galactonoamidines needed to be investigated to ensure that they bound to the active site of the β -galactosidase rather than through an allosteric site. The galactonoamidine inhibitors were determined to be competitive inhibitors of β -galactosidase (*E. coli*), **Figure 4.2A**.⁵⁶ To ensure that the galactonoamidines do not interact with multiple active sites of the homotetramers, a plot of apparent Michaelis-Menten constant vs inhibitor concentration was constructed to measure cooperativity, **Figure 4.2B**.¹⁵⁶ The high correlation of the apparent Michaelis-Menten constant and inhibitor concentration ($R^2=0.999$) revealed that the active sites act independently.¹⁵⁶

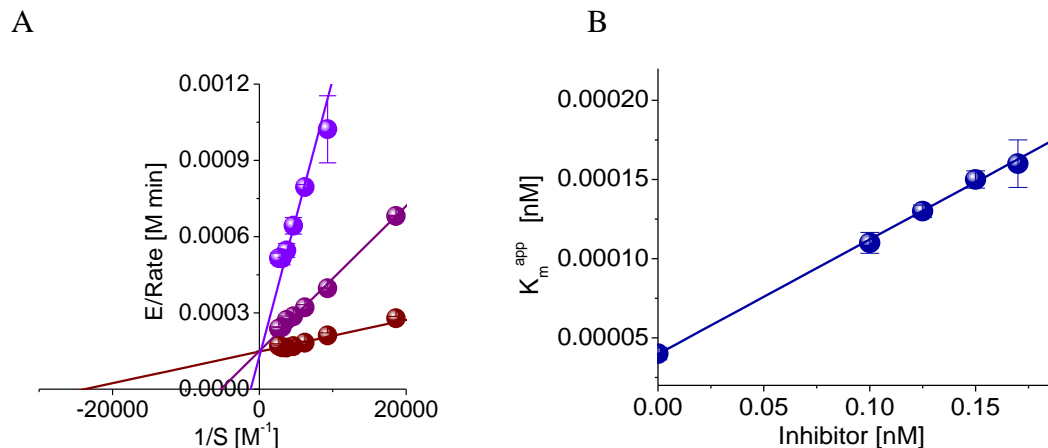
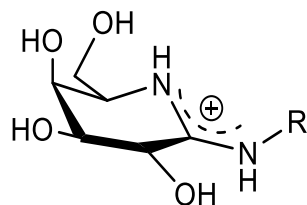


Figure 4.2 (A) Lineweaver-Burk plots of the hydrolysis of **5h** by β -galactosidases (*E. coli*) in the presence of **4b** show competitive inhibition. (B) Cooperativity analysis of interaction of galactonoamidines in the active sites of β -galactosidases (*E. coli*) shows the independence of active sites of the homotetramers.

After determining the galactonoamidines were competitive inhibitors that interact with only one active site at a time, a SAR study was initiated using the library of 20 galactonoamidines. As stated in the introduction, these galactonoamidines have aglycons with various interaction capabilities.⁸⁶ The SAR study revealed that the active site of β -galactosidase (*E. coli*) supports both hydrophobic and π - π interactions over the aglycon with a preference towards aglycons imparting π - π interactions (K_i **4a** < **4s**), **Table 4.1**. The active site only supports cyclic aliphatic aglycons for hydrophobic interactions; inhibitors with linear aliphatic do not bind as well within the active site (K_i **4s** < **4l**). In ability of the active site to stabilize these linear aliphatic aglycons decreases with the size of the aglycon (K_i **4l** < **4m**). This reduction in stability could be due in part to the tightness of the active site and the proximity of loops of other monomers near the active site interfering with proper binding.¹⁴⁶ Nine inhibitors exhibited similar K_i (30-100pM) and IC_{50} values (6.8-37nM), **4a-c**, **4f-g**, **4i-j**, **4p**, and **4s**). Their tight binding led to the consideration of them as possible TSAs for the hydrolysis of substrates by β -galactosidase (*E.*

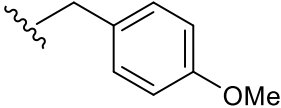
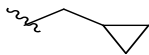
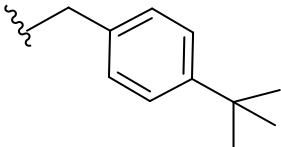
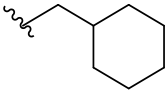
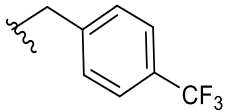
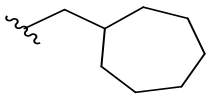
coli). The inhibitors' interactions within the active site were investigated further by molecular docking and modeling studies.

Table 4.1 Inhibition of hydrolysis of 4-nitrophenyl- β -D-galactopyranoside ($k_{\text{cat}} = 5478 \pm 107 \text{ min}^{-1}$ and $K_M = 0.040 \pm 0.004 \text{ mM}$) by β -galactosidase (*E. coli*) in the presence of galactonoamidines. 5mM HEPES buffer solution at pH 7.50 ± 0.05 and $30.0 \pm 0.1^\circ\text{C}$.⁵⁶



Compound	R Group	K_i [nM]	IC_{50} [nM]	Compound	R Group	K_i [nM]	IC_{50} [nM]
4a		0.03 ± 0.01	19	4k		0.25 ± 0.02	35
4b		0.06 ± 0.01^{56}	9.8	4l		0.23 ± 0.03	8.5
4c		0.09 ± 0.01	25	4m		2.6 ± 0.28	8000
4d		0.25 ± 0.02	103	4n		0.15 ± 0.02	244
4e		0.15 ± 0.02	31	4o		0.12 ± 0.01	15
4f		0.03 ± 0.0	37	4p		0.10 ± 0.01	31
4g		0.08 ± 0.01	6.8	4q		1.30 ± 0.14	62

Table 4.1 Cont'd: Inhibition of hydrolysis of 4-nitrophenyl- β -D-galactopyranoside ($k_{\text{cat}} = 5478 \pm 107 \text{ min}^{-1}$ and $K_M = 0.040 \pm 0.004 \text{ mM}$) by β -galactosidase (*E. coli*) in the presence of galactonoamidines. 5mM HEPES buffer solution at pH 7.50 \pm 0.05 and 30.0 \pm 0.1 $^{\circ}$ C

Compound	R Group	K_i [nM]	IC_{50} [nM]	Compound	R Group	K_i [nM]	IC_{50} [nM]
4h		0.25 \pm 0.02	15	4r		0.25 \pm 0.04	37
4i		0.06 \pm 0.01	9.7	4s		0.09 \pm 0.01	9.4
4j		0.06 \pm 0.1	15	4t		0.11 \pm 0.01	24

4.2.2 Molecular docking and modeling of galactonoamidines

Though crystallization of the galactonoamidines within the active site of β -galactosidase (*E. coli*) has been unsuccessful thus far, molecular docking and dynamics of the inhibitor-enzyme complexes are possible. The nine inhibitors (**4a-c**, **4f-g**, **4i-j**, **4p**, and **4s**) with high binding affinities and low IC₅₀ values were further examined through docking and molecular modeling analyses to determine the interactions occurring within the active sites. The interactions observed through these analyses will be compared to the previously discussed interactions known to occur with substrates. Based on previous studies, it is known that a TSA should have interactions with both catalytic residues, and that orientation of the aglycon plays a key role in TSA binding.^{79, 93} Therefore, the initial docking analyses focused on the hydrogen bonding interactions with catalytic residues and the positioning of the galactonoamidines' aglycon.

The attempts at docking the ligands with AutoDock Vina as performed with previous β -galactosidases from bovine liver and *A. oryzae* failed. The algorithms used for determining docking conformations with AutoDock did not accurately model interactions occurring in the active site of β -galactosidase (*E. coli*) due to the two metal ions within the active site. Previously, others revealed similar problems with Autodock Vina and enzymes with metal ions within the active sites.¹⁵⁷ They found that though Autodock Vina gives the most similar ligand orientation to crystalized ligands, the software cannot give the exact orientations found in crystal structures.¹⁵⁷ Thus, the nine galactonoamidines were manually inserted into the active site and overlain with the ligands that were crystallized within the active site. The interactions of the nine inhibitors, along with a ligand representing a reaction intermediate (**2a**, **Figure 4.3**) and an assumed TSA (**3k**), were further characterized by molecular dynamics. Since the interactions of

2a and **3k** have been determined through crystallization studies,¹⁴⁶ the molecular dynamics studies can be validated using these molecules. The inhibitor representing the reaction intermediate, **2a**, was found to have hydrogen binding interactions with His391, Asp201, His540, and Asn604 through the crystallization studies.¹⁴⁶ Whereas, the deep binding inhibitor, **3k**, has hydrogen bonds to His391, Asp201, His540, and Asn604 as well as Asn460, Glu461, and Glu537 in the crystal structure.

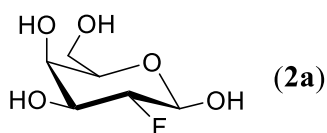


Figure 4.3 Substrate, 2-fluoro-2-deoxy- β -D-galactopyranoside (**2a**), crystallized within the active site of β -galactosidase (*E. coli*), PDB ID 4V45.¹⁴⁶

Protein inhibitor complexes were built with dimers rather than the tetrameric protein for simplicity and examined with GROMOS96 43A1 force field using GROMACS over a 48ns production phase. Initially, the hydrogen bonding interactions of **2a** and **3k** with residues in the active site of β -galactosidase (*E. coli*) were examined to ensure the model was accurate, **Figure 4.5**. These hydrogen bonds were characterized as either strong hydrogen bonding interactions or weak hydrogen bonding interactions based on the distance of acceptor to donor. Strong hydrogen bonds of the complexes of inhibitors with proteins were classified as a bond were the acceptor and donor were within 3.2Å of each other, which was cutoff used for determining hydrogen bonds from the crystallization studies.¹⁴⁶ Weak hydrogen bonding interactions are those in which the donor and acceptor are up to 3.5 Å apart. At first there was concern over some interactions described in the crystal structures not being observed in the simulations. However, we found that the probability of observing a hydrogen bonding interaction in the simulation decreases as the distance of the hydrogen bonding interactions in the crystal structure increases. All missing hydrogen bonding interactions in the simulations were $\geq 3.0\text{\AA}$ from donor to acceptor

in the crystal structure. When the weak hydrogen bonds are examined alongside the strong hydrogen bonds the interactions better match those observed in the crystal structures.

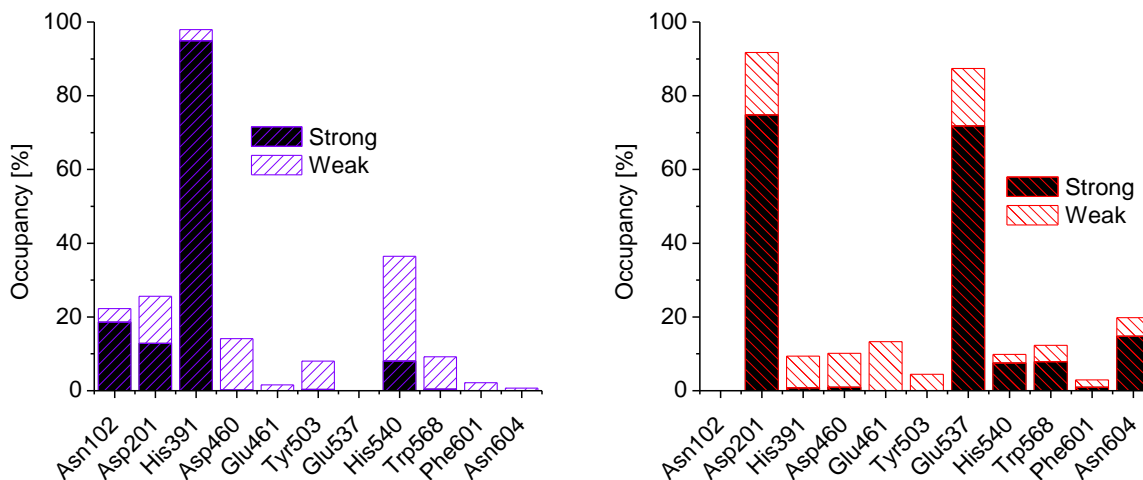


Figure 4.4 Hydrogen bonding interactions of **2a** and **3k** with β -galactosidase (*E. coli*)

After establishing a similar interaction profile with the simulations and crystal structure of the model compounds, the overall structure of the protein was examined to ensure that the protein integrity was maintained through the simulations when using dimers rather than tetramers. Though the hydrogen bond occupancy of **2a** and **3k** are low for the expected residues, the active sites of β -galactosidase (*E. coli*) does not fall apart, **Figure 4.5**. While there are small shifts in the residues surrounding the active site during both simulations the overall structure of the protein within 15Å of the active site remains the same as the crystal structure throughout the simulations (RMSD of 1.13Å for **2a** and 0.985Å for **3k**), **Figure 4.5**. The low occupancy is most likely due to the low binding affinity of these compounds to β -galactosidase (*E. coli*) rather than an error in the simulations. The inhibition constants of both **2a** and **3k** are in the μ M concentration range, whereas the inhibition constants with galactonoamidines are in the pM concentration range. Therefore, we would expect the hydrogen bonding occupancy of **2a** and **3k**

with β -galactosidase (*E. coli*) to be less than those of the galactonoamidines. The overall conservation of hydrogen bonding interactions and protein structure between the crystal structure and the molecular dynamics simulations validates this methodology.

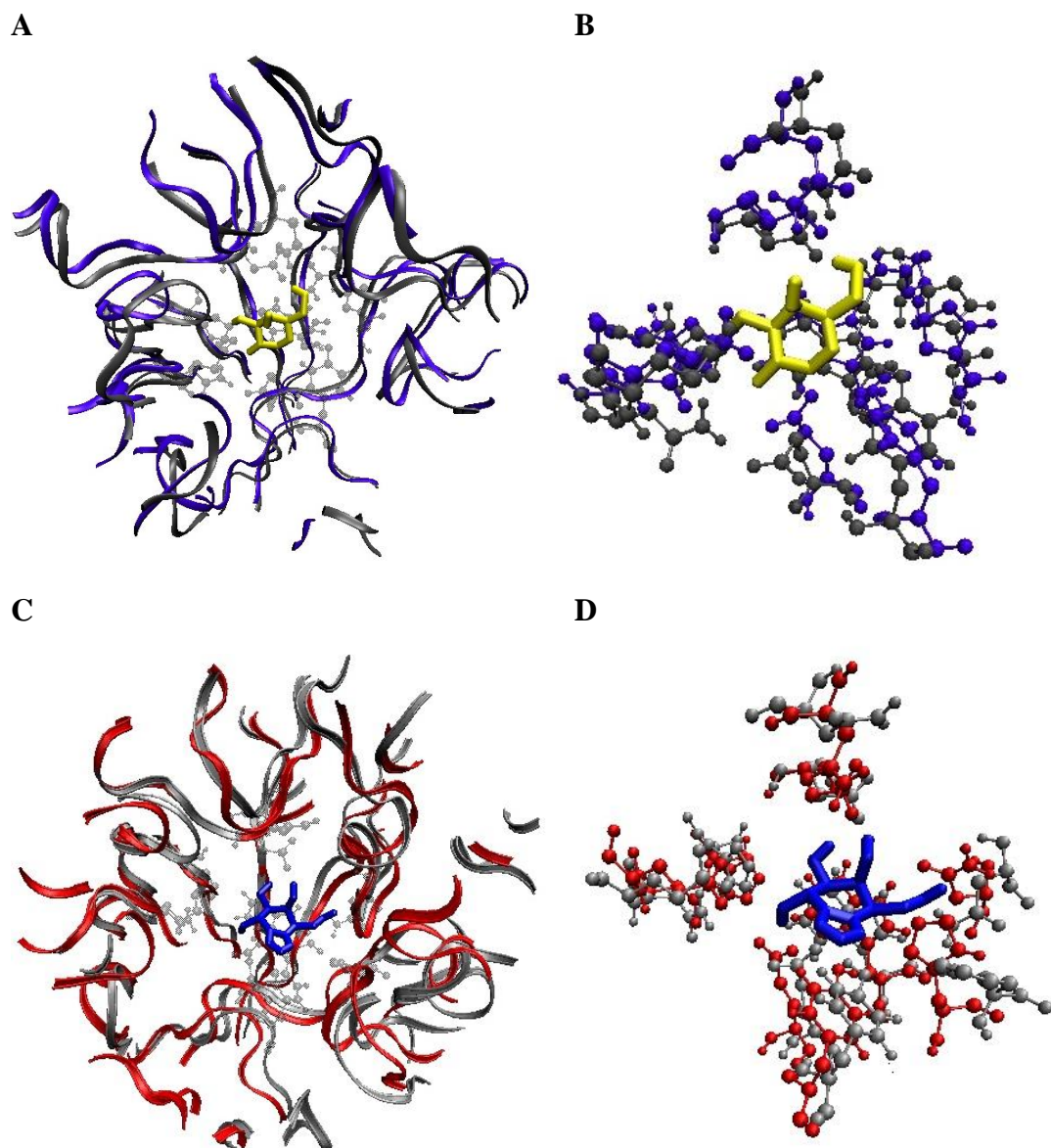


Figure 4.5 A) Crystallized (purple) β -galactosidase (*E. coli*) in complex with 2FG (yellow) and the final coordinates of β -galactosidase (*E. coli*) after 48ns of simulation (grey) within 15Å of the active site. B) Active site residues from the crystal structure (purple) and simulated β -galactosidase (grey) after 48ns with 2FG in yellow. C) Crystallized (red) β -galactosidase (*E. coli*) in complex with GTZ (blue) and the final coordinates of β -galactosidase (*E. coli*) after 48ns of simulation (grey) within 15Å of the active site. D) Active site residues from the crystal structure (red) and simulated β -galactosidase (grey) after 48ns with GTZ shown in blue.

After establishing the model for ligand interactions was correct we moved to examining the interactions of the nine galactonoamides within the active site of β -galactosidase (*E. coli*). First, the hydrogen bonding interactions with the galactonoamides were examined, then the orientation of the glycon within the active site, and finally the interactions of the aglycon. Since the only interaction known to occur with the natural aglycon, glucose, is a stacking interaction with Trp999, this will be the initial focus of the aglycon examinations.

Previous molecular dynamics simulations with TSAs in complex with other β -galactosidases showed that interaction with *both* catalytic residues within the active site are crucial. Complexes with **4a-c**, **4g** and **4s** all have a high probability of interaction with both catalytic residues (Glu461 and Glu537), **Figure 4.6A-C, E, and I**. Complexes with **4f** and **4j** lack of interaction with the proton donor, Glu461, and thus can be eliminated from further scrutiny **Figure 4.6 D and G**. All of the inhibitors show a high probability of interaction with Asp201 and the nucleophile Glu537. Further investigations of the glycon binding of the galactonoamides revealed that six galactonoamides (**4a**, **4b**, **4g**, **4j**, **4p**, and **4s**) stack on Trp568 similarly to inhibitors observed through crystal structures (**Figure 9.2**), with the face of the glycon parallel to the side chain of Trp568. The other three galactonoamides, **4c**, **4f**, and **4i**, are oriented so that the glycon is perpendicular to the side chain of Trp568. The overall hydrogen bonding interactions of **4p** and the active site was significantly less than all other complexes, **Figure 4.6** and **Figure 9.1**. Galactonoamides **4c**, **4f**, **4i**, **4j**, and **4p** were excluded from further scrutiny based on the glycon interactions within the active site.

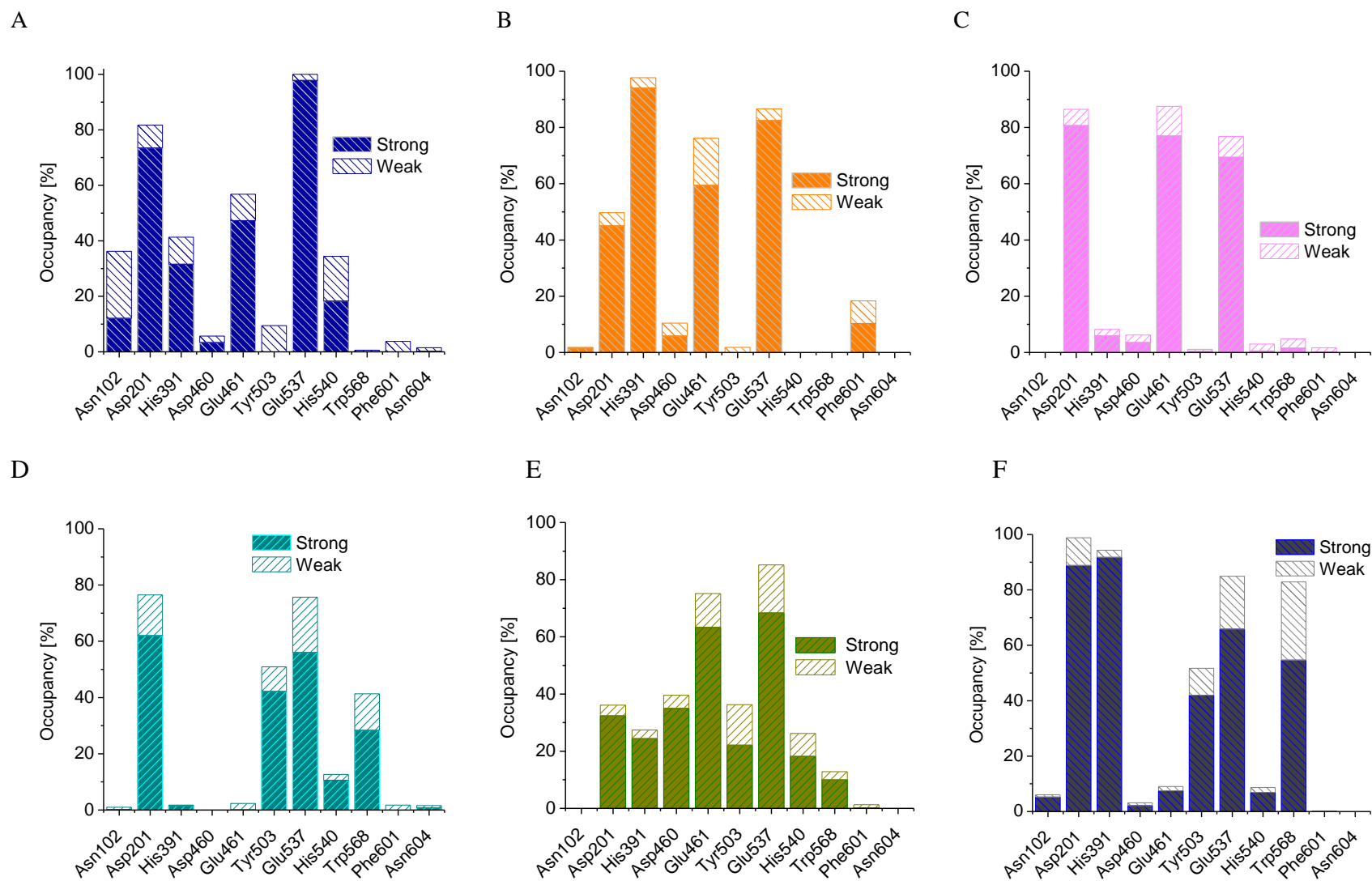
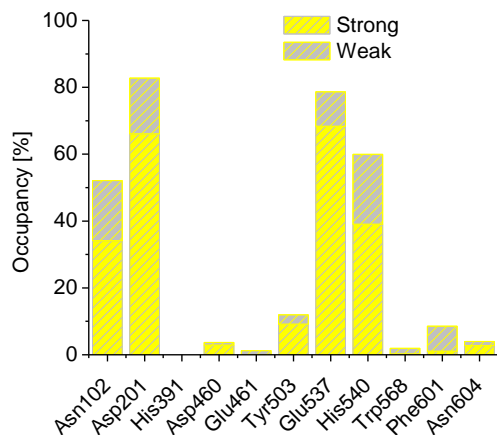
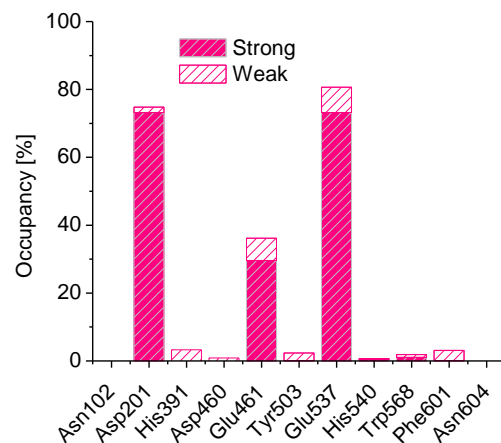


Figure 4.6 Hydrogen bonding interactions of galactonoamidines **4a** (A), **4b** (B), **4c** (C), **4f**(D), **4g**(E) and **4i**(F) with β -galactosidase (*E. coli*)

G



H



I

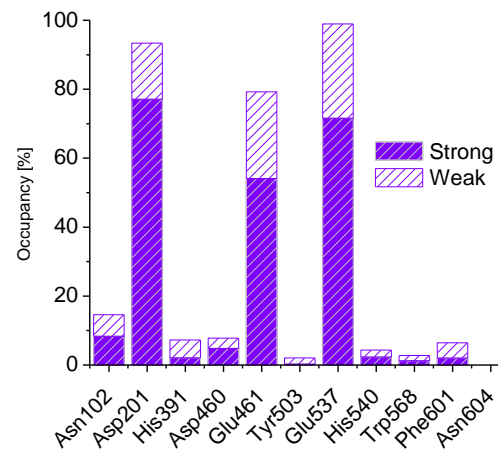
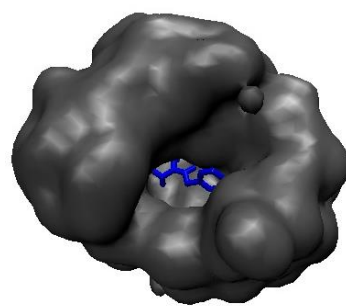


Figure 4.6 cont'd Hydrogen bonding interactions of galactonoamidines **4j** (G), **4p** (H), and **4s**(I) with β -galactosidase (*E. coli*)

A



B

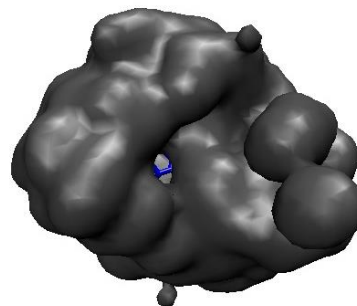


Figure 4.7 Snap shot of the loop closure with complex of β -galactosidase (*E. coli*) and **4a**. Only protein within 10Å of **4a** is shown for clarity.

As already stated the only knowledge about the binding of an aglycon within the active site is the stacking that occurs between glucose and Trp999. Galactonoamidines **4a** and **4b** show π - π stacking interactions with Trp999, **4s** shows CH- π interactions with the aglycon and Trp999, and **4p** has hydrophobic interaction with Trp999, **Figure 9.3**. Galactonoamidine **4g** on the other hand shows interaction with the opposite wall of the active site (Glu281, Arg282, Glu416, Ser462, Glu487, and Lys517). The fluoro-group of the aglycon is imbedded in this hydrophilic pocket of residues that is not observed in any other complex. Along with Trp999, **4a**, **4b** and **4s** have hydrophobic interactions with Phe601, Phe512, Met502 and Val103. Complexes with **4a** and **4b** show additional hydrophobic interactions with Pro511. The aglycon of **4a** has further interactions with Met423, while the aglycon of **4b** has an additional interaction with Pro513.

Further, the galactonoamidines all showed movement of loop 794-803 towards the active site, with complete movement of the loop over the active site for complexes with **4a**, **4b**, and **4s**, **Figure 4.7**. The other inhibitors only showed some movement of the loop towards the active site not complete closure. Based on these molecular dynamics simulations galactonoamidines **4a**, **4b**, and **4s** were further evaluated spectroscopically as TSA

4.2.3 Spectroscopic evaluation of galactonoamidines as TSA.

The galactonoamidines' inhibition of hydrolysis of nine nitrophenyl- β -D-galactopyranoside (**5a-k**)⁷⁰ by β -galactosidase (*E. coli*) was examined through Bartlett method,⁷⁸ **Figure 4.8**. As stated in previous chapters, an inhibitor that is a TSA will result in a double-logarithmic plot with a linear fit and correlation factor (R^2) similar to 1.^{54, 78} All eleven substrates were inhibited in the low picomolar range by the three galactonoamidines (9.5-900pM), **Table 4.2**. The linear fit of the data obtained from inhibition of substrate hydrolysis by **4a** and **4b** was near 1 and both data sets had correlation factors near 1, **Figure 4.9A**. Though the linear fit of the data from **4s**

gave a slope within error of 1, the correlation of the data was very poor ($R^2=0.61$), **Figure 4.9B**.

The afore stated criteria qualified galactonoamidines **4a** and **4b** as TSAs, while excluding **4s**.

With the two TSAs (**4a** and **4b**) in hand, the inhibition ability of the TSAs and the opportunistic inhibitor (**4s**) were examined in solution with multiple proteins. To our knowledge, the inhibition of glycoside hydrolases by TSAs has been not by studied under such conditions.

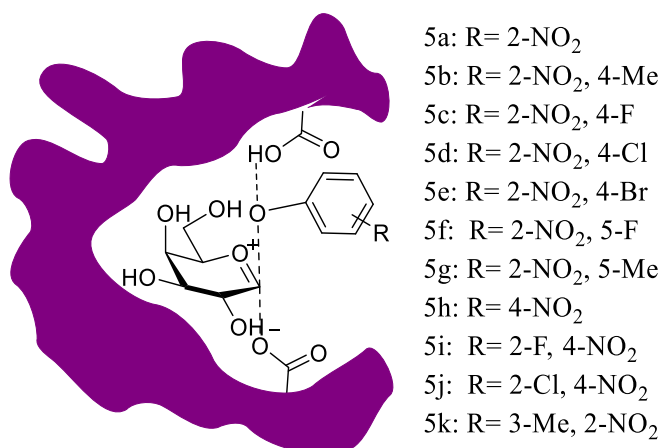
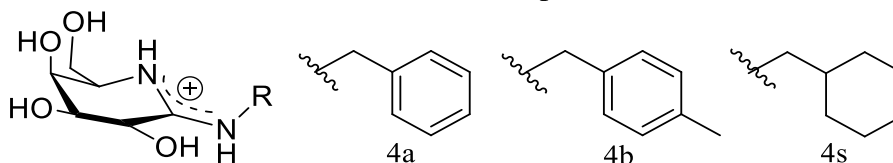


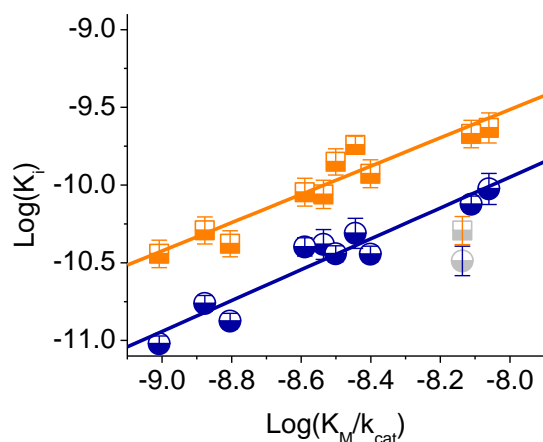
Figure 4.8 Transition state of model substrates' (**5a-k**) hydrolysis by β -galactosidases (grey).⁷⁰

Table 4.2 Galactonoamidine inhibition of hydrolysis of 11 nitrophenyl- β -D-galactopyranosides by β -galactosidase (*E. coli*); 5mM HEPES buffer solution at pH 7.50 \pm 0.05 and 30.0 \pm 0.1°C.



Entry	k_{cat} [sec ⁻¹]	K_M [mM]	K_i 4a [pM]	K_i 4b [pM]	K_i 4s [pM]
5a	860 \pm 20	0.15 \pm 0.008	42 \pm 5	87 \pm 9	151 \pm 50
5b	153 \pm 15	0.08 \pm 0.003	94 \pm 8	233 \pm 40	350 \pm 70
5c	1,320 \pm 89	0.25 \pm 0.003	36 \pm 3	141 \pm 2	155 \pm 23
5d	2,260 \pm 69	0.18 \pm 0.05	17 \pm 3	51 \pm 3	145 \pm 15
5e	1,870 \pm 120	0.11 \pm 0.012	9.5 \pm 0.8	36 \pm 5	16 \pm 4
5f	1,950 \pm 97	0.42 \pm 0.030	49 \pm 4	181 \pm 1	247 \pm 21
5g	3,570 \pm 250	1.66 \pm 0.40	75 \pm 3	213 \pm 7	603 \pm 15
5h	91 \pm 2	0.04 \pm 0.004	33 \pm 5	60 \pm 8	86 \pm 4
5i	504 \pm 25	0.12 \pm 0.009	36 \pm 4	118 \pm 25	900 \pm 10
5j	260 \pm 10	0.04 \pm 0.005	40 \pm 1	90 \pm 7	46 \pm 5
5k	640 \pm 1500	0.06 \pm 0.009	13 \pm 2	42 \pm 1	92 \pm 3

A



B

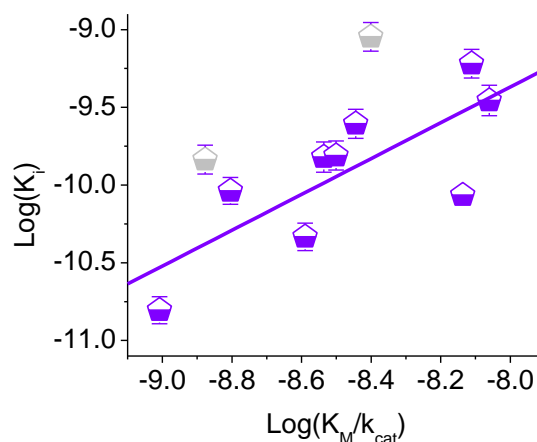


Figure 4.9 Double-logarithmic correlation of inverse catalytic efficiency (K_M/k_{cat}) and the inhibition constant (K_i) with linear fit $y = ax + b$ for the 9 nitrophenyl- β -D-galactopyranosides in the presence of (A); **4a** (navy circle) $a = 0.99 \pm 0.10$, $R^2 = 0.92$ and **4b** (orange square) $a = 0.91 \pm 0.11$, $R^2 = 0.91$; (B) (**4s**) (purple pentagon) $a = 1.15 \pm 0.35$, $R^2 = 0.61$.

4.2.4 Inhibition of β -galactosidase in cell assays

After examining the inhibitors as TSAs, focus turned to the ability of the inhibitors to interact with the β -galactosidase in cell assays. These inhibitors were selected to examine if a TSA will have an increase the inhibitory ability of the galactonoamidines in the presence of other proteins or if the opportunistic binders will bind just as well as seen in the SAR studies with the commercially available enzyme. Initial efforts to investigate the interactions of galactonoamidines within live cells failed. The increase of turbidity observed during the growth of cells impeded efforts to quantify hydrolysis by UV/vis and fluorescence spectroscopy (data not shown). This required lysing of the cells so the cell growth would not affect measurements of product formation. Along these lines, we endeavored to determine the ability of galactonoamidines to inhibit the hydrolysis of substrate by β -galactosidase (*E. coli*) in lysed cells and a crude protein extract from these cells. The turbidity of the lysed cell suspension and crude

protein extract made UV/vis analysis of substrate cleavage impractical, so we turned to evaluations of hydrolysis of 4-methylumbelliferyl β -D-galactopyranoside (**5m**) as the model substrate, **Figure 4.10**. The resulting product, 4-methylumbelliferone (**6**), is easily tracked by fluorescence at an excitation wavelength of 365nm and emission wavelength of 460nm. The turbidity of the lysed cell suspensions was much greater than the crude protein extract, which made the data obtained inconclusive; therefore, we will not speculate to the inhibition of β -galactosidase in these suspensions.

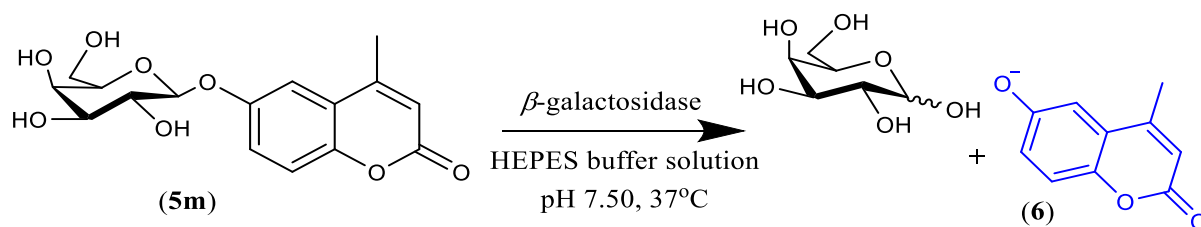


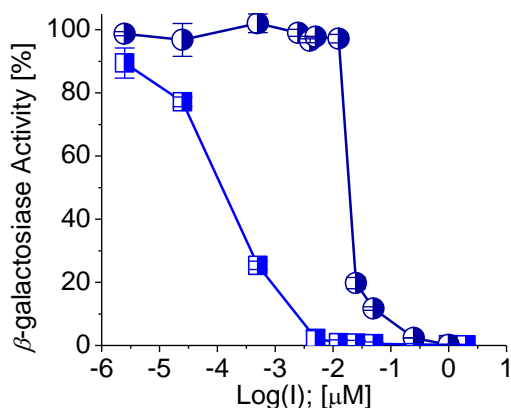
Figure 4.10 Hydrolysis of model substrate, 4-methylumbelliferyl β -D-galactopyranoside (**5m**).

Both the TSAs (**4a** and **4b**) and opportunistic binder (**4s**) reduce the β -galactosidase activity in the crude protein extract at lower concentrations than commercial β -galactosidase (*E. coli*), **Table 4.3**. The galactonoamidine that reduces the activity of the crude protein extract and the β -galactosidase (*E. coli*) to the highest extent at lower concentrations is **4s**, **Figure 4.11C**. Though the **4s** is only an opportunistic binder rather than a TSA it is able to inhibit the β -galactosidase activity to a greater extent. This shows that though the TSAs are better suited to establish the interactions occurring within the active site at the transition state, they are not always the most potent inhibitor for the enzyme. It is possible that the TSAs (**4a** and **4b**) interact with other glycosidases within the crude protein solution and thus more of the TSAs must be in solution to inhibit the activity.

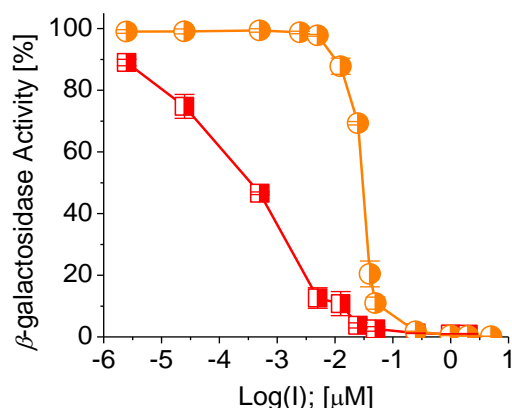
Table 4.3 Inhibition of hydrolysis of 4-methylumberliferyl- β -D-galactopyranoside (**5m**) by β -galactosidase (*E. coli*) in the presence of galactonoamidines. 5mM HEPES buffer solution at pH 7.50 ± 0.05 and $37.0\pm0.1^\circ\text{C}$.

Inhibitor	Crude Protein Extract IC ₅₀ [nM]	Commercial β -gal (<i>E. coli</i>) IC ₅₀ [nM]
4a	0.12 ± 0.010	26.4 ± 2.1
4b	0.35 ± 0.01	31.4 ± 2.2
4s	0.03 ± 0.01	1.74 ± 0.02

A



B



C

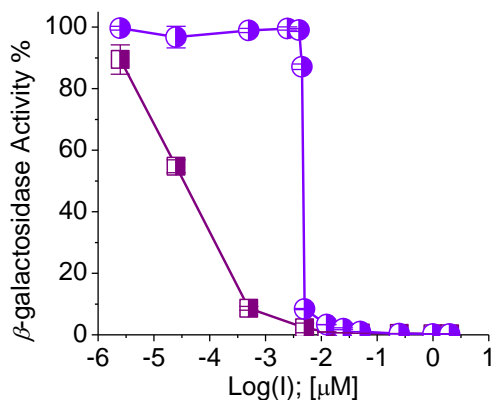


Figure 4.11 Activity of β -galactosidase (*E. coli*) from crude protein extract (half squares) and purified protein (half circles) in the presence of (A) **4a**, (B) **4b**, and (C) **4s**.

4.2.5 Purification of β -galactosidase (*E. coli*)

The ability of the galactonoamidines to bind to the crude protein extract two orders of magnitude more than the commercial protein was concerning. Thus, the β -galactosidase from the crude extract was purified to ensure it was catalytically similar to the commercial enzyme. The purification was accomplished by the method established by Fowler and Zabin with the modifications from Jacobson and Matthews.^{158, 159} Characterization of the purified protein was achieved through circular dichroism, SDS-PAGE electrophoresis, and Gel permeation chromatograph (GPC) analyses by comparison to the commercial β -galactosidase.

GPC analysis of the purified and commercial β -galactosidases resulted in very similar retention times, **Figure 4.12**. Both protein solutions had trace peaks that were determined to be insignificant compared to the β -galactosidase (*E. coli*) peak. The structures of the commercial and purified β -galactosidase were compared using circular dichroism. These data were also compared to a spectrum calculated using PDB2CD software.¹⁶⁰ The calculation of CD spectrum was to ensure that the spectra obtained matched the expected spectrum of the β -galactosidase (*E. coli*). The three spectra overlay nicely showing that there is not a misfolding or denaturation of the proteins that would cause a difference in affinity for the model substrates, **Figure 4.11**.

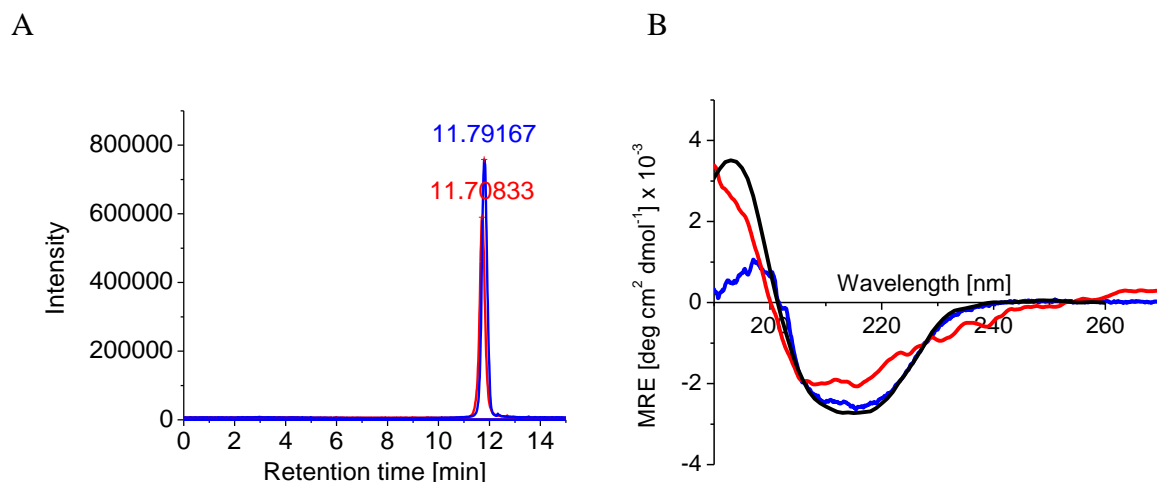


Figure 4.12 A) Comparison of commercial (red) and purified (blue) β -galactosidases by GPC analysis. B) Comparison of estimated $\Delta\epsilon$ by PDB2CD (black) to the experimental CD obtained with purified (blue) and commercial (red) β -galactosidase (*E. coli*).¹⁶⁰

4.2.6 Inhibition of purified (*E. coli*)

With the purified β -galactosidase in hand, we set out to examine the ability of the galactonoamidines to bind to the purified β -galactosidase. The same three galactonoamidines were used to test the inhibition on the purified β -galactosidase compared to the commercial enzyme: the two TSAs (**4a** and **4b**) and the opportunistic binder (**4s**). The inhibition constants of galactonoamidine inhibition of the two β -galactosidases were very similar with an error of only 4% between the two, **Table 4.4**. Thus, the β -galactosidase within the crude protein extract is not binding the galactonoamidines more tightly on its own. Therefore, something about the crude protein extract itself is causing the galactonoamidines to be bound more tightly in this solution.

Table 4.4 Inhibition of hydrolysis of 4-nitrophenyl- β -D-galactopyranoside (**5h**) by β -galactosidase (*E. coli*) in the presence of galactonoamidines. 5mM HEPES buffer solution at pH 7.50 \pm 0.05 and 30.0 \pm 0.1°C.

Inhibitor	Commercial β -gal (<i>E. coli</i>) K_i [pM]	Purified β -gal (<i>E. coli</i>) K_i [pM]
4a	33 \pm 6	31 \pm 3
4b	59 \pm 7	56 \pm 13
4s	86 \pm 4	81 \pm 4

The ability of the inhibitors to inhibit the crude protein extract to such extent without the β -galactosidase within the extract being less active is impressive. This shows that the inhibitors have the ability to bind the β -galactosidase specifically when in a solution of various other proteins. Given other methods of detection, it is highly probable that the galactonoamidines would be able to inhibit β -galactosidases within a cell.

4.3 Conclusions

The active site of β -galactosidase from *E. coli* was probed with 20 galactonoamidines. As expected, the library of galactonoamidines was able to inhibit the hydrolysis of substrate by β -galactosidase (*E. coli*) in the low picamolar concentration level (0.03-1.35nM). Initial SAR studies with 20 galactonoamidines revealed nine galactonoamidines (**4a-c**, **4f-g**, **4i-j**, **4p**, and **4s**) bound with similar IC_{50} values (6.8-37nM) and inhibition constants (30-100pM). Molecular dynamics analyses revealed that six (**4c**, **4f-g**, **4i-j**, and **4p**) of these inhibitors were unlikely to be TSAs based on the binding within the active sites being different than substrates previously crystallized within the active site. Spectroscopic evaluations of the three remaining inhibitors (**4a**, **4b**, and **4s**) revealed **4a** and **4b** are TSAs of the hydrolysis of substrate by β -galactosidase

(*E. coli*). Though β -galactosidase from *E. coli* is one of the most studied enzymes, no TSA had been determined experimentally until now.

Evaluation of the inhibition of β -galactosidase activity within a crude protein extract by galactonoamidines revealed inhibition of the hydrolysis of model substrates two orders of magnitude more than the purified β -galactosidase. This increase in inhibition occurred with both TSA and opportunistic binders, showing that though not all galactonoamidines are TSAs, they are still some of the most potent inhibitors known.

4.4 Materials and Methods

4.4.1 Instrumentation:

CD spectra were obtained on a Jasco J-1500 CD spectrometer Model 150 with a EXOS liquid cooling system from Koolance Inc.¹⁶¹ The supplied Spectra Manager software version 2.12.00 was employed for recording the spectra using a Thomas Scientific Quartz Spectrophotometer cell with a 1mm path length at 37.00±0.01°C.¹⁶¹ An HPLC system from Shimadzu with a CBM-10A communications bus module, an LC-20AD analytical pump, DGU-20A3R three channel online degassing unit, a SIL-20A UFLC autosampler with 96 well capability, a CTO-20A/prominence column oven, ELSD-90LT light scattering and LC solution software (vers. 1.25) from Shimadzu for data collection and analysis was used to establish purity of β -galactosidase (*E. coli*).⁸⁶ GPC analysis of protein purity was performed using a Yarra™ 3uM SEC-3000 column (Phenomenex) at 40°C with nanopure water as the isocratic eluent with a flow rate of 1.0L/min at 60°C.⁸⁶ All cell work was carried out in a Purifier Class II Biosafety Cabinet (Labconco) using aseptic technique. All media and glassware used during propagation of cells were autoclaved in a SG-1200 Steam sterilizer Autoclave (Steris Amsco Scientific). *E. coli*

cells were incubated in a Innova 4330 Incubator Shaker (New Brunswick Scientific; 37.0 ± 0.5 °C). Growth of cells was tracked at Optical Density 600nm (OD₆₀₀) with an Agilent 8453 UV/Vis spectrometer with a tungsten lamp using a disposable semi-micro cuvette (1.5-3mL) with a 10mm pathlength (BrandTech Scientific). The data were visualized with UV-Visible Chem Station B.02.01 SP1 software. Cells were harvested using J2-HS Refrigerated Centrifuge (Beckman Coulter) and Jouan CR412 refrigerated centrifuge (Scimetrics), only used for samples less than 100mL. Cell lysis was carried out using a Digital Sonifier (Branson) with a tapered 1/8 inch micro tip. Lyophilization of lysed cell was performed using a Freezone 1 liter benchtop freeze drying system (Labcono). Purification of β -galactosidase (*E. coli*) was carried out on a Biologic Low-Pressure Liquid Chromatography system (Bio Rad) equipped with a SV-5 Buffer Select Valve, Gradient Mixer, and BioFrac Fraction Collector. A PowerPac HC electrophoresis system (BioRad) with a Mini-Protean Tetra System chamber was used for electrophoresis analysis of purified samples. A Galaxy 5D centrifuge (VWR) was used for concentrating protein samples in Nanosep Centrifugal Devices (PALL Life Sciences) with an 10kDa molecular weight cutoff. All other instrumentation was described in **section 2.4.1**.

4.4.2 Materials:

Commercial β -galactosidase (*E. coli*) was obtained as a lyophilized powder from Sigma Aldric and used as received.⁵⁶ pST5832 was a gift from Carolyn Bertozzi & Jessica Seeliger (Addgene plasmid # 36256).¹⁶² A 30kDa Microsept Advance centrifuge device (Pall Corporation) was used to concentrate fractions from purification. DEAE Sephacel (GE Health Sciences) and p-amino-benzyl-1-thio- β -D-galactopyranoside agarose (Sigma Aldrich) resins were added to separate 1.5x30cm columns (Bio Rad) until a 20mL bed volume was obtained. Isopropyl β -D-thiogalactopyranoside (IPTG) was synthesized by Ifedi Orizu according to a

general procedure described Fairbanks.¹⁶³ Luria Berani media, ethylenediaminetetraacetic acid (EDTA), Calcium chloride, ammonium sulfate, potassium chloride, and agar were purchased from Sigma Aldrich as proteomic grade or higher. Kanamycin sulfate, TRIS buffer, Magnesium chloride, UREA, Phenylmethyl sulfonyl fluoride, TEMED, and Sodium chloride were purchased from VWR as proteomics grade or higher. Trichloroacetic acid (Beantown chemicals), Sodium Dodecyl Sulfate (TCI), and β -mercaptoethanol (Acros organics) at 99% purity were used as received. All other materials have been described in **section 3.4.2**.

4.4.3 *Spectroscopic evaluations of commercial enzyme.*

Stock solution of inhibitors:

Typically, 0.00025, 0.0025, 0.005, 0.05, 0.125, 0.25, 0.5, 2.5, 10, 20, 30, 50 and 100mM inhibitor solutions were prepared by diluting aliquots of 100 μ M aqueous solution of the galactonoamidines with nanopure water. All resulting inhibitor stock solutions were used in 10 μ L aliquots in IC₅₀ and K_i assays and kept at ambient temperature until pipetted into plates. Stock solutions of inhibitors in concentrations of 0.025-0.2nM for **4a-c**, **4e-j**, **4l**, **4n-p**, and **4s-t** and 0.25-1.0nM for **4d**, **4k**, **4m**, **4q-r**, and **4u-v** were used in the determination of K_i values.

Stock solution of substrate:

All substrate solutions were prepared immediately before use and kept at ambient temperature until pipetted into the plates.⁵⁶ Substrate solution was prepared by dissolving 4.61-6.93mg nitrophenyl- β -D-galactopyranoside (**5a-k**) in 20mL 5mM HEPES buffer solution (pH 7.50) in a volumetric flask and then diluted 1:1 with 5mM HEPES buffer solution (pH 7.50) for a final 0.37-0.65mM substrate solution.⁵⁶

Stock solution of commercial enzyme:

A 5mg sample of β -galactosidase (*E. coli*) was dissolved in 1mL of degassed nanopure water.⁵⁶ The sample was aliquoted into 10 μ L samples and stored at -80°C until use.⁵⁶ A BCA of the aliquoted samples revealed a concentration of 33.13 \pm 1.62 μ M.⁵⁶ Prior to use, a single sample was thawed and diluted to 5mL in a volumetric flask with 5mM HEPES buffer solution (pH 7.50 at 30°C).⁵⁶ Then, an 80 μ L aliquot of the solution was diluted to 10mL with the buffer solution in a volumetric flask.⁵⁶ The final monomeric concentration was determined to be 528 \pm 26pM.⁵⁶ The stock solution was kept on ice until use in 20 μ L aliquots.⁵⁶

Kinetic Assay with commercial enzyme:

The kinetic assay was performed as described in **section 2.4.3.5** with the following changes: The plate was then read at a wavelength of 405nm at 30°C for 30 min every 27s.⁵⁶

Data analysis:

The data analysis for kinetic evaluations was described in **section 2.4.3.6**.

4.4.4 Inhibitor cooperativity analysis:

4b was selected as a model galactonoamidine to show only a single class of inhibition sites was available to the galactonoamidine. For class of inhibition analysis, the four apparent K_M s were plotted versus the concentration of galactonoamidine.¹⁶⁴ A linear regression was performed on the data; the R^2 was then examined to determine the linearity of the data. If the linear regression shows a high linearity, R^2 , the inhibitor is only acting on a single class of active sites.¹⁶⁴

4.4.5 Molecular docking and modeling of protein inhibitor complexes

The PDB coordinates of β -galactosidase (*E. coli*) in complex with 2-flouro-2-deoxy- β -d-galactopyranoside (4V45) and galactotetrazole (1JZ6) were obtained from the Protein Data Bank. The water molecules were removed from the PDB coordinates and used without further modification in the case of these two control compounds. However, for all galactonoamidines complexes, the inhibitors were manually inserted in the active site of the *b*-galactosidase and overlain with the crystallized inhibitors. After obtaining the coordinates for the overlain galactonoamidines the inhibitors were removed from the active site along with all water molecules.

Protein inhibitor complexes were built with dimers rather than the tetrameric protein for simplicity using the GROMOS96-43A1 force field with GROMACS 4.6.7 software. The dimeric PDB coordinates were converted to a GROMACS coordinate and topology files by employing the pdb2gmh program. The pdb coordinate files for all inhibitors were converted to GROMACS coordinate files by the free software PRODRG. The chirality of all inhibitors was maintained and all partial charges were defined as GROMOS96-43A1 forces field without further energy minimization by PRODRG. The inhibitor topology files were corrected by reducing all charge groups to 3-4 atoms and correcting all partial charges with guidance from a recent study by Lemkul *et al.*¹

The edited topology and coordinate files of the inhibitors were appended to the dimeric *b*-galactosidases to create protein-inhibitor complexes. The protein inhibitor complexes were centered in a 8304.76nm^3 cubic box and solvated with 266,740-266,754 simple point charge water molecules and neutralized with 64 sodium ions. The systems were equilibrated as previously described and a 48ns NPT simulation was used as production phase.^{2, 3} The hydrogen

bonding interactions of inhibitors were determined using the H-bond plugin in the Visual Molecular Dynamics (VMD) program. Strong hydrogen bonds of the complexes of inhibitors with proteins were classified as a bond were the acceptor and donor were within 3.2Å of each other, which was cutoff used for determining hydrogen bonds from crystallization.⁴ Weak hydrogen bonding interactions are those in which the donor and acceptor are up to 3.5 Å apart.

4.4.6 Propagation of *E. coli* cells for cell assays

The *E. coli* (strain K12) cells containing a pST5832 plasmid were purchased from Addgene.¹⁶² A sterile inoculation loop was used to spread the purchased bacteria over a Luria-Bertani Agar plate with 30µg/mL Kanamycin antibiotic in the plate. The plate was incubated for 20 hours at 37°C. Then, five colonies were selected from the plate and placed in 10mL of sterile LB broth with 30µg/mL Kanamycin. This culture was incubated in an Innova incubator shaker for 16 hours. A 3.3mL aliquot of 50% sterile glycerol solution was added to the 10mL culture and the culture was stored in 500µL aliquots at -80°C until use.

Cells were grown in Luria-Bertani (LB) broth at 37.5°C. Growth of cells was monitored spectrophotometrically at a wavelength of 600nm (OD₆₀₀).¹⁵⁸ Cells grown from 2L cultures were harvested when the logarithmic growth reached an optical density (OD₆₀₀) of 2.5-3.0.¹⁶⁶ Cells were harvested at 6,000rpm and 4°C for 20min. The supernatant was discarded and the cell pellets were re-suspended in 60mL of 5mM HEPES buffer solution. The re-suspended pellets were combined into two pre-chilled High performance VWR centrifuge tubes. The re-suspended cell pellets were then centrifuged at 6,000rpm, 4°C for 15 minutes. The supernatant was discarded and the final cell pellets were stored at -20°C until processed for further use. The cell pellets were processed two ways for the cell assays: lysed cells and a crude protein extract from cells.

4.4.6.1 *Lysed E. coli cells:*

Two of the 5mL cell pellets were thawed and each was suspended in 10mL of buffer solution. The cells were then lysed while suspended in an ice bath using a Branson digital sonicator for 5 minutes at an amplitude of 40%. The sonication was performed with 5sec on followed by 5sec off. After the sonication, the cells were allowed to rest in ice for 5 minutes. Then the sonication and rest cycle was repeated twice for a total of 15 minutes of sonication and 15 minutes of rest. The resulting suspension was then flash frozen with liquid nitrogen and then freeze dried on over 72 hours. A total of 1.3198g lysed *E. coli* cells was obtained.

4.4.6.2 *Crude protein extract from E. coli cells:*

Two cell pellets obtained from an expression of *E. coli* cells were thawed and each were re-suspended in 15mL of the above 5mM HEPES buffer. The cell suspension was sonicated as explained above in **section 4.4.6.1**. The resulting suspension was then transferred to a 50mL VWR High performance centrifuge tube and centrifuged at 19,000rpm and 4°C for 25 minutes. The supernatant containing the crude protein extract was collected (total of 21mL) and aliquoted out into microvials (1mL aliquots). The aliquots were flash frozen with liquid nitrogen and stored at -80°C until further use.

4.4.7 *Purification of β -galactosidase (E. coli)*

4.4.7.1 *Propagation of cells:*

A vial of 500 μ L *E. coli* cells containing the pST5832 plasmid was thawed and pipetted into 5mL of sterile LB broth.¹⁶² The culture was incubated at 250rpm at 37°C for 6 hours; then a 1mL aliquot of this solution was used to inoculate a 100mL sterile LB broth in a 1L flask. The culture solution was shaken at 250rpm at 37°C for 15 hours in a Innova 4330 incubator shaker. After the incubation time, 25mL of the culture was used to inoculate four Erlenmeyer flasks with 500mL

of sterile LB broth, then incubated at 37°C and shaken at 250rpm until the desired optical density (OD 0.4-0.6A.U.) was obtained. The total incubation time until OD₆₀₀ of 0.53AU was reached was 1hr after inoculation.

After the desired OD₆₀₀ was reached, 1M *isopropyl* β -D-1-thiogalactopyranoside (IPTG) was added in 500 μ L aliquots into each of the 500mL cultures. The cultures were incubated for four hours after the addition of IPTG. Following the four-hour expression, the culture was centrifuged for 15minutes at 6,000rpm, 4°C to harvest the cells. The supernatant was discarded and the cell pellets were re-suspended in 30mL of 40mM Tris/0.5mM EDTA/10mM MgCl₂/5mM β -mercaptoethanol buffer solution (pH 7.50). Then, the re-suspended pellets cells were then centrifuged at 6,000rpm, 4°C for 15 minutes in a VWR High Performance centrifuge tube. The supernatant was discarded and the resulting cell pellet was stored at -20°C until use, each expression resulted in two large cell pellets.

4.4.7.2 Purification of β -galactosidase (*E. coli*):

The two cell pellets obtained from an expression of *E. coli* cells were thawed and each were re-suspended in 15mL of the above 5mM HEPES buffer. The cell suspension was sonicated as explained above in **section 4.4.6.1**. The resulting suspension was then transferred to a 50mL VWR High performance centrifuge tube and centrifuged at 19,000rpm and 4°C for 25 minutes. Ammonium sulfate (typically 11.71g) was slowly added to the supernatant (50mL) over 30 minutes until 40% saturation.¹⁵⁸ The suspension was stirred over two hours at 4°C then centrifuged at 19,000rpm for 30 minutes to obtain the protein as a precipitate. The precipitate was dissolved in 20mL 40mM Tris/0.5mM EDTA/10mM MgCl₂/5mM β -mercaptoethanol buffer solution (pH 7.50) and placed in a 15kDa molecular weight cutoff dialysis bag.¹⁵⁸ The crude

protein suspension was dialyzed against the same buffer solution over 24 hours with a total of six buffer exchanges.

After dialysis, the suspension was concentrated to 10mL in a 30kDa Microsept Advance centrifuge device (Pall corporation) and applied to a column (1.5x30cm) of DEAE Sephacel (GE Health sciences) that had been equilibrated with the 40mM Tris/0.5mM EDTA/10mM MgCl₂/5mM β -mercaptoethanol buffer solution (pH 7.50).¹⁵⁸ The column was washed with buffer solution until all non-bound proteins had eluted, typically 240mL. Then, the column was washed with the buffer solution with a linear gradient of aqueous 100mM-400mM NaCl solution applied from a 2M NaCl stock solution.¹⁵⁸ All fractions containing β -galactosidase activity and bands observed in by SDS-PAGE gels, typically from fractions containing 300mM and 400mM NaCl, were pooled and concentrated down to 10mL.

The pooled solution was loaded onto a column of p-amino-benzyl-1-thio- β -D-galactopyranoside agarose that had been equilibrated with 40mM Tris/0.5mM EDTA/10mM MgCl₂/5mM β -mercaptoethanol buffer solution (pH 7.50) with 250mM aqueous KCl solution.¹⁵⁹ After washing with this buffer solution, the buffer was switched to a 200mM Tris/0.5mM EDTA/10mM MgCl₂/10mM β -mercaptoethanol buffer solution (pH 8.50) with 250mM aqueous KCl solution.¹⁵⁹ Protein was eluted from the column using a linear gradient of aqueous 0.25M-1.5M KCl solution.¹⁵⁹ Pure β -galactosidase was obtained from fractions containing 0.5-1.0M KCl.

4.4.7.3 Characterization of purified β -galactosidase (*E. coli*):

Circular Dichroism

A 50 μ L aliquot of the concentrated purified protein was added to 950 μ L of nanopure water and mixed. A 400 μ L aliquot of this solution was then added to the spectrophotometer cell. The

solutions were equilibrated to 37°C then analyzed. Measurements were performed between 190 and 250nm with a CD scale of 200 mdeg/1.0dOD, a data pitch of 0.1nm, a 20nm/min scanning speed, and a 0.5nm band width. A total of three accumulations were obtained and averaged for each sample by the software. Similarly, a 400μL aliquot of a solution of 50μL 5mM HEPES buffer solution mixed with 950μL of nanopure water was analyzed for a baseline.

Data analysis:

The cd [mdeg] of the baseline solution was subtracted from the cd [mdeg] of the protein solution's spectrum.¹⁶¹ The data were smoothed using a Savitzky-Golay smoothing with 5-points to each side of the data with 5 iterations of smoothing.¹⁶¹ Then, the following equations were used to determine the molar ellipticity of the β -galactosidase sample.¹⁶¹

$$\text{Equation I: } [\theta] = \frac{[100*\theta]}{[C*L]}$$

$$\text{Equation II: } \Delta\epsilon = [\theta]/3298.2$$

An estimation of CD spectra for β -galactosidase (*E. coli*) was obtained using PDB2CD by uploading a pdb file (1JZ7) to the server.¹⁶⁰ The obtained spectra were then overlaid with the cd spectra obtained with the purified protein.

4.4.7.4 Gel permeation chromatography

Stock solutions of enzymes

Both solutions of β -galactosidase (*E. coli*) were thawed and used immediately.

*Stock solution of purified β -galactosidase (*E. coli*):* A 500μL aliquot of purified protein was concentrated to a volume of 150μL using a 10kDa Nanosept concentration device (Pall).

Stock solution of purchased β -galactosidase (E. coli): A 100 μ L aliquot of the working solution of purchased β -galactosidase was concentrated to 50 μ L of protein using a 10kDa Nanosept concentration device (Pall).

Assay

The sample was added to a Greiner BioOne 96 well microplate with conical well in 20 μ L aliquots. The samples were injected, in 5 μ L aliquots, onto a YarraTM 3 μ M SEC-3000 column at 40°C (Phenomenex) with nanopure water as solvent using a Shimazu UFLC instrument. A SEDEX 90 SEDERE LT-ELD detector was employed to determine retention times of samples.

Data analysis

The retention times of each sample were plotted against the intensity observed.

4.4.8 Spectroscopic analysis with lysed cells, crude protein extract, and purified protein.

Stock solution of crude protein extract: Typically, a 1mL aliquot of crude protein extract was thawed and diluted to 5mL with 5mM HEPES buffer solution (pH 7.50 at 37°C) in a volumetric flask. The concentration of total protein was determined to be 3.23 \pm 0.17mg/mL by BCA assay.

Stock solution of purified β -galactosidase from E. coli: A 1000 μ L aliquot of purified protein was diluted to 5mL with 5mM HEPES buffer solution (pH 7.50 at 37°C) in a volumetric flask. A BCA assay of the stock solution revealed a concentration of 81.6 \pm 6.8nM.

Stock solution of substrates: Stock solutions were prepared immediately before use and were discarded if not used within four hours after preparation.

Stock solution for crude protein extract: 6.48-6.52mg (0.0192-0.0193mmol) **5m** were dissolved in 500 μ L of DMSO, then brought to 10mL with 5mM HEPES buffer solution (pH 7.50 at 37°C) in a volumetric flask (1.92-1.93mM).

Stock solution for purified protein: 6.67-6.71mg (0.0191-0.0191mmol) **5m** were dissolved in 500 μ L of DMSO, then brought to 5mL with 5mM HEPES buffer solution (pH 7.50 at 37°C) in a volumetric flask (3.94-3.97mM). A 1000mL aliquot of this solution was then diluted to 5mL with 5mM HEPES buffer solution (pH 7.50 at 37°C) in a volumetric flask (0.790-0.793mM)

4.4.9 Assay to determine β -galactosidase activity

A 10 μ L aliquot of stock solution of inhibitor was added into a well in increasing concentration. In the twelfth well of the row, a 10 μ L aliquot of buffer solution was substituted for inhibitor for an uninhibited hydrolysis. Substrate solution was then added to each well in 30 μ L aliquots. Then 40 μ L aliquots of 5mM HEPES buffer solution (pH 7.50 at 37°C) were added to each well. Lastly, the stock solution of protein solution was added to each well in 20 μ L aliquots. After 30 minutes, a 60s medium orbital shake was performed then the fluorescence was read at an excitation wavelength of 360nm and an emission wavelength of 465nm for 24 hours with a read every hour. Assays with the purified protein were shortened to 2.5 hours with a read every 15 minutes due to the reaction completion being reached quicker.

Data analysis:

The appearance of product, 4-methylumbelliferone (**6**), was observed by fluorescence at an excitation wavelength of 360nm and an emission wavelength of 465nm. The fluorescence of inhibited hydrolysis were divided by the fluorescence in absence of inhibitor and transformed into percentage to determine the percentage inhibition of each inhibitor. The percent inhibition was then plotted as a function of the logarithmic concentration for each inhibitor. The IC₅₀ was determined by the concentration at which the enzyme was inhibited 50% by the inhibitor in the duplicate experiments and then averaged for the final value.

4.4.10 Assay to determine inhibition constants with purified β -galactosidase

Stock solution of substrate: Typically, 6.37mg (0.0211mmol) of 4-nitrophenyl β -D-galactopyranoside (**5h**) was dissolved with 5mM HEPES buffer solution (pH 7.50 at 37°C), then diluted to 5mL with the same buffer solution in a volumetric flask (4.23mM). Finally, a 1000mL aliquot was diluted to 5mL with 5mM HEPES buffer solution (pH 7.50 at 37°C) in a volumetric flask (0.846mM).

Assay conditions and data analysis was performed the same as sections **3.4.3.4** and **3.4.3.5**.

5 Conclusions and Outlooks

Glycoside hydrolases are able to stabilize the transition state for hydrolysis of substrates within their active sites to accelerate the hydrolysis 10^{17} over that of non-enzymatic hydrolysis.¹⁶⁷ Establishing the interactions that occur over the transition state (TS) is difficult due to its fleeting nature.⁶⁷ Therefore, the interactions with transition state analogs (TSAs) are examined instead.¹⁶⁸⁻¹⁷⁰ Many inhibitors had previously been designed as TSAs for glycoside hydrolases; however, experimental evidence of true TSAs only existed for xyloside based inhibitors and gluco- and manno-tetrazole based inhibitors.^{54, 69}

Here we have examined the abilities of a library of 25 galactonoamidines to mimic the TS of three β -galactosidases: from *A. oryzae*,⁷⁹ bovine liver, and *E. coli*. An initial structure activity relationship (SAR) screening of the galactonoamidines established the predominate interactions occurring within the active site of the glycoside hydrolases.^{86, 90} The predominate interactions with the galactonoamidines depend on the origin of the β -galactosidase.^{86, 90} The interactions over the aglycon were diverse depending on source: the β -galactosidase (*A. oryzae*) favored hydrophobic interactions,^{79, 86} β -galactosidase (bovine liver) favored π - π and CH- π interactions,⁹⁰ while β -galactosidase (*E. coli*) had all three interaction types. After narrowing down the inhibitors with the highest binding affinities to the enzyme, spectroscopic evaluation of the hydrolysis of 9-11 nitrophenyl- β -D-galactopyranosides revealed a single galactonoamidine, **4b**, was a TSA for all three enzymes.^{79, 90}

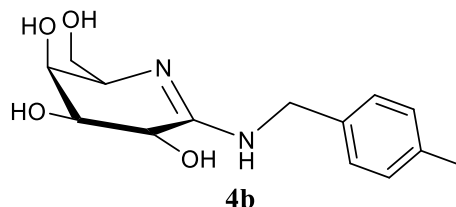


Figure 5.1: Structure of the galactonoamidine (**4b**) that determined to be a TSA of the three examined β -galactosidases.

Molecular docking and modeling analysis revealed that **4b** is stabilized by a synergy of interactions in the enzymes which include hydrogen bonding, hydrophobic interactions, π - π and CH- π interactions, and conformational changes at the active site.^{79, 90} The conformational shift in β -galactosidases from bovine liver and *E. coli* resulted in a loop closure over the active site.⁹⁰ This along with the synergy of other interactions resulted in an increased binding affinity of two orders of magnitude compared to the β -galactosidase from *A. oryzae*.⁹⁰ These conformational shifts when a TSA is bound in the active site occur through the beta/alpha loops at the entrance of the active sites. Since all clan A glycoside hydrolases have the same TIM motif as their catalytic site it is only logical that these beta/alpha loops play a part in stabilizing the transition state of the glycoside hydrolases in this clan.

Further examination of these loops is needed to determine how the conformational shifts are mediated and which residues play the largest role in stabilization. Most mutations of glycoside hydrolase enzymes have been in attempts to establish interactions that occur over the *glycon* during hydrolysis of substrates, while little to no mutations have been performed on residues that interact with the *aglycon*. Mutations to these residues would show which interactions are the most crucial to stabilizing the transition state of these enzymes and thus allow for such a large increase in hydrolysis compared to non-enzymatic reactions.

6 References

1. Gruber, E., Cellulose in der Zukunft. *Papier* **1976**.
2. Sinnott, M. L., Catalytic mechanism of enzymic glycosyl transfer. *Chem. Rev.* **1990**, 90 (7), 1171-1202.
3. Naumoff, D. G., Hierarchical classification of glycoside hydrolases. *Biochemistry.* **2011**, 76 (6), 622-35.
4. Koshland Jr, D., Stereochemistry and the mechanism of enzymatic reactions. *Biol. Rev.* **1953**, 28 (4), 416-436.
5. Henrissat, B.; Callebaut, I.; Fabrega, S.; Lehn, P.; Mornon, J. P.; Davies, G., Conserved Catalytic Machinery and the Prediction of a Common Fold for Several Families of Glycosyl Hydrolases. *Proc. Natl. Acad. Sci. U.S.A.* **1995**, 92 (15), 7090-7094.
6. Juers, D. H.; Huber, R. E.; Matthews, B. W., Structural comparisons of TIM barrel proteins suggest functional and evolutionary relationsps between b-galactosidase and other glycohydrolases. *Protein Science* **1999**, 8, 122-136.
7. Asano, N.; Kizu, H.; Oseki, K.; Tomioka, E.; Matsui, K.; Okamoto, M.; Baba, M., N-alkylated nitrogen-in-the-ring sugars: conformational basis of inhibition of glycosidases and HIV-1 replication. *J. Med Chem.* **1995**, 38 (13), 2349-56.
8. Goins, C. M.; Dajnowicz, S.; Thanna, S.; Sucheck, S. J.; Parks, J. M.; Ronning, D. R., Exploring Covalent Allosteric Inhibition of Antigen 85C from Mycobacterium tuberculosis by Ebselen Derivatives. *ACS Infect. Dis.* **2017**, 3 (5), 378-387.
9. Seppälä, M.; Koistinen, H.; Koistinen, R.; Chiu, P. C. N.; Yeung, W. S. B., Glycosylation related actions of glycodeclin: gamete, cumulus cell, immune cell and clinical associations. *Hum. Reprod. Update* **2007**, 13 (3), 275-287.
10. Wettschureck, N.; Offermanns, S., Mammalian G proteins and their cell type specific functions. *Physiol.l Rev.* **2005**, 85 (4), 1159-204.
11. Bohé, L.; Crich, D., Carbohydrate reactivity: Glycosyl cations out on parole. *Nat. Chem.* **2016**, 8 (2), 99.
12. Vuong, T. V.; Wilson, D. B., Glycoside hydrolases: catalytic base/nucleophile diversity. *Biotechnol. Bioeng.* **2010**, 107 (2), 195-205.
13. Davies, G.; Henrissat, B., Structures and mechanisms of glycosyl hydrolases. *Structure* **1995**, 3 (9), 853-9.
14. Phillips, D. C., The hen egg-white lysozyme molecule. *Pro. Nat. Acad. Sci.* **1967**, 57 (3), 483-495.

15. Post, C.; Karplus, M., Does lysozyme follow the lysozyme pathway? An alternative based on dynamic, structural, and stereoelectronic considerations. *J. Am. Chem. Soc.* **1986**, *108* (6), 1317-1319.
16. Bennet, A. J.; Sinnott, M. L., Complete kinetic isotope effect description of transition states for acid-catalyzed hydrolyses of methyl. cap alpha.-and. beta.-glucopyranosides. *J. Am. Chem. Soc.;*(United States) **1986**, *108* (23).
17. Withers, S. G.; Street, I. P.; Bird, P.; Dolphin, D. H., 2-Deoxy-2-Fluoroglucosides - a Novel Class of Mechanism-Based Glucosidase Inhibitors. *J. Am. Chem. Soc* **1987**, *109* (24), 7530-7531.
18. Martin, A.; Arda, A.; Desire, J.; Martin-Mingot, A.; Probst, N.; Sinay, P.; Jimenez-Barbero, J.; Thibaudeau, S.; Bleriot, Y., Catching elusive glycosyl cations in a condensed phase with HF/SbF₅ superacid. *Nature chemistry* **2016**, *8* (2), 186-191.
19. Cantarel, B. L.; Coutinho, P. M.; Rancurel, C.; Bernard, T.; Lombard, V.; Henrissat, B., The Carbohydrate-Active EnZymes database (CAZy): an expert resource for Glycogenomics. *Nucleic Acids Res.* **2009**, *37* (Database issue), D233-8.
20. Henrissat, B., A classification of glycosyl hydrolases based on amino acid sequence similarities. *Biochem J.* **1991**, *280* (Pt 2) (2), 309-16.
21. Henrissat, B.; Bairoch, A., Updating the sequence-based classification of glycosyl hydrolases. *Biochem. J.* **1996**, *316* (Pt 2) (Pt 2), 695-6.
22. Henrissat, B.; Davies, G., Structural and sequence-based classification of glycoside hydrolases. *Curr. Opin. Struct. Biol.* **1997**, *7* (5), 637-44.
23. Lombard, V.; Golaconda Ramulu, H.; Drula, E.; Coutinho, P. M.; Henrissat, B., The carbohydrate-active enzymes database (CAZy) in 2013. *Nucleic Acids Res.* **2014**, *42* (Database issue), D490-5.
24. Legler, G., Glycoside hydrolases: mechanistic information from studies with reversible and irreversible inhibitors. *Adv. Carbohydr. Chem. Biochem.*, Elsevier: 1990; Vol. 48, pp 319-384.
25. Fersht, A., *Structure and mechanism in protein science: a guide to enzyme catalysis and protein folding*. Macmillan: 1999.
26. Withers, S. G.; Aebersold, R., Approaches to labeling and identification of active site residues in glycosidases. *Protein science : a publication of the Protein Society* **1995**, *4* (3), 361-72.
27. Rempel, B. P.; Withers, S. G., Covalent inhibitors of glycosidases and their applications in biochemistry and biology. *Glycobiology* **2008**, *18* (8), 570-86.

28. Vodovozova, E. L., Photoaffinity labeling and its application in structural biology. *Biochemistry*. **2007**, 72 (1), 1-20.
29. Kuhn, C. S.; Lehmann, J.; Jung, G.; Stevanovic, S., Investigation of the active site of *Escherichia coli* beta-D-galactosidase by photoaffinity labelling. *Carbohydr. Res.* **1992**, 232 (2), 227-33.
30. Romaniouk, A.; Vijay, I. K., Structure-function relationships in glucosidase I: amino acids involved in binding the substrate to the enzyme. *Glycobiology* **1997**, 7 (3), 399-404.
31. Fowler, A. V.; Zabin, I.; Sinnott, M. L., Methionine 500, the site of covalent attachment of an active site-directed reagent of beta-galactosidase. *J. Biol. Chem.* **1978**, 253 (15), 5283-5.
32. BeMiller, J.; Gilson, R.; Myers, R.; Santoro, M., Suicide-substrate inactivation of b-galactosidase by diazomethyl bD-galactopyranosyl ketone. *Carbohydr. Res.* **1994**, 250 (1), 101-112.
33. van der Horst, G. T.; Mancini, G. M.; Brossmer, R.; Rose, U.; Verheijen, F. W., Photoaffinity labeling of a bacterial sialidase with an aryl azide derivative of sialic acid. *J. Biol. Chem.* **1990**, 265 (19), 10801-4.
34. Halazy, S.; Danzin, C.; Ehrhard, A.; Gerhart, F., 1,1-Difluoroalkyl Glucosides - a New Class of Enzyme-Activated Irreversible Inhibitors of Alpha-Glucosidases. *J. Am. Chem. Soc.:(United States)* **1989**, 111 (9), 3484-3485.
35. Sulzenbacher, G.; Schülein, M.; Davies, G. J., Structure of the endoglucanase I from *Fusarium oxysporum*: Native, cellobiose, and 3, 4-epoxybutyl β -D-cellobioside-inhibited forms, at 2.3 Å resolution. *Biochemistry* **1997**, 36 (19), 5902-5911.
36. Keitel, T.; Simon, O.; Borriss, R.; Heinemann, U., Molecular and active-site structure of a *Bacillus* 1,3-1,4-beta-glucanase. *Proc Natl Acad Sci U S A* **1993**, 90 (11), 5287-91.
37. Havukainen, R.; Torronen, A.; Laitinen, T.; Rouvinen, J., Covalent binding of three epoxyalkyl xylosides to the active site of endo-1,4-xylanase II from *Trichoderma reesei*. *Biochemistry* **1996**, 35 (29), 9617-24.
38. Mosi, R. M.; Withers, S. G., Trapping of alpha-glycosidase intermediates. *Methods Enzymol* **2002**, 354, 64-84.
39. Wicki, J.; Rose, D. R.; Withers, S. G., Trapping covalent intermediates on beta-glycosidases. *Methods Enzymol* **2002**, 354, 84-105.
40. Withers, S. G.; Street, I. P., Identification of a Covalent Alpha-D-Glucopyranosyl Enzyme Intermediate Formed on a Beta-Glucosidase. *J. Am. Chem. Soc* **1988**, 110 (25), 8551-8553.

41. Gebler, J.; Aebersold, R.; Withers, S., Glu-537, not Glu-461, is the nucleophile in the active site of (lac Z) beta-galactosidase from Escherichia coli. *J. Biol Chem* **1992**, 267 (16), 11126-11130.
42. Vocadlo, D. J.; Davies, G. J.; Laine, R.; Withers, S. G., Catalysis by hen egg-white lysozyme proceeds via a covalent intermediate. *Nature* **2001**, 412 (6849), 835-8.
43. McIntosh, L. P.; Hand, G.; Johnson, P. E.; Joshi, M. D.; Korner, M.; Plesniak, L. A.; Ziser, L.; Wakarchuk, W. W.; Withers, S. G., The pKa of the general acid/base carboxyl group of a glycosidase cycles during catalysis: a ¹³C-NMR study of bacillus circulans xylanase. *Biochemistry* **1996**, 35 (31), 9958-66.
44. Heightman, T. D.; Vasella, A. T., Recent insights into inhibition, structure, and mechanism of configuration-retaining glycosidases. *Angew. Chem. Int. Ed.* **1999**, 38 (6), 750-770.
45. Tong, M. K.; Papandreou, G.; Ganem, B., Potent, Broad-Spectrum Inhibition of Glycosidases by an Amidine Derivative of D-Glucose. *J. Am. Chem. Soc.* **1990**, 112 (16), 6137-6139.
46. Heck, M. P.; Vincent, S. P.; Murray, B. W.; Bellamy, F.; Wong, C. H.; Mioskowski, C., Cyclic amidine sugars as transition-state analogue inhibitors of glycosidases: Potent competitive inhibitors of mannosidases. *J. Am. Chem. Soc.* **2004**, 126 (7), 1971-1979.
47. Legler, G.; Finken, M.-T., N1-Alkyl-d-gluconamidines: Are they 'perfect' mimics of the first transition state of glucosidase action? *Carbohydr. Res* **1996**, 292, 103-115.
48. Lal  gerie, P.; Legler, G.; Yon, J. M., The use of inhibitors in the study of glycosidases. *Biochimie* **1982**, 64 (11-12), 977-1000.
49. Patai, S., *Chemistry of amidines and imidates*. Wiley: 1975.
50. Williams, S. J.; Notenboom, V.; Wicki, J.; Rose, D. R.; Withers, S. G., A new, simple, high-affinity glycosidase inhibitor: Analysis of binding through X-ray crystallography, mutagenesis, and kinetic analysis. *J. Am. Chem. Soc.* **2000**, 122 (17), 4229-4230.
51. McCarter, J.; Adam, M.; Withers, S., Binding energy and catalysis. Fluorinated and deoxygenated glycosides as mechanistic probes of Escherichia coli (lacZ) β -galactosidase. *Biochem J* **1992**, 286 (3), 721-727.
52. Notenboom, V.; Birsan, C.; Warren, R. A. J.; Withers, S. G.; Rose, D. R., Exploring the cellulose/xylan specificity of the β -1, 4-glycanase Cex from Cellulomonas fimi through crystallography and mutation. *Biochemistry* **1998**, 37 (14), 4751-4758.
53. Papandreou, G.; Tong, M. K.; Ganem, B., Amidine, Amidrazone, and Amidoxime Derivatives of Monosaccharide Aldonolactams - Synthesis and Evaluation as Glycosidase Inhibitors. *J. Am. Chem. Soc.:(United States)* **1993**, 115 (25), 11682-11690.

54. Ermert, P.; Vasella, A.; Weber, M.; Rupitz, K.; Withers, S. G., Configurationally Selective Transition-State Analog Inhibitors of Glycosidases - a Study with Nojiritetrazoles, a New Class of Glycosidase Inhibitors. *Carbohydr. Res* **1993**, 250 (1), 113-128.
55. Hoos, R.; Naughton, A. B.; Thiel, W.; Vasella, A.; Weber, W.; Rupitz, K.; Withers, S. G., d-Gluconhydroximo-1, 5-lactam and Related N-Arylcarbamates Theoretical Calculations, Structure, Synthesis, and Inhibitory Effect on β -Glucosidases. *Helv. Chim. Acta* **1993**, 76 (7), 2666-2686.
56. Fan, Q.-H.; Pickens, J. B.; Striegler, S.; Gervaise, C. D., Illuminating the binding interactions of Galactonoamidines during the inhibition of β -galactosidase (E. coli). *Borg. Med. Chem* **2016**, 24, 661-671.
57. Ermert, P.; Vasella, A., Synthesis of a Glucose-Derived Tetrazole as a New β -Glucosidase Inhibitor. A New Synthesis of 1-Deoxynojirimycin. *Helv. Chim Acta* **1991**, 74 (8), 2043-2053.
58. Tatsuta, K.; Miura, S.; Ohta, S.; Gunji, H., Syntheses and glycosidase inhibiting activities of nagstatin analogs. *J. Antibiot* **1995**, 48 (3), 286-8.
59. Tatsuta, K.; Ikeda, Y.; Miura, S., Synthesis and glycosidase inhibitory activities of nagstatin triazole analogs. *J Antibiot* **1996**, 49 (8), 836-8.
60. Jensen, H. H.; Bols, M., Synthesis of 1-azagalactofagomine, a potent galactosidase inhibitor. *J Chem Soc Perk T I* **2001**, (8), 905-909.
61. S  hoel, H.; Liang, X.; Bols, M., Isogalactofagomine lactam. A neutral nanomolar galactosidase inhibitor. *J. Chem Soc, Perk T I* **2001**, (14), 1584-1585.
62. Heightman, T. D.; Vasella, A. T., Recent Insights into Inhibition, Structure, and Mechanism of Configuration-Retaining Glycosidases. *Angew. Chem. Int. Ed* **1999**, 38, 750-770.
63. Heightman, T. D.; Ermert, P.; Klein, D.; Vasella, A., Synthesis of Galactose-and N-Acetylglucosamine-Derived Tetrazoles and their evaluation as β -glycosidase inhibitors. *Helv. Chim Acta* **1995**, 78 (2), 514-532.
64. Withers, S. G.; Namchuk, M.; Mosi, R., Potent Glycoside Inhibitors: Transition State Mimics or Simply Fortuitous Binders? *Iminosugars as glycosidase inhibitors: nojirimycin and beyond* **1998**, 188-206.
65. Mader, M. M.; Bartlett, P. A., Binding Energy and Catalysis: The Implications for Transition-State Analogs and Catalytic Antibodies. *Chem Rev* **1997**, 97 (5), 1281-1302.
66. Wolfenden, R., Transition state analogues for enzyme catalysis. *Nature* **1969**, 223 (5207), 704-5.
67. Eyring, H., The activated complex in chemical reactions. *J. Chem. Phys.* **1935**, 3 (2), 107-115.

68. Lienhard, G. E., Enzymatic catalysis and transition-state theory. *Science* **1973**, *180* (4082), 149-54.
69. Wicki, J.; Williams, S. J.; Withers, S. G., Transition-state mimicry by glycosidase inhibitors: a critical kinetic analysis. *J Am Chem Soc* **2007**, *129* (15), 4530-1.
70. Fan, Q. H.; Striegler, S.; Langston, R. G.; Barnett, J. D., Evaluating N-benzylgalactonoamidines as putative transition state analogs for beta-galactoside hydrolysis. *Org Biomol Chem* **2014**, *12* (17), 2792-800.
71. Lillelund, V. H.; Jensen, H. H.; Liang, X.; Bols, M., Recent developments of transition-state analogue glycosidase inhibitors of non-natural product origin. *Chem Rev* **2002**, *102* (2), 515-53.
72. Sigurskjold, B. W.; Berland, C. R.; Svensson, B., Thermodynamics of inhibitor binding to the catalytic site of glucoamylase from *Aspergillus niger* determined by displacement titration calorimetry. *Biochemistry* **1994**, *33* (33), 10191-9.
73. Berland, C. R.; Sigurskjold, B. W.; Stoffer, B.; Frandsen, T. P.; Svensson, B., Thermodynamics of inhibitor binding to mutant forms of glucoamylase from *Aspergillus niger* determined by isothermal titration calorimetry. *Biochemistry* **1995**, *34* (32), 10153-61.
74. Biarnés, X.; Ardevol, A.; Iglesias-Fernández, J.; Planas, A.; Rovira, C., Catalytic itinerary in 1, 3-1, 4-β-glucanase unraveled by QM/MM metadynamics. Charge is not yet fully developed at the oxocarbenium ion-like transition state. *J. Am. Chem. Soc.* **2011**, *133* (50), 20301-20309.
75. Davies, G.; Ducros, V.-A.; Varrot, A.; Zechel, D., Mapping the conformational itinerary of β-glycosidases by X-ray crystallography. Portland Press Limited: 2003.
76. Wheatley, R. W.; Huber, R. E., An allolactose trapped at the lacZ β-galactosidase active site with its galactosyl moiety in a 4H3 conformation provides insights into the formation, conformation, and stabilization of the transition state. *Biochem. Cell Biol.* **2015**, *93* (6), 531-540.
77. Sabini, E.; Wilson, K. S.; Danielsen, S.; Schuelein, M.; Davies, G. J., Oligosaccharide binding to family 11 xylanases: both covalent intermediate and mutant product complexes display 2, 5B conformations at the active centre. *Acta Crystallogr. D Biol. Crystallogr.* **2001**, *57* (9), 1344-1347.
78. Bartlett, P. A.; Marlowe, C. K., Phosphonamidates as Transition-State Analog Inhibitors of Thermolysin. *Biochemistry* **1983**, *22* (20), 4618-4624.
79. Pickens, J. B.; Mills, L. G.; Wang, F.; Striegler, S., Evaluating hydrophobic galactonoamidines as transition state analogs for enzymatic β-galactoside hydrolysis. *Bioorg. Chem.* **2018**, *77*, 144-151.
80. Withers TSA study with Cex xylanase: 3n: Slope of 1.06 ± 0.11 , $R^2 = 0.93$, 3o: 1.05 ± 0.09 , $R^2 = 0.095$, 3p 1.11 ± 0.08 , $R^2 = 0.097$.

81. Field, R. A.; Haines, A. H.; Chrystal, E. J. T.; Luszniak, M. C., Histidines, Histamines and Imidazoles as Glycosidase Inhibitors. *Biochem, J* **1991**, 274 (3), 885-889.
82. Kalso, R.; Yancey, E. A.; Striegler, S., N-Benzylgalactonoamidines as potent b-galactosidase inhibitors. *Tetrahedron* **2012**, 68 (47-52).
83. Fan, Q. H.; Striegler, S.; Langston, R. G.; Barnett, J. D., Evaluating N-benzylgalactonoamidines as putative transition state analogs for beta-galactoside hydrolysis. *Org Biomol Chem* **2014**, 12 (17), 2792-800.
84. Kroger, L.; Thiem, J., Synthesis and evaluation of glycosyl donors with novel leaving groups for transglycosylations employing beta-galactosidase from bovine testes. *Carbohydr. Res.* **2007**, 342 (3-4), 467-81.
85. Linear free energy relationship gave a slope of 1.07 and R² of 0.946 with b-galactosidase (*A. oryzae*) and RK221.
86. Fan, Q.-H.; Claunch, K. A.; Striegler, S., Structure-Activity Relationship of Highly Potent Galactonoamidine Inhibitors toward b-Galactosidase (*Aspergillus Oryzae*). *J. Med. Chem* **2014**, 57 (8999-9009).
87. Schramm, V. L., Transition States and transition state analogue interactions with enzymes. *Acc Chem. Res.* **2015**, 48 (4), 1032-9.
88. Blériot, Y.; Genre-Grandpierre, A.; Tellier, C., Synthesis of a benzylamidine derived from D-mannose. A potent mannosidase inhibitor. *Tetrahedron Lett* **1994**, 35 (12), 1867-1870.
89. Legler, G.; Finken, M.-T., N1-Alkyl-d-gluconamidines: Are they 'perfect' mimics of the first transition state of glucosidase action? *Carbohydr Res* **1996**, 292, 103-115.
90. Pickens, J. B.; Wang, F.; Striegler, S., Picomolar inhibition of β -galactosidase (bovine liver) attributed to loop closure. *Bioorg. Med. Chem.* **2017**.
91. Maksimainen, M. M.; Lampio, A.; Mertanen, M.; Turunen, O.; Rouvinen, J., The crystal structure of acidic β -galactosidase from *Aspergillus oryzae*. *Int. J. Biol Macromol.* **2013**, 60, 109-115.
92. Fan, Q. H.; Striegler, S.; Langston, R. G.; Barnett, J. D., Evaluating N-benzylgalactonoamidines as putative transition state analogs for beta-galactoside hydrolysis. *Org. Biomol Chem* **2014**, 12 (17), 2792-2800.
93. Pickens, J. B.; Striegler, S.; Fan, Q.-H., Arabinoamidine synthesis and its inhibition toward β -glucosidase (sweet almonds) in comparison to a library of galactonoamidines. *Bioorg Med Chem* **2016**, 24 (16), 3371-3377.
94. Fan, Q. H.; Claunch, K. A.; Striegler, S., Structure-activity relationship of highly potent galactonoamidine inhibitors toward beta-galactosidase (*Aspergillus oryzae*). *J. Med Chem.* **2014**, 57 (21), 8999-9009.

95. Fan, Q.-H.; Striegler, S.; Langston, R. G.; Barnett, J. D., Evaluating N-benzylgalactonoamidines as putative transition state analogs for β -galactoside hydrolysis. *Org. Biomol. Chem.* **2014**, *12* (17), 2792-2800.
96. Berman, H. M.; Westbrook, J.; Feng, Z.; Gilliland, G.; Bhat, T. N.; Weissig, H.; Shindyalov, I. N.; Bourne, P. E., The Protein Data Bank. *Nucleic Acids Res.* **2000**, *28* (1), 235-242.
97. Sanner, M. F., Python: a programming language for software integration and development. *J Mol Graph Model* **1999**, *17* (1), 57-61.
98. Morris, G. M.; Huey, R.; Lindstrom, W.; Sanner, M. F.; Belew, R. K.; Goodsell, D. S.; Olson, A. J., AutoDock4 and AutoDockTools4: Automated docking with selective receptor flexibility. *J Comput Chem* **2009**, *30* (16), 2785-91.
99. Hess, B.; Kutzner, C.; van der Spoel, D.; Lindahl, E., GROMACS 4: Algorithms for Highly Efficient, Load-Balanced, and Scalable Molecular Simulation. *J Chem. Theory Comp.* **2008**, *4* (3), 435-47.
100. Scott, W. R. P.; Hunenberger, P. H.; Tironi, I. G.; Mark, A. E.; Billeter, S. R.; Fennen, J.; Torda, A. E.; Huber, T.; Kruger, P.; van Gunsteren, W. F., The GROMOS biomolecular simulation program package. *J Phys Chem A* **1999**, *103* (19), 3596-3607.
101. Schuttelkopf, A. W.; van Aalten, D. M., PRODRG: a tool for high-throughput crystallography of protein-ligand complexes. *Acta Crystallogr. D, Biol Crystallogr* **2004**, *60* (Pt 8), 1355-63.
102. Lemkul, J. A.; Allen, W. J.; Bevan, D. R., Practical considerations for building GROMOS-compatible small-molecule topologies. *J. Chem Inf Model* **2010**, *50* (12), 2221-35.
103. Lemkul, J. A.; Allen, W. J.; Bevan, D. R., Practical considerations for building GROMOS-compatible small-molecule topologies. *J Chem Inf Model* **2010**, *50* (12), 2221-2235.
104. Berendsen, H. J. C.; Grigera, J. R.; Straatsma, T. P., The Missing Term in Effective Pair Potentials. *J Phys Chem-Us* **1987**, *91* (24), 6269-6271.
105. Bussi, G.; Donadio, D.; Parrinello, M., Canonical sampling through velocity rescaling. *J. Chem. Phys.* **2007**, *126* (1), 014101.
106. Darden, T.; York, D.; Pedersen, L., Particle Mesh Ewald - an N.Log(N) Method for Ewald Sums in Large Systems. *J. Chem. Phys.* **1993**, *98* (12), 10089-10092.
107. Essmann, U.; Perera, L.; Berkowitz, M. L.; Darden, T.; Lee, H.; Pedersen, L. G., A Smooth Particle Mesh Ewald Method. *J Chem Phys* **1995**, *103* (19), 8577-8593.
108. Verlet, L., Computer Experiments on Classical Fluids .I. Thermodynamical Properties of Lennard-Jones Molecules. *Phys Rev* **1967**, *159* (1), 98-+.

109. Hess, B.; Bekker, H.; Berendsen, H. J. C.; Fraaije, J. G. E. M., LINCS: A linear constraint solver for molecular simulations. *J. Comput Chem* **1997**, *18* (12), 1463-1472.
110. Nose, S., Constant-Temperature Molecular-Dynamics. *J Phys-Condens Mat* **1990**, *2* (S), Sa115-Sa119.
111. Ray, J. R.; Rahman, A., Statistical Ensembles and Molecular-Dynamics Studies of Anisotropic Solids. *J Chem Phys* **1984**, *80* (9), 4423-4428.
112. Humphrey, W.; Dalke, A.; Schulten, K., VMD: visual molecular dynamics. *J Mol Graph* **1996**, *14* (1), 33-8, 27-8.
113. Consortium, T. U., UniProt: a hub for protein information. *Nucleic Acids Res* **2015**, *43* (Database issue), D204-12.
114. Ganem, B.; Papandreou, G.; Tong, M., Amidine, Amidrazone, and Amidoxime Derivatives of Monosaccharide Aldonolactams: Synthesis and Evaluation as Glycosides Inhibitors. *J. Am. Chem. Soc* **1993**, *115*, 11682-11690.
115. Seppälä, M.; Koistinen, H.; Koistinen, R.; Mandelin, E.; Oehninger, S.; Clark, G. F.; Dell, A.; Morris, H. R., Glycodelins: role in regulation of reproduction, potential for contraceptive development and diagnosis of male infertility. *Hum Reprod* **1998**, *13* (suppl 3), 262-269.
116. Mahajan, C.; Patel, K.; Khan, B. M.; Rawal, S. S., In silico ligand binding studies of cyanogenic β -glucosidase, dhurrinase-2 from Sorghum bicolor. *J Mol Model* **2015**, *21* (7), 184.
117. Ogunmolu, F. E.; Jagadeesha, N. B. K.; Kumar, R.; Kumar, P.; Gupta, D.; Yazdani, S. S., Comparative insights into the saccharification potentials of a relatively unexplored but robust *Penicillium funiculosum* glycoside hydrolase 7 cellobiohydrolase. *Biotechnol. Biofuels* **2017**, *10* (1), 71.
118. Kaufmann, K. W.; Lemmon, G. H.; Deluca, S. L.; Sheehan, J. H.; Meiler, J., Practically useful: what the Rosetta protein modeling suite can do for you. *Biochemistry* **2010**, *49* (14), 2987-98.
119. Kim, D. E.; Chivian, D.; Baker, D., Protein structure prediction and analysis using the Robetta server. *Nucleic Acids Res* **2004**, *32* (suppl 2), W526-W531.
120. Fernandez-Fuentes, N.; Madrid-Aliste, C. J.; Rai, B. K.; Fajardo, J. E.; Fiser, A., M4T: a comparative protein structure modeling server. *Nucleic Acids Res* **2007**, *35* (Web Server issue), W363-8.
121. Benkert, P.; Tosatto, S. C.; Schomburg, D., QMEAN: A comprehensive scoring function for model quality assessment. *Proteins* **2008**, *71* (1), 261-77.
122. McGuffin, L. J., The ModFOLD server for the quality assessment of protein structural models. *Bioinformatics* **2008**, *24* (4), 586-7.

123. Smith, J. U.; Smith, P., 'MODEVAL': Quantitative methods to evaluate and compare SOM models. **1995**.
124. Papandreou, G.; Tong, M. K.; Ganem, B., Amidine, Amidrazone, and Amidoxime Derivatives of Monosaccharide Aldonolactams: Synthesis and Evaluation as Glycosidase Inhibitors. *J. Am. Chem. Soc.* **1993**, *115*, 11682-11690.
125. Namchuk, M. N.; Withers, S. G., Mechanism of Agrobacterium beta-glucosidase: kinetic analysis of the role of noncovalent enzyme/substrate interactions. *Biochemistry* **1995**, *34* (49), 16194-202.
126. Juers, D. H.; Heighten, T. D.; Vasella, A.; Mackenzie, L.; Withers, S. G.; Matthews, B. W., A Structural View of the Action of Escherichia coli (lacZ) b-Galactosidase. *Biochemistry* **2001**, *40*, 14781-14794.
127. McCarter, J. D.; Withers, S. G., Mechanisms of enzymatic glycoside hydrolysis. *Curr. Opin Struct Biol* **1994**, *4* (6), 885-92.
128. Nerinckx, W.; Desmet, T.; Claeysens, M., A hydrophobic platform as a mechanistically relevant transition state stabilising factor appears to be present in the active centre of all glycoside hydrolases. *FEBS letters* **2003**, *538* (1-3), 1-7.
129. Rigden, D. J.; Jedrzejas, M. J.; de Mello, L. V., Identification and analysis of catalytic TIM barrel domains in seven further glycoside hydrolase families. *FEBS letters* **2003**, *544* (1-3), 103-111.
130. Fernandez-Fuentes, N.; Rai, B. K.; Madrid-Aliste, C. J.; Fajardo, J. E.; Fiser, A., Comparative protein structure modeling by combining multiple templates and optimizing sequence-to-structure alignments. *Bioinformatics* **2007**, *23* (19), 2558-65.
131. Rykunov, D.; Steinberger, E.; Madrid-Aliste, C. J.; Fiser, A., Improved scoring function for comparative modeling using the M4T method. *J Struct Funct Genomics* **2009**, *10* (1), 95-9.
132. Chivian, D.; Kim, D. E.; Malmstrom, L.; Bradley, P.; Robertson, T.; Murphy, P.; Strauss, C. E.; Bonneau, R.; Rohl, C. A.; Baker, D., Automated prediction of CASP-5 structures using the Robetta server. *Proteins* **2003**, *53 Suppl 6* (S6), 524-33.
133. Zhang, Y., Protein structure prediction: when is it useful? *Curr. Opin Struct Biol* **2009**, *19* (2), 145-155.
134. Fiser, A.; Do, R. K.; Sali, A., Modeling of loops in protein structures. *Protein science : a publication of the Protein Society* **2000**, *9* (9), 1753-73.
135. Richard, J. P.; Zhai, X.; Malabanan, M. M., Reflections on the catalytic power of a TIM-barrel. *Bioorg Chem* **2014**, *57*, 206-12.

136. Fan, Q.-H.; Striegler, S.; Langston, R. G.; Barnett, J. D., Evaluating N-benzylgalactonoamidines as putative transition state analogs for β -galactoside hydrolysis. *Org Biomol Chem* **2014**, *12* (17), 2792-2800.
137. Kanso, R.; Striegler, S., Multi gram-scale synthesis of galactothionolactam and its transformation into a galactonoamidine. *Carbohydr Res* **2011**, *346* (7), 897-904.
138. Rai, B. K.; Fiser, A., Multiple mapping method: a novel approach to the sequence-to-structure alignment problem in comparative protein structure modeling. *Proteins* **2006**, *63* (3), 644-61.
139. Šali, A.; Blundell, T. L., Comparative protein modelling by satisfaction of spatial restraints. *J Mol Biol* **1993**, *234* (3), 779-815.
140. Trott, O.; Olson, A. J., Software News and Update AutoDock Vina: Improving the Speed and Accuracy of Docking with a New Scoring Function, Efficient Optimization, and Multithreading. *J Comput Chem* **2009**, *31* (2), 455-461.
141. Trott, O.; Olson, A. J., Software News and Update AutoDock Vina: Improving the Speed and Accuracy of Docking with a New Scoring Function, Efficient Optimization, and Multithreading. **2009**, *31* (2), 455-461.
142. DeLano, W. L., Pymol: An open-source molecular graphics tool. *CCP4 Newsletter On Protein Crystallography* **2002**, *40*, 82-92.
143. Sharma, P.; Kaila, P.; Guptasarma, P., Creation of active TIM barrel enzymes through genetic fusion of half-barrel domain constructs derived from two distantly related glycosyl hydrolases. *Febs J* **2016**, *283* (23), 4340-4356.
144. Malabanan, M. M.; Amyes, T. L.; Richard, J. P., A role for flexible loops in enzyme catalysis. *Curr Opin Struct Biol* **2010**, *20* (6), 702-10.
145. O'Rourke, K. F.; Jelowicki, A. M.; Boehr, D. D., Controlling Active Site Loop Dynamics in the (β/α) 8 Barrel Enzyme Indole-3-Glycerol Phosphate Synthase. *Catalysts* **2016**, *6* (9), 129.
146. Juers, D. H.; Heightman, T. D.; Vasella, A.; McCarter, J. D.; Mackenzie, L.; Withers, S. G.; Matthews, B. W., A structural view of the action of Escherichia coli (lac Z) β -galactosidase. *Biochemistry* **2001**, *40* (49), 14781-14794.
147. Juers, D. H.; Jacobson, R. H.; Wigley, D.; Zhang, X.-J.; Huber, R. E.; Tronrud, D. E.; Matthews, B. W., High resolution refinement of b-galactosidase in a new crystal form reveals multiple metal binding sites and provides a structural basis for a-complementation. *Protein Science* **2000**, *9*, 1695-1699.
148. Juers, D. H.; Matthews, B. W.; Hyber, R. E., LacZ b-Galactosidase: Structure and function of an enzyme of historical and molecular biological importance. *Protein Science* **2012**, *21*, 1792-1807.

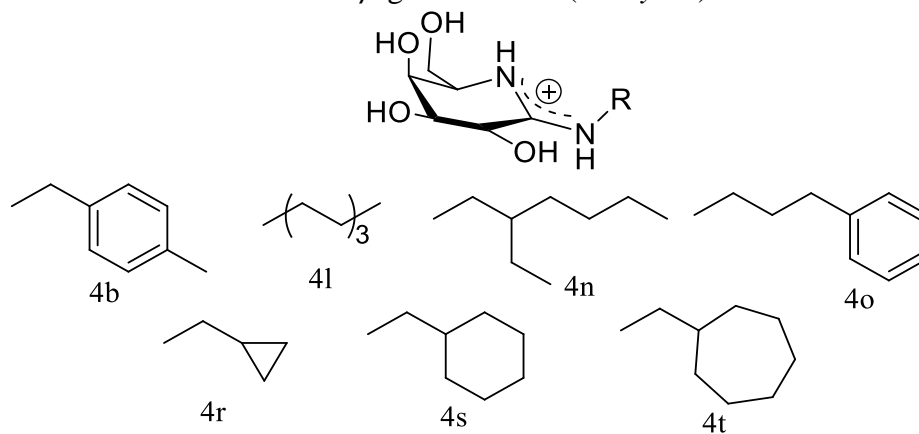
149. Wheatley, R. W.; Kappelhoff, J. C.; Hahn, J. N.; Dugdale, M. L.; Dutkoski, M. J.; Tamman, S. D.; Fraser, M. E.; Huber, R. E., Substitution for Asn460 Cripples β -galactosidase (*Escherichia coli*) by increasing substrate affinity and decreasing transition state stability. *Arch. Biochem Biophys* **2012**, *521* (1), 51-61.
150. Wheatley, R. W.; Lo, S.; Jancewicz, L. J.; Dugdale, M. L.; Huber, R. E., Structural explanation for allolactose (lac operon inducer) synthesis by lacZ β -galactosidase and the evolutionary relationship between allolactose synthesis and the lac repressor. *J Biol Chem* **2013**, *288* (18), 12993-13005.
151. Juers, D. H.; Hakda, S.; Matthews, B. W.; Huber, R. E., Structural basis for the altered activity of Gly794 variants of *Escherichia coli* β -galactosidase. *Biochemistry* **2003**, *42* (46), 13505-13511.
152. Dugdale, M. L.; Vance, M. L.; Wheatley, R. W.; Driedger, M. R.; Nibber, A.; Tran, A.; Huber, R. E., Importance of Arg-599 of β -galactosidase (*Escherichia coli*) as an anchor for the open conformations of Phe-601 and the active-site loop. *Biochem Cell Biol* **2010**, *88* (6), 969-979.
153. Jancewicz, L. J.; Wheatley, R. W.; Sutendra, G.; Lee, M.; Fraser, M. E.; Huber, R. E., Ser-796 of β -galactosidase (*Escherichia coli*) plays a key role in maintaining a balance between the opened and closed conformations of the catalytically important active site loop. *Arch. Biochem Biophys* **2012**, *517* (2), 111-122.
154. Wheatley, R. W.; Lo, S.; Jancewicz, L. J.; Dugdale, M. L.; Huber, R. E., Structural Explanation for Allolactose (lac Operon Inducer) Synthesis by lacZ β -galactosidase and the Evolutionary Relationship between Allolactose Synthesis and the lac Repressor. *J Biol Chem* **2013**, *288* (18), 12993-13005.
155. Pilipenko, O. S., Dissociation and catalytic activity of oligomer forms of β -galactosidases. *Russ. J. Phys. Chem. A* **2007**, *81* (6), 990-994.
156. Wang, Y. J.; Zhang, G. W.; Pan, J. H.; Gong, D. M., Novel Insights into the Inhibitory Mechanism of Kaempferol on Xanthine Oxidase. *J Agric Food Chem* **2015**, *63* (2), 526-534.
157. Chen, D.; Menche, G.; Power, T. D.; Sower, L.; Peterson, J. W.; Schein, C. H., Accounting for ligand-bound metal ions in docking small molecules on adenylyl cyclase toxins. *Proteins* **2007**, *67* (3), 593-605.
158. Fowler, A. V.; Zabin, I., Purification, structure, and properties of hybrid beta-galactosidase proteins. *The Journal of biological chemistry* **1983**, *258* (23), 14354-8.
159. Jacobson, R. H.; Matthews, B. W., Crystallization of β -galactosidase from *Escherichia coli*. *J. Mol. Biol.* **1992**, *223* (4), 1177-82.
160. Mavridis, L.; Janes, R. W., PDB2CD: a web-based application for the generation of circular dichroism spectra from protein atomic coordinates. *Bioinformatics* **2017**, *33* (1), 56-63.

161. Striegler, S.; Pickens, J. B., Discrimination of chiral copper(II) complexes upon binding of galactonoamidine ligands. *Dalton T* **2016**, 45 (38), 15203-15210.
162. Seeliger, J. C.; Topp, S.; Sogi, K. M.; Previti, M. L.; Gallivan, J. P.; Bertozzi, C. R., A riboswitch-based inducible gene expression system for mycobacteria. *PloS one* **2012**, 7 (1), e29266.
163. France, R. R.; Compton, R. G.; Davis, B. G.; Fairbanks, A. J.; Rees, N. V.; Wadhawan, J. D., Selective electrochemical glycosylation by reactivity tuning. *Org Biomol Chem* **2004**, 2 (15), 2195-202.
164. Sharma, B.; Pickens, J. B.; Striegler, S.; Barnett, J. D., Biomimetic Glycoside Hydrolysis by a Microgel Templated with a Competitive Glycosidase Inhibitor. *ACS Catalysis* **2018**, 8 (9), 8788-8795.
165. Berman, H. M.; Westbrook, J.; Feng, Z.; Gilliland, G.; Bhat, T. N.; Weissig, H.; Shindyalov, I. N.; Bourne, P. E., The protein data bank. *Nucleic Acids Res* **2000**, 28 (1), 235-242.
166. Rodriguez-Colinas, B.; de Abreu, M. A.; Fernandez-Arrojo, L.; de Beer, R.; Poveda, A.; Jimenez-Barbero, J.; Haltrich, D.; Ballesteros Olmo, A. O.; Fernandez-Lobato, M.; Plou, F. J., Production of galacto-oligosaccharides by the β -galactosidase from *Kluyveromyces lactis*: Comparative analysis of permeabilized cells versus soluble enzyme. *J. Agric. Food Chem.* **2011**, 59 (19), 10477-10484.
167. Wolfenden, R.; Lu, X. D.; Young, G., Spontaneous hydrolysis of glycosides. *J. Am. Chem. Soc* **1998**, 120 (27), 6814-6815.
168. Wolfenden, R., Transition state analogues for enzyme catalysis. *Nature* **1969**, 223, 704-705.
169. Lienhard, G. E., Enzymatic catalysis and transition-state theory. *Science* **1973**, 180 (4082), 149-154.
170. Mader, M. M.; Bartlett, P. A., Binding energy and catalysis: the implications for transition-state analogs and catalytic antibodies. *Chemical Rev.* **1997**, 97 (5), 1281-1302.

7 Appendix 1: Supplemental Information from Chapter 2

7.1 Molecular docking analysis with β -galactosidase (*A. oryzae*)

Table 7.1 Hydrogen bonding interactions of the galactonoamidines (**4b**, **4l**, **4n-o**, and **4r-t**) and amino acid residues in the active site of β -galactosidase (*A. oryzae*). From **Section 2.2.1**



Interacting partners		4b	4l	4o	4t	4s	4n	4r
C2 OH	Glu142	2.1Å		2.4Å				
	Glu200	2.2Å						
C3 OH	Glu298	2.4Å	2.1Å	2.1Å		2.1Å	2.2Å	2.2Å
C4 OH	Ala141	2.3Å	2.5Å	2.4Å	2.3Å	2.5Å	2.6Å	2.6Å
	Tyr342	2.2Å	2.6Å		2.1Å		2.5Å	
C6 OH	Asn199		2.2Å	2.2Å	1.9Å	1.1Å	1.9Å	1.9Å
	Glu298		2.5Å		2.0Å		1.9Å	2.7Å
Endo NH	Glu200		2.0Å	2.0Å	2.8Å	2.3Å	1.9Å	2.3Å
Exo NH	Glu200		2.5Å	2.7Å	2.8Å	2.6Å	1.9Å	

8 Appendix 2: Supplemental Information from Chapter 3

8.1 Determination of molar absorptivity of nitrophenylates.

8.1.1 *Stock solution of phenols:*

For phenol solutions, 3.14mg-5.79mg of the phenol were dissolved in 25mL 5mM HEPES buffer solution at pH 7.50 (0.82-1.47mM). The phenol solutions were kept at ambient temperature until pipetted into microplates.

8.1.2 *Molar absorptivity Assay:*

The stock solutions of phenols were pipetted in 10-70 μ L aliquots into a 96-well plate, then brought to 100 μ L with 5mM HEPES buffer solution.⁷⁰ The solutions were thermostated at 30°C for thirty minutes then a low orbital shake was performed within the plate reader.⁷⁰ The absorbance was then read at a wavelength of 405nm as an endpoint read.⁷⁰

8.1.3 *Data analysis:*

The absorbances of the phenol solutions were plotted against concentrations of phenol solution.⁷⁰ The linear regression obtained by this plot gave the extinction coefficient, ϵ_{405} , multiplied by the pathlength of the 96-well microplate containing 100 μ L of phenol solution in 5mM HEPES buffer solution at pH 7.50 and 30°C.⁷⁰ These apparent extinction coefficients were then averaged for the three impartial concentrations of the phenol.⁷⁰ From these data, the molar extinction coefficients were calculated based on path length described by the manufacture and correcting for the volume within each cell.⁷⁰

Molar extinction coefficients for phenolates produced by the hydrolysis of model substrates were determined at pH 7.50 and 30°C in 5mM HEPES buffer **5a** ϵ_{405} : 2871 M⁻¹cm⁻¹, **5b** ϵ_{405} : 943 M⁻¹cm⁻¹, **5c** ϵ_{405} : 2964 M⁻¹cm⁻¹, **5d** ϵ_{405} : 1674 M⁻¹cm⁻¹, **5e** ϵ_{405} : 1590 M⁻¹cm⁻¹, **5f** ϵ_{405} : 4499 M⁻¹cm⁻¹

¹, **5g** ϵ_{405} : 780 M⁻¹cm⁻¹, **5h** ϵ_{405} : 13300 M⁻¹cm⁻¹, **5i** ϵ_{405} : 14400 M⁻¹cm⁻¹ and, **5j** ϵ_{405} : 15700 M⁻¹cm⁻¹
¹ and **5k** ϵ_{405} 14100 M⁻¹cm⁻¹

8.2 Molecular Dynamics snapshots of FQ248 in complex with β -galactosidase (bovine liver)

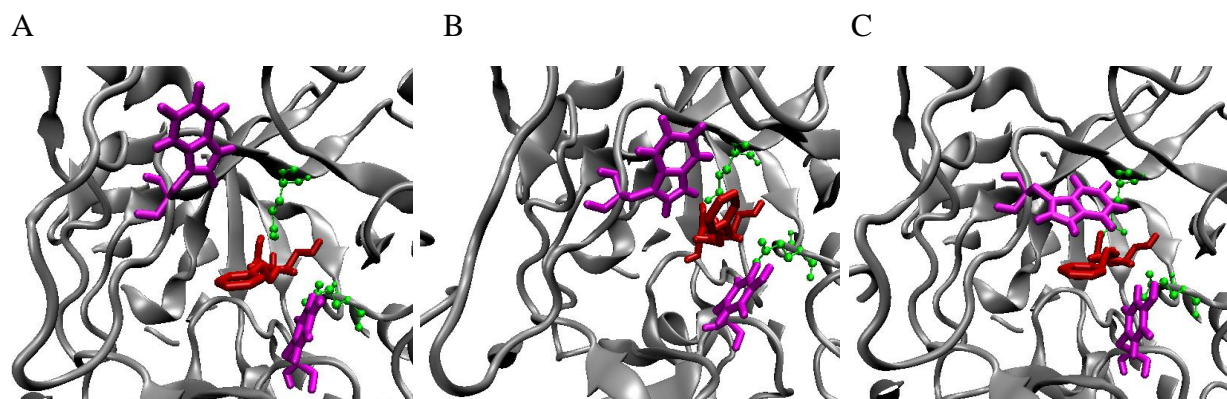
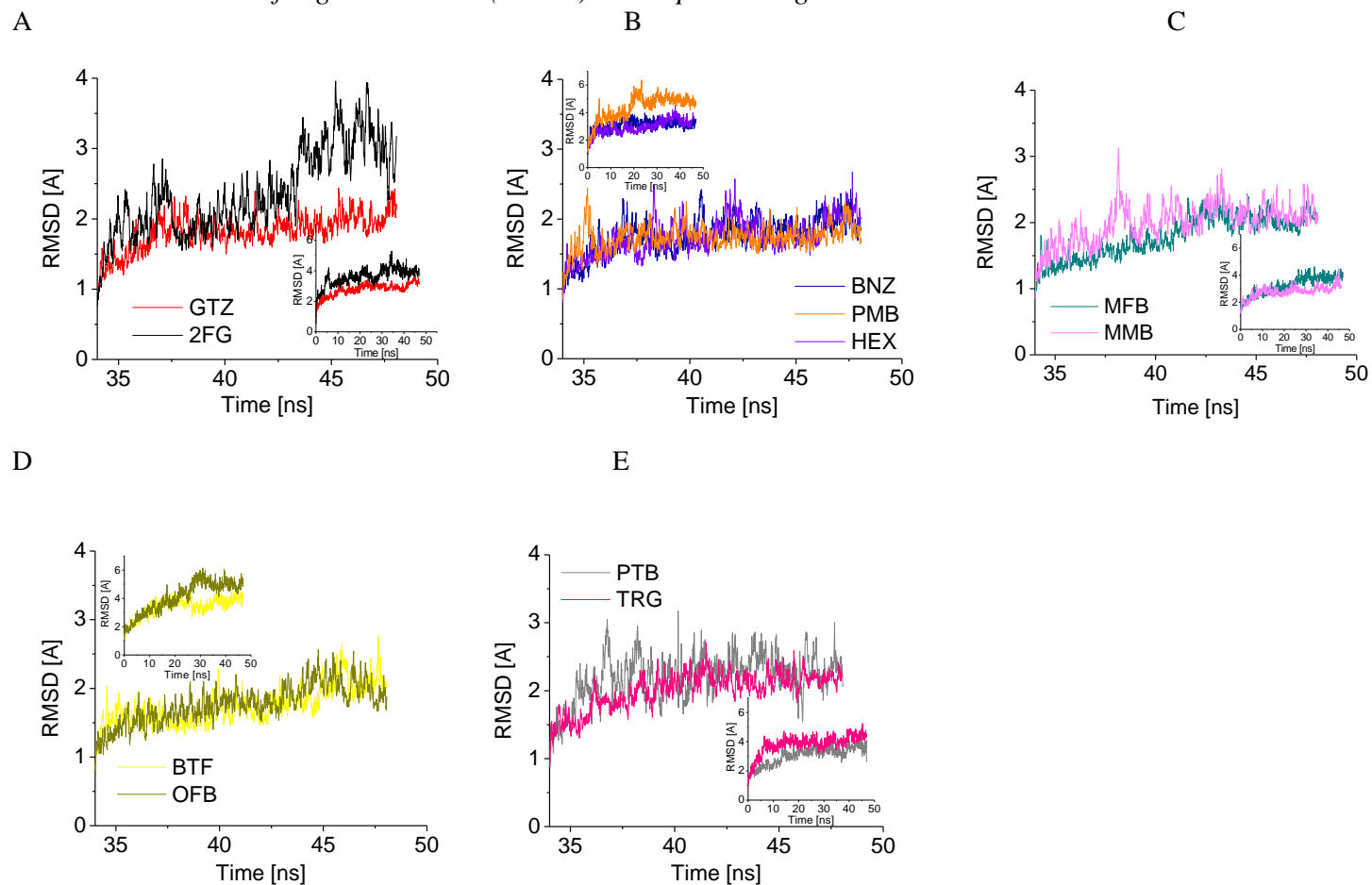


Figure 8.1 Snap shots of from the 30 ns simulation of the **4o** (red) and β -galactosidase (bovine liver) complex showing the active site (A) before, (B) during, and (C) after the loop closure event. The catalytic residues are shown in green and TRP272 and TYR484 are shown in magenta.

9 Appendix 3: Supplemental information for Chapter 4

9.1 Molecular Dynamics Simulations

9.1.1 RMSD Plots of *b*-galactosidase (*E. coli*) in complex with galactonoamidines:



RMSD of the backbone of a dimer of β -galactosidase (*E. coli*) in complex with (A) 2FG and GTZ, (B) RK217, RK221, and FQ162, (C) FQ065 and RK203, (D) FQ187 and RK222, and (E) FQ202 and FQ245 over the relaxation phase (35 to 48ns) and the RMSD from the entire production phase (0 to 48ns) as an insert in each image.

9.1.2 Hydrogen bond Formation

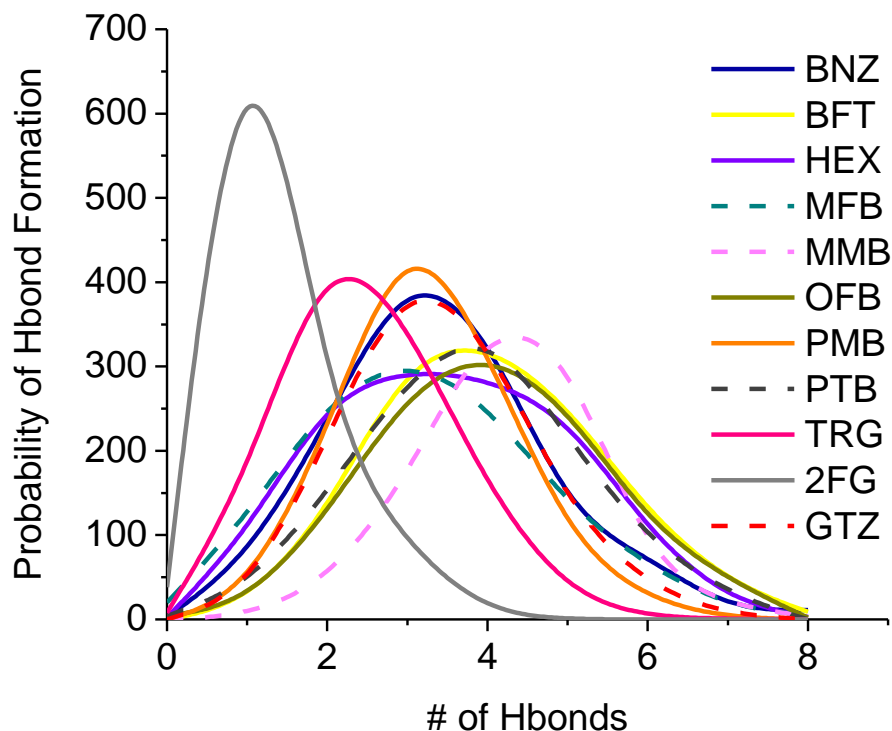


Figure 9.1 Frequency of hydrogen bonding interactions in correlation to the number of hydrogen bonding of galactonoamidines with β -galactosidase (*E. coli*).

9.1.3 Images

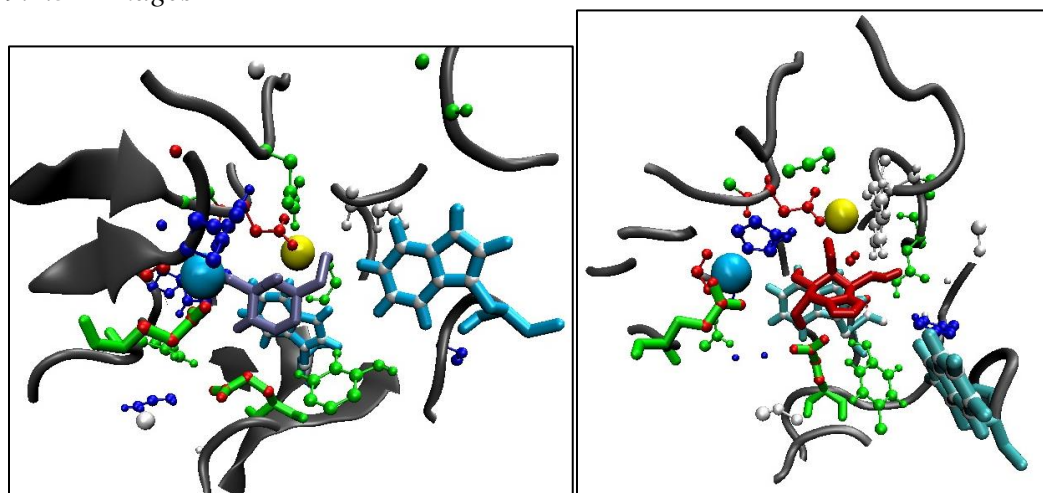


Figure 9.2 Snap shots of **2a** and **3k** within the active site of β -galactosidase (*E. coli*). Catalytic residues are shown as green sticks, Trp999 and Trp568 are shown as cyan sticks, and the metal ions are shown as spheres (cyan = Mg^{2+} and yellow = Na^{+})

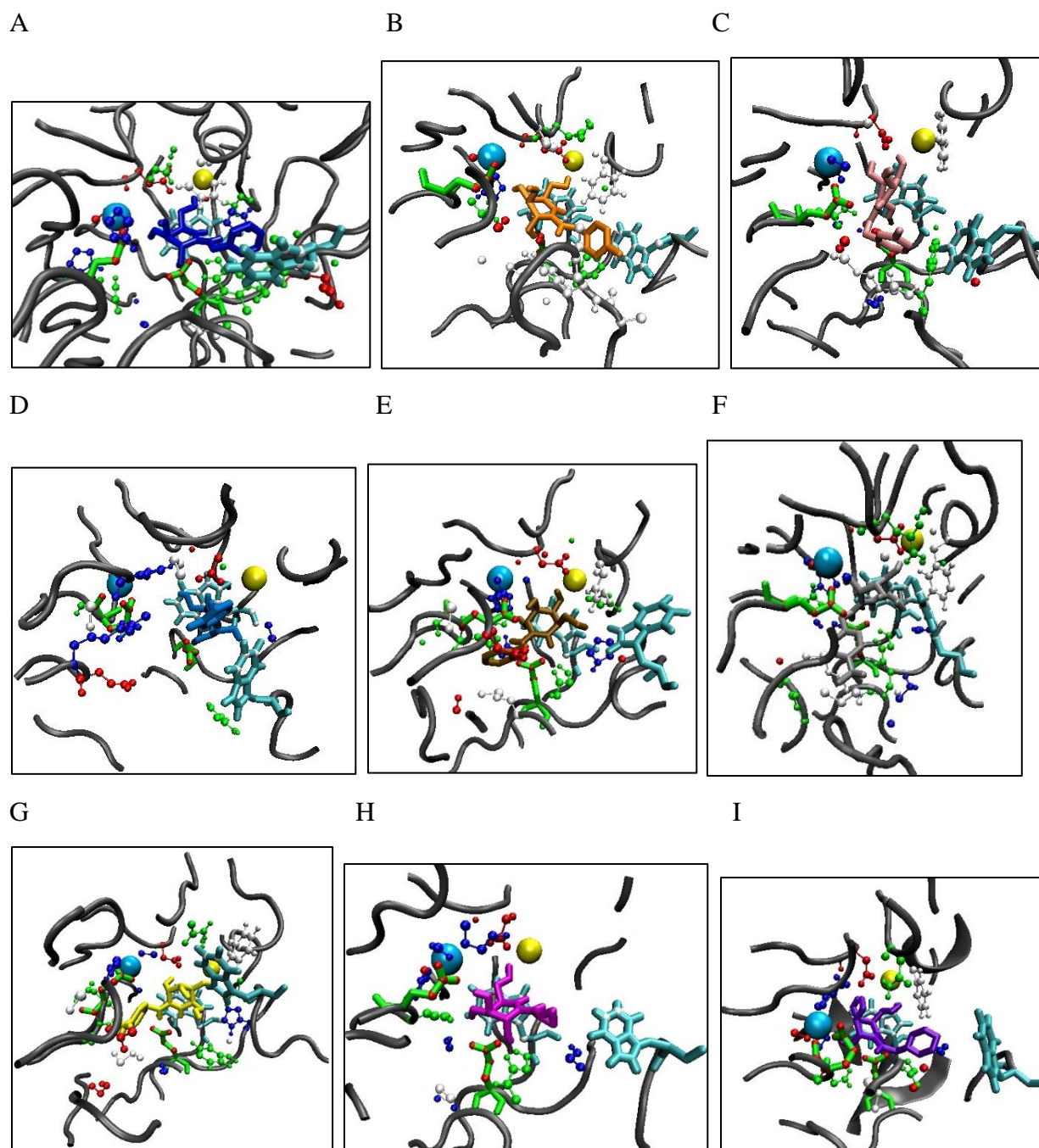


Figure 9.3 Snap shots of the galactonoamidines within the active site of b-galactosidase (*E. coli*). Green sticks are catalytic residues, cyan sticks are Trp999 and Trp568, and the metal ions are shown as spheres (cyan = Mg^{2+} and yellow = Na^{+}). (A) **4a**, (B) **4b**, (C) **4c**, (D) **4f**, (E) **4g**, (F) **4j**, (G) **4i**, (H) **4p**, and (I) **4s**.

9.2 SDS-PAGE

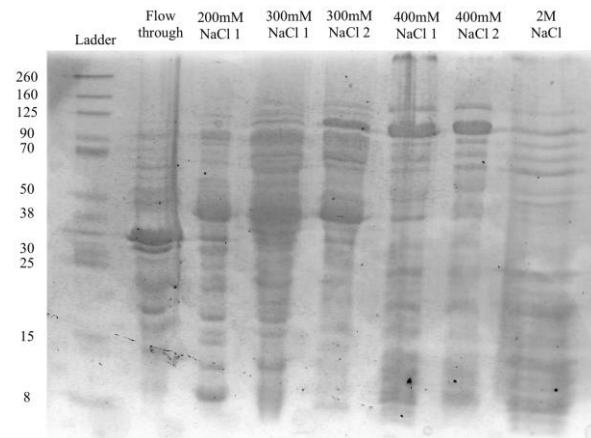


Figure 9.4 SDS PAGE analysis of fractions from the ion exchange column, DEAE Sephacel. The fractions containing β -galactosidase (*E. coli*) were from the 300mM and 400mM NaCl buffer solutions.

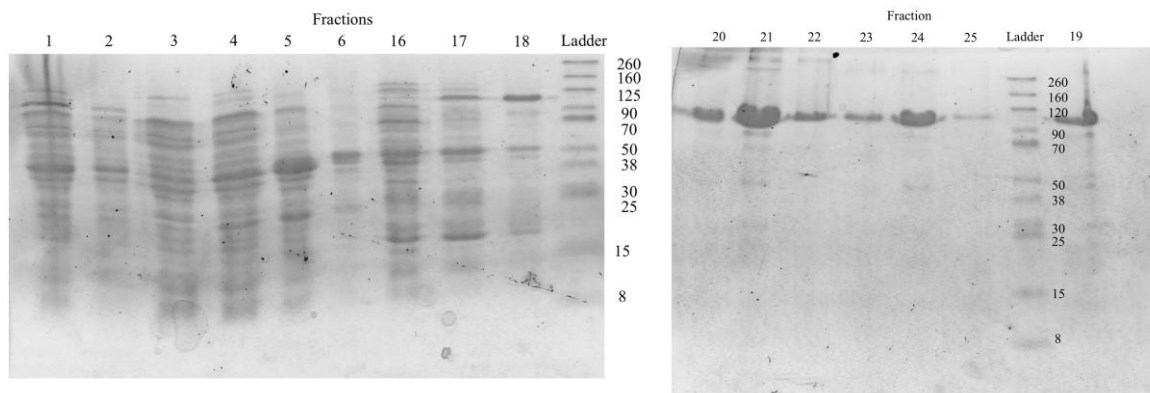


Figure 9.5 SDS PAGE analysis of fractions from the affinity column, p-aminobenzyl-1-thio-b-D-galactopyranoside agarose. Pure β -galactosidase (*E. coli*) eluted in fractions 19-25. Since fraction 21 contained some contamination it was not pooled with the other fractions for the final stock solution.

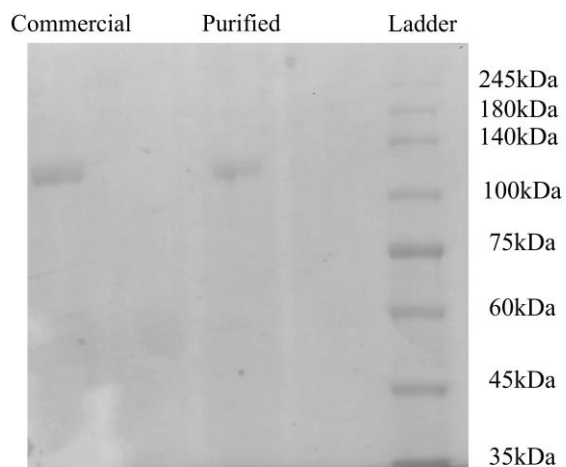


Figure 9.6 SDS PAGE comparison of purified β -galactosidase (*E. coli*) and the commercial β -galactosidase (*E. coli*).

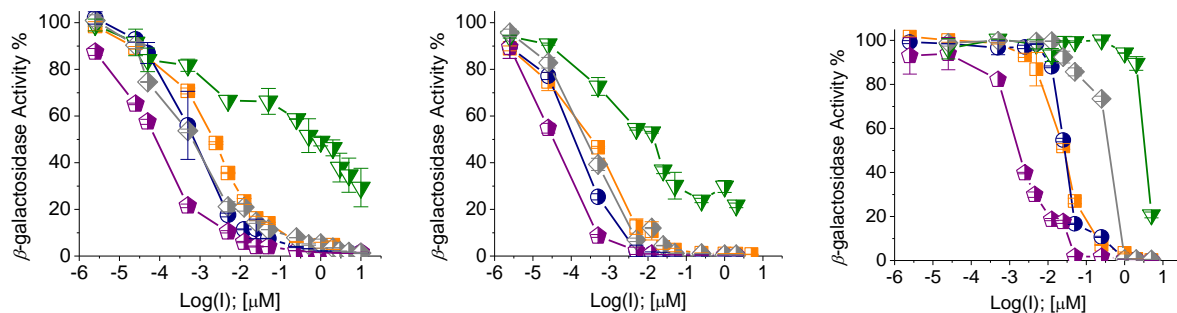


Figure 9.7 Activity of β -galactosidase (*E. coli*) from (A) lysed cells, (B) crude protein extract, and (C) purified protein in the presence of **4a** (navy circle), **4b** (orange square), **4i** (grey diamond), **4n** (green triangle), and **4s** (purple pentagon).